Computational Model of Forward and Opposed Smoldering Combustion with Improved Chemical Kinetics

by

Guillermo Rein Soto-Yarritu

B.S. (Universidad Pontificia Comillas de Madrid ICAI, Spain) 1999
M.S. (University of California Berkeley) 2003

A dissertation submitted in partial satisfaction of the

requirements for the degree of

Doctor of Philosophy
in

Engineering-Mechanical Engineering

in the

GRADUATE DIVISION

of the

UNIVERSITY OF CALIFORNIA, BERKELEY

Committee in charge:

Professor A. Carlos Fernandez-Pello, Chair
Professor Jyh-Yuan Chen
Professor Scott L. Stephens

Fall 2005

The dissertation of Guillermo Rein Soto-Yarritu is approved:

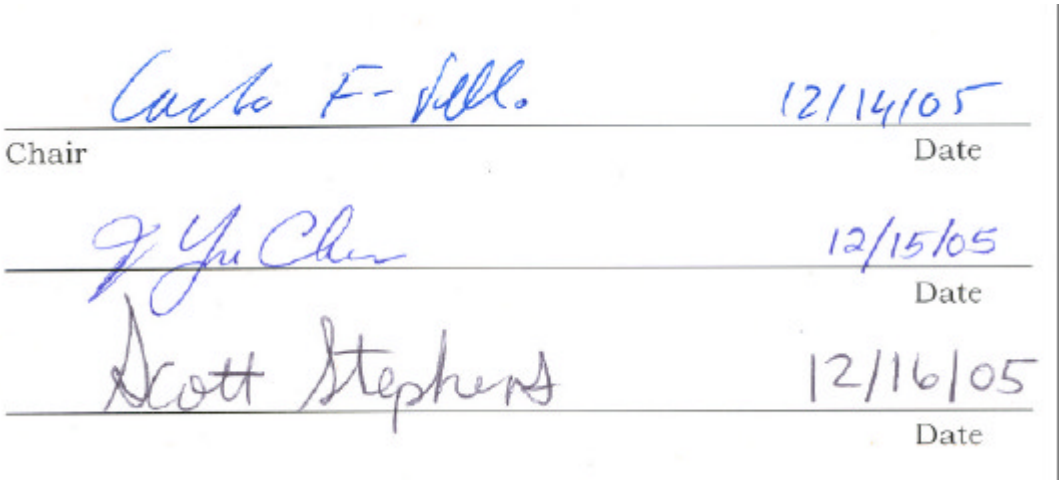

University of California, Berkeley

Fall 2005

Computational Model of Forward and Opposed Smoldering Combustion with Improved Chemical Kinetics

by

Guillermo Rein Soto-Yarritu

Abstract

Computational Model of Forward and Opposed Smoldering Combustion with Improved Chemical Kinetics

by

Guillermo Rein Soto-Yarritu

Doctor of Philosophy in Engineering-Mechanical Engineering

University of California, Berkeley

Professor A. Carlos Fernandez-Pello, Chair

A computational study has been carried out to investigate smoldering ignition and propagation in polyurethane foam. The one-dimensional, transient, governing equations for smoldering combustion in a porous fuel are solved accounting for improved solid-phase chemical kinetics. A systematic methodology for the determination of solid-phase kinetics suitable for numerical models has been developed and applied to the simulation of smoldering combustion. This methodology consists in the correlation of a mathematical representation of a reaction mechanism with data from previous thermogravimetric experiments. Genetic-algorithm and trail-and-error techniques are used as the optimization procedures. The corresponding kinetic parameters for two different mechanisms of polyurethane foam smoldering kinetics are quantified: a previously proposed 3-step mechanism and a new 5-step mechanism. These kinetic mechanisms are used to model one-dimensional

smoldering combustion, numerically solving for the solid-phase and gas-phase conservation equations in microgravity with a forced flow of oxidizer gas. The results from previously conducted microgravity experiments with flexible polyurethane foam are used for calibration and testing of the model predictive capabilities. Both forward and opposed smoldering configurations are examined. The model describes well both opposed and forward propagation. Specifically, the model predicts the reaction-front thermal and species structure, the onset of smoldering ignition, and the propagation rate. The model results reproduce the most important features of the smolder process and represent a significant step forward in smoldering combustion modeling.

Professor A. Carlos Fernandez-Pello

Chair, Dissertation Committee

To my parents, Tomás and Maria Amelia.

To Fernando, Mencía and Javito.

Table of Contents

Nomenclature

A_i	Preexponential factor of reaction i
A_{gs}/V	Surface area between gas and solid to volume ratio
A_L/A_c	Lateral to cross-sectional areas ratio
A_L/V	Lateral area to volume ratio
c_s	Specific heat of solid
c_{pg}	Specific heat of gas
d_f	Fiber diameter
d_p	Pore diameter
D	Diameter
D_{diff}	Mass diffusivity
Da	Damkohler number
e	Wall thickness
E_i	Activation energy of reaction i
h'''	Enthalpy per unit volume
Δh_i	Enthalpy of reaction i
hr	Heating rate
h_{in}	Convective Heat transfer in the foam
h_{gs}	Heat transfer coefficient between gas and solid
h_m	Mass transfer coefficient between gas and solid
K_i	Permeability of species i
k	Conductivity
l_m	Mean penetration distance
L	Sample length or Smolder-front characteristic length
L_t	Smolder-front characteristic thermal-length
L_c	Critical length
m_i	Mass of solid species i

m_0	Mass of solid at initial conditions
$\dot{m}''$	Mass flux
$\overline{MW}$	Average molecular weight
n_i	Reaction order on solid reactant of reaction i
P	Pressure
Pr	Prandtl number
$\dot{q}''$	Heat flux
Q	Global heat of smolder
R	Universal gas constant
Re	Reynolds number
t	Time
T	Temperature
u	Velocity
U	Global heat-loss coefficient
V	Total volume
V_{O_2}	Diffusivity velocity of oxygen
w_i	Mass of solid species i respect to initial solid mass
x	Spatial location
y_i	Mass fraction of species i in the gas

Greek symbols

α	Ratio of smolder-thickness to thermal-thickness
γ	Constant of relative influence in the fitness
δ	Smolder front thickness
δ_i	Reaction order on gas reactant of reaction i
$\dot{\theta}_j$	Non-dimensional reaction rate of reaction j
λ	Graetz number
$\nu_{j,i}$	Mass yield of species j per reactant in reaction i
ξ	Non-dimensional spatial location
Π	Non-dimensional temperature

ρ	Bulk density
ρ_0	Bulk density of the initial solid
$\tilde{\rho}$	Solid density
σ	Stephan-Boltzmann constant
ϑ	Specific volume
τ	Characteristic chemical time
ϕ	Porosity of the foam
Φ	Fitness of individual
$\dot{\omega}_i$	Reaction rate (per unit time) of reaction i

Subscripts

0	Initial or ambient environment conditions
c	Char solid species / Char oxidation reaction
calc	Calculations
cell	Cellulose solid species
cd	Conduction
cv	Convection
exp	Experimental
diff	Diffusion
f	Foam solid species
for	Forced
fwd	Forward propagation
g	Gas
gp	Gas products species
ig	Igniter or Ignition
loss	Heat losses to the external environment
L	Condition at $x = L$
m	Mean
oβ	β-foam oxidation reaction
o	Foam oxidation reaction
opp	Opposed propagation

O_2	Oxygen
p	Foam pyrolysis reaction
pβ	β-foam pyrolysis reaction
r	Residue solid species
s	Solid
su	Surface of pore
sml	Smoldering
β	β-foam solid species

Acknowledgements

We are like dwarfs sitting on the shoulders of giants. We see more, and things that are more distant, than they did, not because our sight is superior or because we are taller than they, but because they raise us up, and by their great stature add to ours.

John of Salisbury, The Metalogicon, 1159.

To Prof. Carlos Fernandez-Pello, who suffered innumerable times my difficult writing and thought my style was “as baroque as Cervantes’s style itself” (this was meant to be a protest). For giving me the opportunity of being his teacher assistant. For encouraging me to travel so much to present our work. For being a friend, an excellent mentor and a tough boss. Muchas gracias, Carlos, de veras.

To Prof. Jose Luis Torero (University of Edinburgh), my mentor and guide since the very fist moment I decided to do research in combustion back in 1999. He is in fact my second (non official though) advisor.

To Prof. Jyh-Yuan Chen, member of the committees of this thesis and of my qualifying oral exam in 2004. He encouraged me to start the application of genetic algorithms. To Prof. Stephens who served in my thesis committee and introduced me in the fascinating world of wildland fires.

I would not even have started the path of research if it were not for the guidance, help and wise advices of Prof. Janet Ellzey (University of Texas at Austin), my former B.S. advisor in 1999.

To Dr. Dave Urban (NASA) for the help and opportunities provided to the project. His inspiration and encouragement was especially crucial fostering the research on solid kinetics and the core of this thesis. The National Aeronautics and Space Administration financially and technically supported this research under NASA grant NAG3-2026.

To Prof. Robert Diddle, who chaired my qualifying oral exam and served in my Master's committee in 2003. He showed me through his example that it is possible to be very successful in academia at the same time as entertaining to peers. To Prof. Ömer Savas, who served in my qualifying exam and roused my enchantment for fluid dynamics. I would have never dare to read Batchelor's book if it were not for his excellent lectures. Prof. John Verboncoeur, who also served in my qualifying exam and taught me in his lectures about the quintessence of computational modeling.

The contents of this thesis have been presented in many meeting and conferences sponsored by The Combustion Institute and its Western States Section. These two institutions and the Graduate Division of UC Berkeley provided precious financial support for traveling expenses around the US and overseas.

To Dr. Alan Hindmarsh (Lawrence Livermore National Laboratory) who never met me personally but endured with tons of patience my multiple emails charged with questions about the VODE solver. I greatly appreciate his help.

To Norm Alvares (Fire Science Applications), who taught me so many things about happiness, professionalism and fire.

To the members of the mailing list of the International Association for Fire Safety Science, who share with us, and on a weekly basis, their enormous knowledge about fire.

Thanks to Prof. Colomba Di Blasi (Università di Napoli Federico II), Dr. Takashi Kashiwagi (NIST) and Dr. Thomas Ohlemiller (NIST), who without directly knowing it provided me with motivation to carry out this work and gave me plenty of first-class examples of how a good paper should be like.

Thanks to Prof. Christopher Chao (Hong-Kong University of Science and Technology), Prof. Michael Antal (University of Hawaii at Manoa) and Prof. Gabor Varhegyi (Hungarian Academy of Sciences) for providing very useful comments and thermogravimetric data.

Special thanks to my coworkers, Chris Lautenberger, Olivier Putzeys, Elizabeth Kallman, Amnon Bar-Ilan, Robin Titus and David Sadeli, true fountains of knowledge, quarrel and consensus, and always always of good help. To the open-ended and the one-and-only great officemate Dr. Mark Mikofski. To MaryAnne Peters (our Hesse advisor), Scott McCormick, Michael Neufer, Pete Graham, for their kindness and friendship, and especially for making Hesse Hall an even better place. To my colleagues David Rich, Andrea Ronza, Jorge Sendagorta, Bennett Sprague, Dr. David Walther, Kelvin Fu, Jaime Herren, Sang-Won Park, Ronda Ropes, Andreja Stevanovic, Sonia Fereres, Nina Bjerkebo, Shivani Metha, Kevin Macko, Yoshifumi Tsuji, Tomomi Ohnishi, Thomas Lo, Aaron Knobloch and Jorge Hernández.

To Dona Craig, Anayancy Paz and Pat Giddings for their vital assistance to survive the Mechanical Engineering Department.

To the best team of reviewers I could asked for: Norm Alvares, Maria Vu, Rebecca, Rebecca again (she read two chapters), and half Dottore Alessandro Pinto.

To Terminator whose signature in my degree could potential make it be worth more.

A Chema, evidentemente, por hacer cada día que 1807 Addison fuera nuestra casa y con quien aprendí las mercedes de la democracia. A Alex, Rubén, Maud, Tanja, Rafa, Katya, Lou, Rebecca (claro que sí), Dorothea, Larissa, Marianna (Dottoressa Belloc), Eran, Leticia, Pistachito, Pinto, y a todos los amigos que encontré en Berkeley. A Jorge, Beita, Luis, Eloy, Moisés, Alba, Javi, Alberto, Víctor, Curra, a todos los amigos que no me olvidaron (sin casi casi yo merecerlo). A Casacostus por eliminar las distancias. A Melquíades por dar a conocer nuevos inventos.

A Fernando, que está a puntito de nacer, a Mencía que hoy tiene menos de un mes y a Javito que cumple un año en breve.

A Tomi, a Belén, a Carla, a papá y mamá, porque me escapé de casa para escribir esto.

Chapter 1

Introduction and Background

"saw a likeness between the two, and he felt the strain between them, almost as if he saw a line of smouldering fire, drawn eye to eye, that might suddenly burst into flame".

The Return of the King, John R.R. Tolkien (1892-1973).

1.1 Overview of Smoldering Combustion

Smoldering phenomenon is a flameless form of combustion, deriving its heat from heterogeneous reactions occurring on the surface of a solid fuel when heated in an oxidizer environment (Ohlemiller 2002). It is of interest both as a fundamental combustion problem and as a practical fire hazard. Common examples of smoldering combustion are the initiation of upholstered furniture fires by weak heat sources and the persistent combustion of biomass occurring in wildland fires behind the flaming front.

The fundamental difference between smoldering and flaming combustion is that in smoldering, oxidation of the reactant species occurs on the surface of the solid rather than in the gas phase. The characteristic temperature and heat released during smoldering are low compared to those in the flaming combustion of a solid. Typical values in smoldering are around 600 °C for the peak temperature and 5 kJ/g-O_2 for the heat released (Ohlemiller 2002); typical values during flaming are around 1500 °C and 13 kJ/g-O_2 respectively (Drysdale 1999). These characteristics make smolder to propagate at low velocities, typically around 0.1 mm/s, which is about two orders of magnitude lower than the velocity of flame spread over a solid. In spite of its weak-combustion characteristics, smoldering is a significant fire hazard. Smoldering can be initiated by weak sources of heat; yields a high conversion of fuel to toxic products per unit mass smoldered (particularly CO and heavy molecules); is difficult to detect and extinguish; and it can abruptly transition to flaming combustion.

Many materials can sustain a smoldering reaction, including coal, cotton, tobacco, paper, duff, peat, wood and most charring polymers. In general, a smolder fuel consists of an aggregate and permeable medium formed by particulates, grains, fibers or a porous matrix. These aggregate fuel elements facilitate the surface reaction with oxygen by providing a large surface area per unit volume. They also act as thermal insulation that reduces heat losses but, at the same time, permit oxygen transport to the reaction sites by convection and diffusion. From the chemical point of view, smoldering leaves behind a significant amount of solid combustible char and generates flammable and toxic gas

products. This char is considerably richer in carbon content than the original fuel and has a high enthalpy of oxidation (Ohlemiller 1985). As a result, char oxidation represents an important source of heat release in smoldering. Hence, it is considered that any material that forms char during thermal decomposition can potentially sustain a smoldering process (Ohlemiller 2002). The combustion reaction in smoldering is characteristically incomplete and so it emits toxic gas compounds at a higher yield than flaming fires. These gas compounds are also flammable and could later on be ignited in the gas-phase, triggering the transition from smoldering to flaming.

From a fundamental point of view, smoldering is a basic combustion problem involving heterogeneous chemical reactions, and the transport of heat, mass and momentum in the gas and solid phases. Smoldering initiation requires the supply of heat flux to the solid fuel. The subsequent temperature increase of the solid triggers its thermal-degradation reactions (endothermic pyrolysis and exothermic oxidation) until the net heat released is high enough to balance the heat required for propagation. This net heat released by the reactions is partially transferred by conduction, convection and radiation ahead of the reaction and partially lost to the surrounding environment. The oxidizer is transported to the reaction zone by diffusion and convection, in turn feeding the oxidation reactions. Once ignition occurs, the smolder reaction propagates through the material in a creeping fashion. It has been observed that for most materials and typical conditions, the two limiting factors in smoldering propagation are the oxidizer flux to and the heat losses from the reaction zone (Ohlemiller 1981).

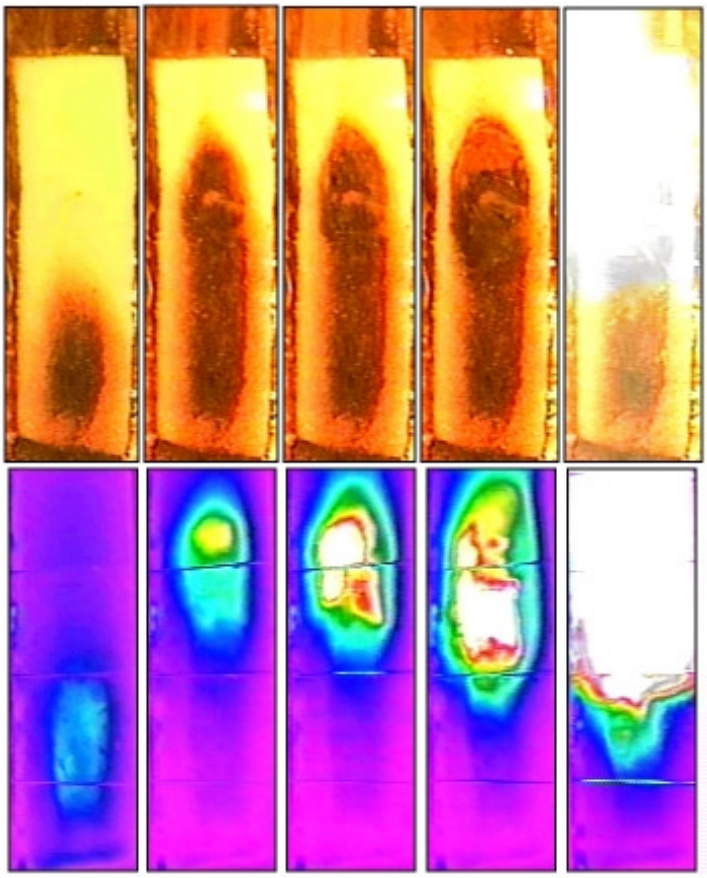

Figure 1.1: Snapshots of the transition from smoldering to flaming in a 50x125 mm polyurethane foam sample (Bar-Ilan *et al.* 2005); (top) visible imaging; (bottom) infrared imaging.

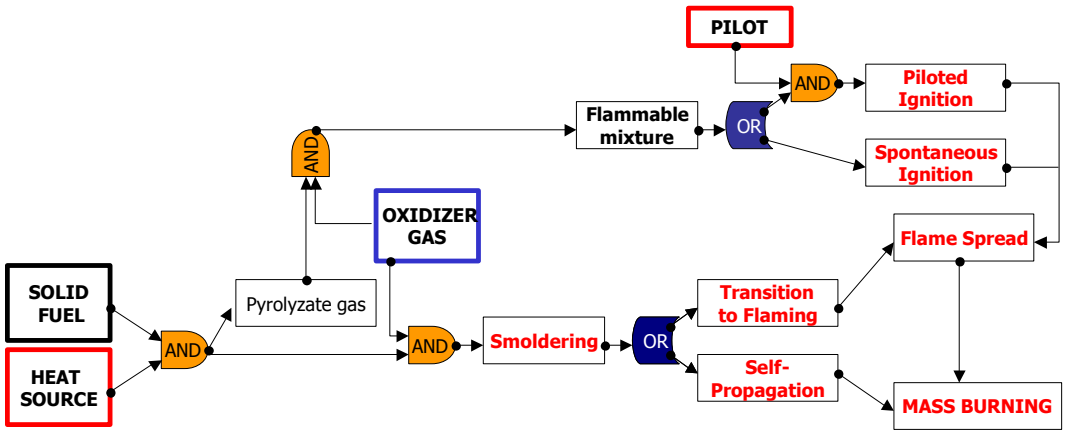

Figure 1.2: Flowchart for identification of possible fire scenarios from a heated solid

The transition from smolder to flaming is a spontaneous gas-phase ignition supported by the smolder reaction which acts both as the source of gaseous fuel (pyrolyzate, CO, etc.) and of heat to carry the reaction. Fig. 1.1 shows snapshots of smoldering propagation and the eventual transition to flaming of a polyurethane foam sample exposed on its free surface to a radiant heat-flux. The transition occurs eventually when critical conditions inside the pores of the solid are met, triggering the onset of gas-phase reactions. The critical conditions include the flammability of the gas mixture inside the pores and a net excess of heat released by strong solid-phase oxidation reactions. The heat flux needed to attain smoldering ignitions is significantly lower than that for flaming ignition. For instance, smoldering ignition of polyurethane foam in air atmospheres has been reported to occur with a heat flux of 2 kW/m^2 using a contact heater (Walther *et al.* 1999), while direct flaming ignition with a radiant heater occurs only above 8 kW/m^2 (Grexa *et al.* 1996). Thus, the transition from smoldering to flaming combustion provides a hazardous shortcut to flaming fires, which could be initiated with heat sources that are too weak to directly ignite a flame on the solid fuel. Figure 1.2 shows a basic flowchart for possible fire scenarios originating from a heated solid. It highlights the similarities and divergences between smoldering and flaming combustion of a solid.

When studying smolder propagation through the interior of combustible materials, it is common to consider the simpler one-dimensional process and to classify it in two main configurations; opposed and forward propagation. These are defined according to the direction in which the smolder reaction propagates relative to the oxidizer flow (Fig. 1.3); in opposed smolder, the reaction front

propagates in the direction opposite to the oxidizer flow, and in forward smolder, the front propagates in the same direction. A common case of forward smolder is a burning cigarette being puffed. The equivalent opposed case would imply the rare situation of a burning cigarette being blown.

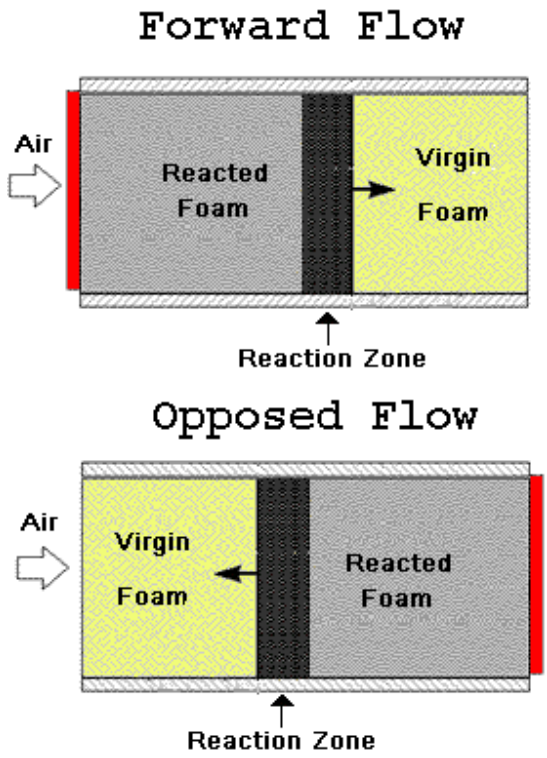

Figure 1.3: Configurations in one-dimensional smoldering (in a porous foam): forward and opposed.

These two configurations are distinguished by the roles played by the transport mechanisms and chemical reactions (Ohlemiller and Lucca, 1983). In forward propagation, the fresh oxidizer flows through the char, reacts at the smolder zone and then the oxidizer-depleted flow goes through the virgin fuel. This configuration favors that the oxidation reactions occur at the rear of the

smolder zone and pyrolysis at the front. Convective transport is in the direction of the virgin fuel ahead, preheating it before the smolder zone arrives. In opposed propagation, the fresh oxidizer flows through the virgin fuel and reacts at the smolder zone favoring that both the oxidation and the pyrolysis reactions occur at approximately the same location. Convective transport is in the direction of the char behind the front, reducing the preheating of the fuel.

In two- and three-dimensional propagation, the classification of all the possible configurations becomes too complicated, but in general terms the same classification can be applied considering only the principal direction of propagation and the principal direction of the oxidizer flow.

1.2 Analysis of Smoldering Propagation

A global energy balance at the smolder front yields a simple mathematical representation of the propagation and serves to quantify the controlling mechanisms involved in the process. In a control volume that contains the smolder front, the propagation rate is determined by the balance among the heat released per unit mass of oxygen reacted, the energy required to heat the virgin fuel and the incoming air to the smolder temperature, and the heat losses to the environment. Assuming that all oxygen is consumed, the application of such an energy balance into mathematical terms provides the following expression for the smoldering propagation velocity in opposed configuration (Dosanjh *et al.* 1987, Bar-Ilan *et al.* 2004):

$$u_{sml} = \frac{\dot{m}''_{O_2} Q_{sml} - \dot{m}''_g c_{pg}\left(T_{sml} - T_0\right) - \dot{q}''_{loss}\,{}^{A_L}\!/_{A_c} + \dot{q}''_{ig}}{\rho_s c_{ps}(1-\phi)\left(T_{sml} - T_0\right)} \tag{1.1}$$

The heat transferred from the igniter $\dot{q}''_{ig}$ can be neglected when studying self-sustained smolder because the propagation occurs away from the igniter influence. For the typical range of gas velocities, the energy required to heat the incoming airflow to the smolder temperature ($\dot{m}''_g c_{pg}\left(T_{sml} - T_0\right)$) is small in comparison with the other energy terms. Consequently, in the above expression, Eq. (1.1), the two major terms determining the smolder propagation velocity are the heat released by the reaction ($\dot{m}''_{O_2} Q_{sml}$) and the heat losses to the external environment ($\dot{q}''_{loss}\,{}^{A_L}\!/_{A_c}$). The coefficient ${}^{A_L}\!/_{A_c}$ multiplying the heat losses term expresses the ratio of the lateral area to the cross-sectional area at the smolder front. The properties of the solid ($\rho_s c_{ps}(1-\phi)$) only scale the magnitude of the velocity. Then, considering only the major terms, Eq. (1.1) simplifies to:

$$u_{sml} = \frac{\dot{m}''_{O_2} Q_{sml} - \dot{q}''_{loss}\,{}^{A_L}\!/_{A_c}}{\rho_s c_{ps}(1-\phi)\left(T_{sml} - T_0\right)} \tag{1.2}$$

According to Eq. (1.2), the propagation velocity in the oxidizer-limited regime is linearly proportional to the mass flux of oxidizer, as it has been verified experimentally (Rogers and Ohlemiller 1980, Torero 1993, Bar-Ilan *et al.* 2004b). It is seen in Eq. (1.2) that the effect of the heat losses to the external environment is to hamper smoldering propagation. The heat losses term includes the effect of the size of the fuel sample through the ration ${}^{A_L}\!/_{A_c}$. This ratio reflects that heat loss is proportional to the surface area whereas heat generated is proportional to

the volume. As the sample is made smaller, the ratio A_L/A_c increases, and the effect of the heat losses increases until smolder propagation cannot occur below a critical size. The critical size for smoldering propagation can be analyzed by making Eq. (1.2) equal to zero (limit of no propagation). For a sample of square cross-sectional area, side length L and smolder-zone thickness δ, the ratio A_L/A_c becomes equal to $4\delta/L$. The flux of heat losses can be expressed as the function of a global heat-losses coefficient U_{loss} and the temperature gradient with the exterior. Then, setting u_{sml} to zero and rearranging the expression, the critical sample size L_c is expressed as:

$$L_c = \frac{4\delta}{Q_{sml}} \frac{U_{loss}(T_{sml} - T_0)}{\dot{m}''_{O_2}} \tag{1.3}$$

The expression Eq. (1.3) can be used to provide an estimate of the critical size. The smolder-zone thickness δ, the smolder temperature T_{sml} and the heat of smolder Q_{sml} depend on the smoldering properties of the fuel. For example, for polyurethane foam the required parameters are available from Bar-Ilan *et al.* (2004) and yields the critical size L_c of 160 mm. Experimental studies of smoldering (Torero and Fernandez-Pello 1995) indicate that the critical size for rectangular polyurethane foam samples under natural convection is 150 mm. Thus, for a polyurethane-sample which size is below this critical value, achieving self-sustained smoldering requires the reduction of the heat losses or the increase of the heat generated, or both. The former can be accomplished by

thermally insulating the sample and the latter by increasing the oxidizer flux (Bar-Ilan *et al.* 2005, Putzeys *et al.* 2005).

1.3 Chemical Kinetics

As shown above, the propagation rate of self-sustained smoldering is typically controlled by oxygen transport and net heat losses. Yet, heterogeneous chemical kinetics governs the front structure and dictates the effective value of the global heat of smolder $\mathrm{Q}_{\mathrm{sml}}$. Chemical kinetics is particularly important for the kinetically controlled regimes of ignition, extinction, and the transition to flaming. In addition to the thermophysical aspects of smoldering, kinetics are also ultimately responsible in determining under what conditions a material ignites and smolders (and thus poses a hazard). Proper understanding and modelling of the process require information on the heterogeneous reactions taking place in the solid.

Established and quantified kinetic mechanisms of smoldering solids are not readily available in the literature. The degradation of a solid involves complex pathways to chemical and physical changes, and these pathways are not yet fully understood. Most of the studies on solid thermal-decomposition do not provide all the information needed to understand smoldering combustion. They usually focus on thermal-decomposition by pyrolysis only and provide a kinetic scheme of degradation not complete for oxidative environments. Furthermore, conventional mechanisms do not describe well smoldering in its different

propagation modes, and as a consequence different mechanisms are used for each propagation mode (Dosanjh *et al.* 1987, Dosanjh and Pagni 1987).

The polymer for which smoldering kinetics are known the best is cellulose. The thermal degradation of cellulose is now established and quantified (Kashiwagi and Nambu 1992, Grønli *et al.* 1999). More work is needed for other smoldering fuels. A kinetic mechanism that has been most frequently used for general polymeric fuel is the three-step chemical-reaction scheme, proposed by Ohlemiller (1985). The reduced mechanism, based on the degradation kinetic of cellulose, describes the major chemical and heat effects occurring at the smoldering front. It includes fuel pyrolysis, fuel oxidation and char oxidation, accounting for three solid species; fuel, char and ash.

The application of Ohlemiller's mechanism to smoldering has been found to give acceptable results with some polymers, like cellulose (Di Blasi 1995, Leach *et al.* 1997) and polyurethane (Leach *et al.* 2000, Rein *et al.* 2005, Kelley and Schult 2006), although the main problem lies in the quantification of the kinetic parameters for the solid fuels of interest. It is customary to assume that each one of the reaction paths has an Arrhenius-type reaction rate, which general form is:

$$\dot{\omega}_i = A_i e^{-\frac{E_i}{RT}} \left(\frac{W_i}{W_0} \right)^{n_i} y_{O_2}^{\delta_i} \tag{1.4}$$

Each solid fuel would kinetically behave differently and the kinetic parameters expressed in Eq. (1.4) for each reaction need to be determined for every fuel of interest. Determining these parameters is usually accomplished using experimental data, especially thermogravimetric analysis. However, the procedure is of considerable difficulty due to the high complexity of solid

thermal-decomposition. In this work a methodology to obtain a reduced mechanism of smoldering combustion is developed and tested (see Chapter 3).

1.4 Smoldering Episodes

On the practical side of the problem posed by smoldering fires, two groups of fuels have received the most attention. Polyurethane foams and cellulosic fabrics are one group. They are investigated due to their hazard to residential fire-safety as upholstery and bedding materials. Smoldering fires are the leading cause of fire deaths in the United States (Hall 2004), probably with similar figures in most other developed countries (Brereton and Laing 1992). The other group of smoldering fuels receiving attention consists of forest biomass, like duff and wood logs. They are of interest due to their considerable prevalence in wildland fires. In wildland fires, smoldering combustion has a great impact, being responsible for a large amount of the fuel consumed and the pollutants emitted (Fransden 1991).

1.4.1 Smoldering Combustion in Fire Safety

Fire statistics draw attention on the magnitude of smoldering fires as the leading cause of fire deaths (Hall 2004). More than 25 % of the annual fire-deaths in the United States are attributed to smoldering-initiated fires, both due to a sudden transition from smoldering to flaming and a higher conversion

to toxic species. During 2001 alone, there were an estimated 31,200 smoldering fires in structures, and $386 million in property damage (Hall 2004). A fire-initiation scenario that is particularly common is when a cigarette ignites by smoldering a piece of upholstered furniture. Then cigarette can lead to a smoldering fire that lasts for a long period of time (could be hours), spreading slowly until critical conditions are attained and flames suddenly erupt.

Smoldering combustion is a fire-safety concern in space-flight programs (see section 1.5 “Smoldering in the Absence of Gravity” of this chapter). Incidents involving smoldering in the air-transportation industry are also of concern. One example is the 1998 Swissair flight 111 aircraft fire (Fiorino 2003) which appears to have been caused by faulty wiring that ignited an adjacent Mylar insulation sheathing, probably through smolder initiation and subsequent transition to flaming.

Smoldering intrinsically emits products of incomplete combustion. The yield of carbon monoxide is significantly higher although emitted at a smaller rate than in flaming fires, and other gas toxic compounds only increase this risk. The studies of Hilado *et al.* (1979) with mice addressed the lethal toxicity of smoldering gases from a wide range of polymers. Mice in a 244-liter animal chamber were exposed to the smoldering gases of an 80x20 cm piece of upholstery. With cotton fabric and polyurethane foam cushion, 12% of the mice died in the 90 minutes of the experiment and an additional 40% died in the following 14 days after the exposure was discontinued. With cotton fabric and cotton cushion, all the mice died during the first 35 minutes of experiment due

to carbon monoxide poisoning. Quintiere *et al.* (1982) studied the hazard to humans of smoldering fires in enclosure due carbon monoxide. They determined that life-threatening conditions from CO doses occurred in most cases in the 50-150 minute range of the experiment. They also noted that the time to transition to flaming occurred within the same time window.

The ability of standard smoke detectors to activate in the presence of a smoldering source is undermined by two characteristics of smoldering products. In general, smoke detectors are located near the ceiling of an enclosure because the hot products of combustion move there due to the buoyant natural ventilation. The typical low magnitude of the heat-released rate by smoldering implies that in its weak plume the gases of combustion are cooled sooner than gases from a flaming fire, and therefore depend strongly on the enclosure's forced ventilation. Thus, it takes longer to move to the ceiling height (Hotta *et al.* 1987, Watanabe and Tanaka 2004). As a result, smoldering fires could take considerably longer times to be detected by conventional detectors if the forced ventilation is not taken into account when placing them. Another issue is that the size of the smoke particulates and their spatial distribution in the smoke plume from a smoldering source varies greatly from flaming fires, and this forces the detectors to require a different calibration to be triggered, especially the ionization ones (Meacham and Motevalli 1992, Mulholland and Ohlemiller 1982).

There are several works in the literature addressing the effect of fire retardants on flaming vs. its effect on smoldering. Some suggest that fire retardant treatments to reduce flame ignition also reduce smoldering ignition

(Wakelyn *et al.* 2005). However, it has been observed often that materials with good resistance to flame ignition have poor resistance to smoldering ignition and vice versa (Rogers *et al.* 1978, Chao and Wang 2001a, Wang *et al.* 2004, Wakelyn *et al.* 2005). Inhibition of smoldering combustion requires very different types of chemical retardant mechanisms than those required for inhibition of flaming combustion. The analysis by Chao and Wang (2001a) with polyurethane foams shows that flame-retarded foams transition to flaming in a wider range of conditions than non flame-retarded foam do, primarily due to the higher yield of char of the former (Chao *et al.* 2001b). Wang *et al.* 2004 studied wood ignition and showed that Borax tends to reduce flame spread but promotes smoldering, conversely boric acid suppresses smoldering but has little effect on flame spread. This conflictive interaction of current flame-retardants with smoldering and flaming ignitions poses a dilemma in fire safety and requires further research.

In spite of its prevalence in fire safety, smoldering receives relatively little attention from the fire sciences community. A possible explanation for this fact is that the menace of smoldering fires generally originates from the objects inside a building rather than the building itself; thus, it is perceived as a consumer product oriented issue and not a building code issue.

1.4.2 Smoldering Combustion in Forest Fires

Smoldering combustion of the forest ground does not have the visually dramatic impact of flaming combustion. However smoldering is an important component of forest fires since it might result in the transition to flaming and also cause the killing of roots, seeds and plant stems at the ground surface. Smoldering of forest biomass can linger for days or weeks after flaming has ceased, resulting in large quantities of biomass consumed and becoming a globally significant source of emissions to the atmosphere. Biomass fuels prone to smolder during wildfires are stumps, snags, downed logs and large branches, duff, roots and organic soils. These fuels are characterized by having a significantly greater thermal time than fine fuels; characteristic that favors the slow burning of smolder combustion. In forests where large quantities of fuel prone to smolder are present on the surface and the ground, the majority of the energy released is by smoldering combustion.

Smoldering is responsible for a significant fraction of the total fuel consumed during a wildfire. It has been reported that smoldering can consume around 50% or more of the total burned biomass in temperate and boreal fires (Fransden 1991, Bertschi *et al.* 2003), and in Amazonian tropical-woodland fires (Kauffman 1998). Bertschi *et al.* (2003) and Rabelo *et al.* (2004) report consistently high fuel-consumption fractions by smoldering. Smoldering of forest fuels is also responsible for a significant fraction of the total pollutants emitted into the atmosphere during a wildfire. Bertschi *et al.* (2003) studied the emissions from smoldering biomass fuels and calculated the emission from real

wildfires. Based on their results and compared to the emissions from the flaming phase of a tropical savanna fire, smoldering produces 130% more CO and 670% more hydrocarbons, but 15% less CO_2 and no NOx. Compared to the emissions from a boreal fire, smoldering produces 30% more CO and 20% more hydrocarbons, but 13% less CO_2 and no NOx. Many smoke management problems in the US associated with prescribed fires involved smoldering emission (Hardy *et al.* 2002).

Duff (layer of partly decayed, organic matter on the soil surface) consumption is mostly determined by the smoldering phase while the flaming phase has significantly lesser impact. In general terms, flaming fires produced substantial flame lengths but minimal heating to the surface, as compared to smoldering combustion which produces many times longer duration heating, and reaches lethal temperatures at the surface (Hartford and Frandsen 1992). The longer duration and the higher heat transferred to the forest floor by smoldering has been identified as an important factor in fire mortality together with damage to tree crowns (Stephens and Finney 2002). In the organic layers of the ground, the smolder front propagates downward and laterally consuming the fuel (Fig. 1.4). The front structure is similar to a forward-smoldering configuration: the drying and the pyrolysis fronts move ahead of the oxidization front which stays in contact with the oxygen in the open air. Smolder can also propagate inside wood logs (Fig. 1.5).

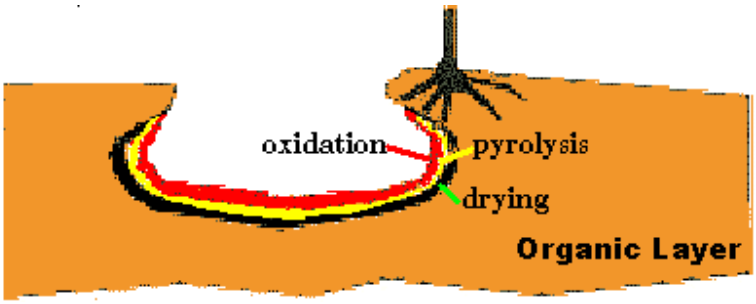

Figure 1.4: Spread of a smoldering ground fire (after Frandsen 1997).

Figure 1.5: Cavity left by smoldering inside a log (Costa and Sandberg 2004, reproduced with permission).

The moisture and the organic content have been identified as the main controlling parameters for smolder ignition of biomass. Frandsen (1997) determined that the smolder-ignition limits of peat moss mixed with mineral soil are a moisture content lower than 110% (on a dry base) and an organic content lower than 82%. Contents higher that these would result in no ignition of the moss. The strong dependence of spatial duff-consumption by smoldering on moisture content was studied by Hille and Stephens (2005), and Miyanishi and Johnson (2002). They found a strong correlation between higher duff consumption and distance from the base of the tree, because crown cover

reduces the rainfall on the duff beneath tree crowns and it is drier. The geometry of the fuel is also important because it determines the ratio between heat generated and heat lost to the surroundings. For instance, fuel geometry effects are observed (Rabelo *et al.* 2004) when smoldering of wood logs is favored in configurations, such as where logs cross each other (reduced heat losses), logs in contact with the ground (reduced heat losses) or inclined logs (increased buoyant preheating and oxidizer flow).

The transition to flaming is also observed in forest fires. Logs can naturally burn for long periods of time oscillating between flaming and smoldering combustion after the flame front has passed (Rabelo *et al.* 2004). Smoldering can also re-ignite previously extinguished wildfires. This mechanism is believed to have contributed to the ignition of the 1991 Oakland Hills Fire, California (Pagni 1993). The fire destroyed nearly 2000 homes and caused up to $10 billion in damages. Smoldering is as well related to the hazard of smoldering embers in wildland fires. These embers are lofted by the fire plume and transported some distance away from the originating fire front (Anthenien *et al.* 2005). Once landed, the hot ember could ignite a smoldering fire on dead forest fuels, underbrush or grass and later produce a new fire front.

Worth noting is that there exist in wildland fire management, a beneficial use of smoldering combustion. In prescribed fires aiming to reduce the load of ground fuels, smoldering is useful in some cases due to the ease to control its propagation (Biswell 1989). If the duration of the burning time is kept low, smoldering is of lower severity to the ecosystem.

1.4.3 Other Smoldering Episodes

Underground fires occurring many feet below the surface are another type of smoldering events of natural and anthropologic causes (Prakash 2005). Underground fires (Fig. 1.5) in coal mines, peatlands and landfills are rare events but when active they can smolder for very long periods of time, emitting enormous quantities of combustion products into the atmosphere and causing deterioration in air quality and health problems (Page *et al.* 2002, Stracher and Taylor 2004). Some of the oldest and largest coal fires in the world occurred in the United States and India, but it is especially in China where they have been more intense and some have been burning for several centuries now. These fires are fed by small but continuous quantities of air flowing through fractured strata, cracks, openings or abandoned mines shafts, which permits oxidizer to circulate into the subsurface. The reduced heat losses and the high thermal inertia of the underground, together with the high fuel availability and the small oxidizer flow promote long-term smoldering combustion and allows for creeping but extensive propagation both in depth and in area. These fires prove difficult to be detected and frustrate most efforts to be extinguished.

There are several well-documented cases of underground smoldering. In 1962, an abandoned mine pit in Centralia, Pennsylvania (USA) was accidentally lit. Several unsuccessful attempts were made to extinguish it, but the fire continues to burn after more than forty years. It is currently being monitored with the front advancing approximately 20 m/year (Nolter and Vice 2004). Underground smoldering was also greatly involved in the 1997 occurrence of

widespread fires throughout the peatlands of Indonesia (Page *et al.* 2002), which produced a dense haze that blanketed a large part of Southeast Asia. During the *El Niño* dry season of 1997, many peat fires spread out of control, emitting an equivalent to 13-40% of the mean annual global carbon emissions from fossil fuels, and contributed greatly to the largest annual increase in atmospheric CO_2 concentration ever measured. During 2005 the state of Colorado (USA) reported more than 30 actives underground fires in coal mines (Renner 2005), involving 2% of the total number of known abandoned coal mines.

Figure 1.5: Collapse of a smoldering wall during a coal mine fire, Northern China. (©Anupma Prakash, Geophysical Institute, UAF, reproduced with permission).

Smoldering combustion has a few beneficial applications besides the aforementioned one in prescribed wildland fires. Smoldering of tires is employed for tar production, fostering the recycling of tires and partially avoiding their waste (Vantelon *et al.* 2005). In-situ combustion of petroleum sites is becoming more often used for oil recovery when traditional-extraction methods become inefficient or too costly (Akkutlu and Yortsos 2003). The most recent beneficial application of smoldering is that of remediation of contaminated soils (Torero and Gerhard 2005), which is currently under research and development.

1.5 Smoldering Combustion in the Absence of Gravity

Smoldering combustion intrinsically involves the production of high-temperature gases whose low densities trigger buoyant motion under a gravity field. Thus buoyancy-induced flows increase the convective transport of heat and mass in the direction opposite to the gravity field. Gravity affects both primary controlling mechanisms of self-sustained smoldering, oxidizer supply and heat losses. In a gravity field, convective heat losses are increased by buoyancy thus hindering smoldering. The buoyant mass-flux could hinder smoldering in the downward propagation, but it promotes smoldering in upward propagation. In absence of gravity, these natural buoyant flows are not established and only diffusion or forced convection exists.

The importance of studying smoldering in the absence of gravity (microgravity) is three-fold: fire safety in space facilities, fundamental research under simplified flow conditions, and as an ideal benchmark to test theories.

There is a founded and strong concern for an accidental fire occurring in a space-based facility (Palmer 1989, Faeth 1989). In the closed environment of a spacecraft or extraterrestrial base, with no avenue for escape, a fire is greatly to be feared (Friedman 1998). Should a fire occur in a space facility, there is a strong probability that it would be a smolder-originated fire (T'ien *et al.* 2001). The Space Shuttles have registered on average one charred-cable incident for every ten missions (Paulos *et al.* 1994, NASA 2003). A charred cable is symptomatic of smolder-prone conditions and could lead to sustained smoldering or ignition of nearby fuels. Also the MIR orbital station and other Russian/USSR spacecrafts suffered several smolder-related incidents (Oberg 2001). The impact of smoldering during a space mission is also critical from the points of view of its impact on the environmental health to the astronauts (Irons *et al.* 1994) and the difficulty to detect and extinguish a smoldering fire (Weinberg *et al.* 2003). These topics need to be assessed in the context of long-term space habitation. With the currently orbiting International Space Station and future long-term missions (*i.e.*, mission to the Moon and Mars), there is an increased interest in the study of smoldering in reduced gravity because of the need to pre-empt the possibility and to minimize the effect of a smolder-initiated fire during the operation of a space-based facility. Thus, it is of great interest to understand and characterize the smoldering behavior of materials used in these facilities under the expected ambient conditions.

Research on microgravity combustion is also of importance because it offers a unique capability for experimentalists to establish an ideal flow environment and to extend the range of test conditions that can be studied (*i.e.*, low-velocity flows, low heat losses, purely diffusive transport regimes, etc) (Law 1994, King and Ross 1998). Buoyant flows complicate the execution and interpretation of experiments on Earth, since buoyant motion triggers also the onset turbulence and unsteadiness. Absence of gravity allows the development of new insights into the fundamental phenomena of smoldering combustion.

Furthermore, microgravity environments provide ideal benchmark cases against which existing theories and new theories can be tested (King and Ross 1998). These theories often neglect buoyancy effects and/or assume one-dimensional flow in situations where in reality buoyant effects induce two- or three-dimensional behavior. Microgravity continues to offer the unique ability to test truly one-dimensional flow experiments in combustion science. A numerical model of smoldering in microgravity does not need to model the buoyant transport of heat and mass inside the porous fuel and thus is simpler and needs fewer assumptions.

1.6 The Current Contributions

The objective of this work is to develop a mathematical model of smoldering ignition and propagation. Modeling of smoldering combustion is of particular interest because of its potential use for estimating smolder-ignition resistance,

production rate of toxic species and conditions for transition to flaming, as well as for forensic reconstruction. It also provides a cost-effective alternative to experiments when testing is too costly, such as in microgravity conditions. In this work, emphasis is given to polyurethane foam (PU) as the fuel. PU is selected because in addition to its major importance in fire-safety, there is a large amount of experimental data on its smoldering behavior. Moreover, the only smoldering experiments conducted to date in microgravity conditions used PU as fuel.

The governing equations for smolder combustion in a porous fuel have been derived. The transient behavior of the process is studied in different configurations, and the boundary and initial conditions are set to mimic the existing experimental setup in order to allow for the comparison with the available experimental results. But the computational model requires the chemical mechanism and the kinetic parameters of the reacting porous fuel, and available studies on polyurethane thermal-decomposition do not provide all the information needed for models of smoldering combustion. Furthermore, conventional mechanisms of PU foam do not describe sufficiently well smoldering in its different propagation modes. This work proposes the application of the efficient multidimensional optimization technique of genetic algorithms to the extraction of the parameters from thermogravimetric experiments. The computational study tests these kinetic mechanisms simulating the ignition and propagation of smoldering combustion in polyurethane and then comparing the results with the experiments.

The current contributions summarized and organized by chapters are:

- Chapter 1. Evaluation of the prevalence and consequences of smoldering combustion on fire safety, wildland fires and microgravity environments.
- Chapter 2. Literature review of the state of the art of: mechanisms of smoldering combustion, smoldering of polyurethane foam, chemical kinetics of solid thermal-degradation, numerical models of smoldering, microgravity research, and transition to flaming.
- Chapter 3. Development and test of a methodology to obtain reduced mechanisms of smoldering combustion for application in computer models using thermogravimetric experiments of polyurethane. Extraction of the kinetic parameters for Ohlemiller's 3-step mechanism and proposition and validation of a new 5-step mechanism with its corresponding parameters. Using a simple mass-species conservation model of smoldering combustion, the 5-step mechanism is seen to be valid to model smoldering behavior in both opposed and forward propagation.
- Chapter 4. One-dimensional modelling of forward smolder combustion in polyurethane foam. Test the new kinetic parameters for Ohlemiller's 3-reaction mechanism for polyurethane foam (from chapter 3). Calculation and inclusion into the model of the heat losses to the external environment. Used the experimental results from microgravity experiments to validate the results and calibrate the unknown parameters.
- Chapter 5. One-dimensional modelling of opposed and forward smoldering combustion in polyurethane foam. Further develop the

theoretical framework of smoldering combustion in a porous medium. Test the new 5-reaction mechanism for polyurethane foam with the kinetic parameters (from chapter 3). Used the experimental results from microgravity experiments to validate the results and calibrate the unknown parameters.

- Chapter 6. Conclusions of the this thesis.

Chapter 2

Literature Review

"A case can be made for fire being, next to the life processes, the most complex of phenomena to understand"

Hoyt Hottel (1903-1998).

2.1 Fundamentals of Smoldering Combustion

The following section is a literature review of the most important studies available about the fundamental mechanisms of smoldering combustion that are relevant to the objective of this thesis. Emphasis is given to smoldering combustion of polyurethane (PU) foam. Other reviews on smoldering can be found in Ohlemiller (1985), Torero (1993), Walther (1998), Ohlemiller (2002) and Bar-Ilan (2004).

Ohlemiller (1985) presented a review of the most significant mechanisms involved in smoldering combustion of polymers. The study focuses on the

coupled chemical and physical processes involved in self-sustained propagation of smoldering. The main sources and sinks of heat are identified and examined. Three heat sources: virgin polymer oxidation, char oxidation, and gas-phase oxidation. And two heat sinks: virgin polymer pyrolysis and water vaporization. He presented the general equations as functions of about 50 dimensionless groups. He concluded that at that time (1985), the chemical mechanisms involved in these processes were too complex and too poorly understood to be included in a smolder propagation model, and that the general smoldering case is too complex to be tractable. The current state of the art in numerical models of smoldering combustion has improved significantly since 1985 as can be seen in Leach *et al.* (2000), and chapters 4 and 5 of this thesis. In a more recent publication, Ohlemiller (2002) gives at the same time an introduction and an excellent review to smoldering. The paper stands a one of the critical references in the field. He addresses the fire hazard, the basic mechanisms, the controlling variables, the possible configurations and the transition to flaming. He also collected and summarized the most important experimental results available for many different smoldering fuels. Ohlemiller and Lucca (1983) compared experimentally the essential differences between forward and opposed propagation. They concluded that whereas both modes of propagation are ultimately limited by oxygen transport, there are marked qualitative and quantitative differences between them. Opposed smolder reaches a steady propagation speed determined mainly by heat transfer. Forward smolder propagation is unsteady and moves at a lower rate, probably limited by the stoichiometry of the oxidations.

Torero *et al.* studied opposed (Torero *et al.* 1993) and forward (Torero and Fernandez-Pello 1996) forced-flow, and natural convection (Torero and Fernandez-Pello 1995) smoldering combustion of PU. These studies provided a great understanding of the controlling mechanisms of smoldering combustion and solid verification of simple heat-balance models of the process. Buoyancy was observed to affect the propagation especially at low mass-fluxes and to depend on the sample length as a consequence of the pressure drop along the porous sample (see section 2.4 for more on Torero *et al.*).

Walther *et al.* (2000) studied the ignition of smoldering of PU with forced flow. Their experiments include both forward and opposed configurations, with variable flow velocities and oxygen concentrations. Their results show a well-defined smoldering ignition regime, which is primarily determined by the igniter heat-flux and the exposure time. Their ignition map spans from a heat flux of 2.5 kW/m^2 with a 3000 s exposure time, to over 9 kW/m^2 with less than 300 s exposure. With a simple analytical model of heat transfer in a semi-infinite solid, they concluded that the ignition regime is given by a minimum igniter/foam temperature (290 °C for forward and about 330 °C for opposed, which promote a strong smolder reaction) and a minimum depth of smolder propagation (about 45 mm, which produces an insulating char-layer). The tests with variable oxidizer concentrations indicate that the ignition has a weak dependence on the oxygen concentration (Walther *et al.* 2001). This study clearly identifies heat transfer and kinetics as the limiting mechanisms in ignition, whereas oxygen transport is of secondary importance.

Anderson *et al.* (2000) studied the ignition of smoldering of PU in natural convection. They identified three stages in the process: warm-up, weak smolder, and self-sustained smolder. The first two stages are controlled primarily by heat-transfer, being the last one controlled also by oxidizer transport. Due to the lack of a forced flow, self-sustained smolder in natural convection could only be achieved in the heat-flux window from 6.1 to 6.8 kW/m^2. When the heat-flux is below the minimum, the temperature inside the foam is not high enough to promote the oxidation reactions over the pyrolysis. If the heat flux is higher than the maximum, the foam exposed to the igniter heat-flux is rapidly consumed by pyrolysis and the increased heat-losses quenched the smolder reaction. In their experiments a minimum temperature (300 °C) and a minimum exposure time (about 1000 s) were identified as needed in order to ignite the foam.

2.2 Chemical Kinetics

One of the biggest impediments preventing an increased usage of smolder models for predictions is the current limited ability to characterize practical materials in terms of their thermal and oxidative degradation (Ohlemiller 1985, Kelley and Schult 2006)). Even for the most-studied case of cellulose, the chemical mechanisms involved in smoldering are too complex and not yet fully understood (Ohlemiller 1985). Significantly simplified kinetic schemes are currently inevitable and the kinetic parameters are based on empirical estimation. In spite of the complex kinetic-behavior of a solid during smoldering,

experimental evidence suggests that it can be approximated by a reduced mechanism consisting of only a few global reactions, which capture the most significant behavior. These descriptions are formal rather than mechanistic and seek to understand the controlling factors in the propagation process with the ultimate goal of describing smolder tendencies. Detailed description of the chemical processes occurring in smoldering combustion can rapidly lead to enlarged complexity and prevent tractability.

A global mechanism that has been frequently used is the three-step chemical-reaction scheme for smoldering of a polymeric fuel (Eqs. 2.1-2.3), proposed by Ohlemiller (1985). The mechanism includes fuel pyrolysis, fuel oxidation and char oxidation, accounting for three solid species; fuel, char and ash. The application of this reduced mechanism to smoldering of cellulose (Di Blasi 1995, Leach *et al.* 1997) and PU foam (Leach *et al.* 2000, and chapter 4 of this thesis) has been found to give relatively good results, although predicting excessive mass-loss due to the consideration of a single one-step pyrolysis.

$$Foam \rightarrow \nu_{c,p}\, Char + \nu_{g,p}\, Gas \tag{2.1}$$

$$Foam + \nu_{O_2,o}\, O_2 \rightarrow \nu_{c,o}\, Char + \nu_{g,o}\, Gas \tag{2.2}$$

$$Char + \nu_{O_2,c}\, O_2 \rightarrow \nu_{a,c}\, Ash/Residue + \nu_{g,c}\, Gas \tag{2.2}$$

The analysis of the chemical reactivity of a solid material as it is heated can be done experimentally through thermogravimetric (TG) analysis. It provides information regarding the different reactions taking place in the solid material and is widely used in the study of thermal degradation. The estimation of the

corresponding kinetic parameters from TG experimental data is an established methodology and a wide variety of techniques are available in the literature (Kissinger 1957, Grønli *et al.* 1999, Conesa *et al.* 2001). The validity of the application of TG-estimated parameters outside the realm of TG presents some controversies (Schneider 1992, Galwey 2004) such as: discrepancy in the kinetic parameters derived from different studies for the same material; the scatter in TG curves; potentially different kinetic behavior of given material from different manufacturers; and possible transport effects in TG experiments and subsequent inaccuracy in the kinetic model. But in spite of it, TG remains the experimental technique offering the most reliable data to estimate kinetic parameters (Grønli *et al.* 1999).

Most of the studies on PU thermal-decomposition do not provide all the information needed for numerical models of smoldering combustion. They either provide a kinetic scheme of thermal degradation not complete for oxidative environments (Auerbach 1989, Ravey and Pearce 1997, Font *et al.* 2001) or kinetic parameters that are not appropriate for numerical models (Bilbao *et al.* 1996, Chao and Wang 2001). Furthermore, most of the conventional reduced-mechanisms of smoldering combustion do not describe well the process in its different propagation modes, and as a consequence different mechanisms are used for each propagation mode (Dosanjh *et al.* 1987, Dosanjh and Pagni 1987, see chapter 3 of this thesis). The thermochemistry, namely the heats of reactions, of solid fuels is the least available information in the literature. Only rough orders of magnitude are available (Rogers and

Ohlemiller (1980), Chao and Wang (2001b) and Dick *et al.* (2000). As a consequence of the little experimental information on oxygen consumptions and heats of reaction, some authors determined these unknown parameters through comparison between numerical models and experiments (Leach *et al.* 2000, and chapters 4 and 5 of this thesis).

In their early studies, Ohlemiller and Rogers (1978), showed that the smolder behavior of PU foam varies due to competition between tar and char formation during degradation, since this competition is sensitive to chemical and physical factors that influence either degradation path. However, they highlighted that the oxygen-limited character of self-sustained smolder makes the process relatively insensitive to fuel chemistry variations, except during ignition and extinction. Rogers and Ohlemiller (1981) studied the pyrolysis kinetics of PU foam by thermogravimetry. Their TG experiments showed that the degradation in inert atmosphere occurs in two overall steps. The first pyrolysis step yields a viscous liquid, which further decomposes to gas products. The activation energies and pre-exponential factors of the two steps were provided.

Chao and Wang (2001) conducted thermogravemetric (TG) experiments of flexible PU foam under nitrogen and air atmospheres at three heating rates (5, 10 and 20 °C/min). Their TG results show that the thermal degradation in nitrogen occurs in two stages (pyrolysis), and that the oxidative degradation in air occurs in three stages (combined oxidation and pyrolysis). The authors derived different sets of kinetic parameters for each stage (classified in different temperature ranges). Unfortunately, this approach to express the reaction rates is not valid for

numerical models. Nevertheless their experimental results are very valuable and are explored in detail in chapter 3 of this thesis.

Branca *et al.* (2003) studied the oxidative degradation of rigid PU foam. Based on TG observations, they proposed and quantified a 3-step mechanism to describe the process including three solid species. The proposed reaction paths are general mass-loss reactions and are not typified as pyrolysis or oxidation. Using a simple mathematical mass-loss model, the Arrhenius kinetic-parameters were estimated by evaluations of measured TG-curves. With these parameters, the mechanism is shown to provide a good description of the degradation process for heating rates between 5 and 20 C°/min. Electron microscopy micrographs are shown to characterized the morphological changes as the rigid foam reacts in a cone calorimeter.

In their mathematical study on the role of multi-reaction mechanisms in the extinction of opposed smoldering, Kelley and Schult (2006) concluded that a one-step mechanism cannot predict extinction of opposed smolder under oxygen depleted conditions. Thus, the authors advocate for multi-reaction mechanisms to be developed and included into numerical models of smoldering.

2.3 Models of Smoldering Combustion

There is substantial interest in using modeling to predict smolder behavior of practical materials, geometries and realistic environments. Modeling of

smoldering combustion is of particular interest in fire safety engineering because of its potential use for estimating smolder-ignition resistance, propagation speed, production rate of toxic species and conditions for transition to flaming, as well as for forensic reconstruction. It also provides a cost-effective alternative to experiments when testing is too costly, such as in microgravity conditions or during early phases of product development. Due to the high cost of testing in space-based laboratories, most of the smolder combustion studies have to be conducted in normal gravity and the results applied to microgravity. Theoretical and modeling studies also provide the methodology to apply normal-gravity results to microgravity environments. A recent review of smoldering combustion models can be found in Kallman (2005).

This review classifies the models into categories according to their approach, objective and methodology. The three general modeling categories are:

- Analytical models. They are approximate in nature and relatively simple to solve, but provide a good estimation of the order of magnitude of the variables in the process, specially the overall characteristics like temperature distributions and propagation speed. The principal use of these models is in the analysis of experimental observations.
- Computer physical models. These models include various coupled mechanisms, *e.g.* heat, mass and momentum transport, chemical reactions, heat radiation. These models include a chemical kinetic mechanism and require kinetic parameters to compute the reactions rates. They are predictive models and can be used to model realistic hazard situations.

- Mathematical models. These models are more conceptual that the physical models but less realistic. They are intended to capture qualitative features of the process, not to provide quantitative predictions. They are primary characterized by their focus on the mathematical behavior of the system and its theoretical implications (*e.g.* stability of the solutions, bifurcations, oscillations, transition to chaos). Usually, these studies put as a secondary objective the physical meaning of the input and output data.

2.3.1. Analytical models

The most noteworthy model is that by Dosanjh *et al.* (1987), which was later applied and improved by Torero *et al.* (1993), Torero and Fernandez-Pello (1996), and Bar-Ilan *et al.* (2004). This model has been used for forward and opposed forced flow and natural convection smoldering. This approach captures the most important mechanism in self-sustaining smoldering propagation: heat balance (see Eq. (1.1) in the introductory chapter). The values for the unknown thermodynamic parameters (heats of reactions) are extracted from comparison to experimental results, yielding a remarkable correlation with tests. They provided further verification of theoretical models of the process. Torero and Fernandez-Pello (1995) and Bar-Ilan *et al.* (2004) included into the model the buoyancy flux and its effect on smolder propagation.

Peng *et al.* (2005) developed recently a one-dimensional model of forward smoldering combustion. The model consists a infinitely thin smoldering front

where a one-step reaction takes place. Integrating the energy equation yields a simple expression for the rate of propagation. The application of this expression to smoldering combustion of PU gives results that compare well with their experiments. The authors used the model to explain the experimentally observed trends of the smolder velocity dependence with the forced flow; at low flows, the air velocity increases propagation speed by increasing the oxidizer flux, but beyond an air velocity of 1.2 mm/s, convective heat losses start to dominate the process and the smoldering propagation is hindered.

Analytical models of biomass smoldering and their impact on wildfire are available in the literature. There are two main groups of smoldering models, ignition models and soil heating models (Pastor *et al.* 2003). Most of them rely on empirical constants. These models only estimate average duff consumptions at the stand level and cannot provide calculations on the spatial variations and patterns. Costa and Sandberg (2004) developed an analytical model for a one-dimensional steady-state smoldering front propagating inside a wood log. The model includes drying, pyrolysis and oxidation front with heat transfer by conduction, convection and radiation. Their results compared qualitatively well with experiments. However, the governing variables of the model (smolder temperature and propagation speed) were not solved independently and the results depend on the experimental measurement of at least one of these variables.

Some models of cigarette smoldering are available in the literature. Yi *et al.* (2001a and 2001b) developed a steady-state two-dimensional model of smoldering cylindrical carbonaceous porous fuel (*e.g.* a cigarette). The

smoldering process was separated into two model: a pyrolysis and a combustion zone, linked together through a temperature conditions (experimentally determined). The model was used to conduct a sensitivity analysis of model parameters.

2.3.2. Computer physical models

Ohlemiller and his coworkers formulated the framework for smoldering combustion models (Ohlemiller 1985, reviewed in section 2.1) and developed one of the first transient models of the process (Ohlemiller *et al.* 1979). Their model simulated the one-dimensional opposed propagation of a smolder wave against a forced flow of air. It solved for mass, momentum, energy and species conservation in the solid and gas. The degradation chemistry of the PU foam was reduced to two oxidations reactions. The model solutions captured the front structure and predicted the correct order of magnitude for the propagation velocity and the peak temperature.

Summerfield *et al.* 1978 developed a one-dimensional thermophysical model of steady-draw smoking to predict the overall cigarette behavior. They solved for mass, momentum, energy and species, and two chemical reactions are included (pyrolysis and oxidation) .The kinetic parameters were derived from thermal analysis measurements of tobacco. Model predictions on the effect of flow rate on the propagation speed and pressure drop were compared with experimental results yielding a reasonable agreement.

Di Blasi (1995) developed a two-dimensional, unsteady model of smoldering combustion of a cellulosic bed in still air. The chemical processes accounted for Ohlemiller 3-step mechanism (Ohlemiller 1985) with a combination of kinetic parameters for different fuels: cellulose, polyurethane foam and others. The physical processes were mass, momentum and energy in the porous solid and gas. The domain boundaries were three insulating walls and a free surface from where the oxidizer enters the domain. The resulting two-dimensional structure of the smoldering front was studied, showing that the pyrolysis of the virgin fuel leaded the propagation front and penetrated deep into the fuel layer away from the free surface. The char oxidation was confined to the outer part of the propagation front, close to the free surface were oxygen was available. The heat losses to, and the oxygen transport from, the external ambient were showed to control the intensity and velocity of the process. Only some quantitative comparisons with experimental observations were provided.

Leach *et al.* (1997, 1998 and 2000) developed a one-dimensional model of smoldering ignition and propagation in a porous solid. The physical processes accounted for were mass, momentum and energy conservation in the solid and gas, not forcing thermal nor chemical equilibrium between two phases. This model was applied to model different fuels and configurations using different chemical mechanism and kinetic parameters. The first application of the model was for opposed smoldering combustion in polyurethane foam, implementing a 2-step kinetics (pyrolysis and oxidation of the foam) in a cellulose-like fuel (Leach *et al.* 1997). The paper studied the effect of the different physical mechanisms in the propagation characteristics and compared the trends with the experimental

results of Torero *et al.* (1993). In particular, they noted the significant impact in the results of the mass diffusion and heat conduction of the gas, and the radiative conduction of the solid. The model was able to predict smoldering extinction due to over-blowing by the forced flow. The next application (Leach *et al.* 1998) modeled opposed propagation in polyurethane foam implementing the 3-step kinetic mechanism by Ohlemiller with modified kinetic parameters for cellulose. This paper studied the possible mechanisms leading to the extinction of the opposed smoldering wave in the experiments by Torero *et al.* (1993). The authors concluded that kinetics dominates the extinction process but that heat convection and pyrolysis have also some effects on it. The last application (Leach *et al.* 2000) modeled forward smoldering combustion in polyurethane foam using the similar kinetics as before. The authors first calibrated the kinetics to match the experiments by Torero and Fernandez-Pello (1996) and then conducted an extensive parametric study of the effect of the fuel properties on the smoldering characteristics. The model by Leach *et al.* is used in chapter 4 of this thesis with the kinetics of polyurethane foam, and it is also the based for the model in chapter 5.

Numerical models of cigarette smoldering are available in the literature. Saidi *et al.* (2004) developed a three-dimensional kinetic modeling of tobacco/cigarette smoldering/puffing. The model solved for mass and momentum conservation, including the kinetic reactions, but did not solve for the energy equation. The authors obtained the temperature-time history of tobacco in a puffing cigarette

from existing experimental data. The numerical results show a good agreement with the experimental data for the yield rates of combustion gases.

Debenest *et al.* (2005a) developed a three-dimensional microscale model of smoldering combustion in porous media. Their model accounted in detail for transport processes by convection and diffusion for heat and the chemical species in the gas, and by heat conduction in the solid. In a companion paper (Debenest *et al.* 2005b), the authors applied a similar but two-dimensional model to simulate smoldering of oil shale grains in a fixed bed. The chemical kinetics was represented by a single-step heterogeneous reaction on the surface of the solid grains. The results were used to define a typology of the regimes for smoldering combustion in packed beds.

2.3.3. Mathematical models

Schult *et al.* (1995 and 1996) studied the mathematical behavior of opposed and forward combustion waves. Their opposed model (Schult *et al.* 1995) include a 1-step reaction (fuel converted into char) and employed asymptotic methods to find uniformly propagating, planar smolder wave solutions. They determined spatial profiles of gas velocity and composition, temperature and solid conversion. The model predicted extinction due to large gas flows only for fuel-limited combustion (while experimentally observed extinction had been reported to be in oxygen-limited conditions). Their forward model (Schult *et al.* 1996) detected two types of propagating fronts: ‘reaction leading‘ occurs when the velocity of the combustion front exceeds that of the heat transfer front, and

'reaction trailing' structure is obtained when the combustion front is slower than the heat transfer front. The solutions obtained were qualitative compared to experimental observations yielding a general agreement.

Buckmaster and Lozinski also presented opposed and forward smoldering models. A simple model of opposed smoldering combustion in a porous medium (Lozinski and Buckmaster 1995) was analyzed using asymptotic methods. The reaction scheme is a 2-step mechanism with the secondary reaction being the pyrolysis. The model successfully predicted extinction when oxygen limited conditions were assumed, but the kinetic scheme used seems of little chemical sense since a secondary reaction which is globally endothermic has not been observed yet in smoldering combustion. An elementary model of one-dimensional unsteady forward smoldering (Buckmaster and Lozinski 1996), purged of all unnecessary physics, was used to focus on the nature of a traveling thermal wave. A solution was constructed, characterized by two reaction fronts (pyrolysis and oxidation). They deduced that the smolder temperature and the ratio of the front speeds are independent of the airflow rate, and examined the structure of the reaction fronts.

Bayliss and Matkowsky (1990) numerically studied the solution stability and routes to chaos of the equations governing a simple combustion wave in a reacting solid. Some solutions to this system were known to exhibit pulsating behavior. While varying the controlling parameter, Bayliss and Matkowsky found sequences of period doublings, intermittency, long laminar regions, bursts and finally chaos in the solution bifurcation map. This topic was further investigated by Decker and Schult (2004), who examined the dynamics of opposed smoldering

close to its extinction limit. Using asymptotic methods and a full time-dependent model, they studied the stability of the traveling-wave's solutions near the extinction limit due to convective heat-losses from the incoming gas. The transient one-dimensional numerical model includes a one-step reaction, assumes thermal equilibrium between the gas and the solid and does not include heat losses. They concluded that the system oscillates and then proceeds through a period doubling cascade of bifurcations to chaotic behavior before extinction occurs (see Fig. 2.1).

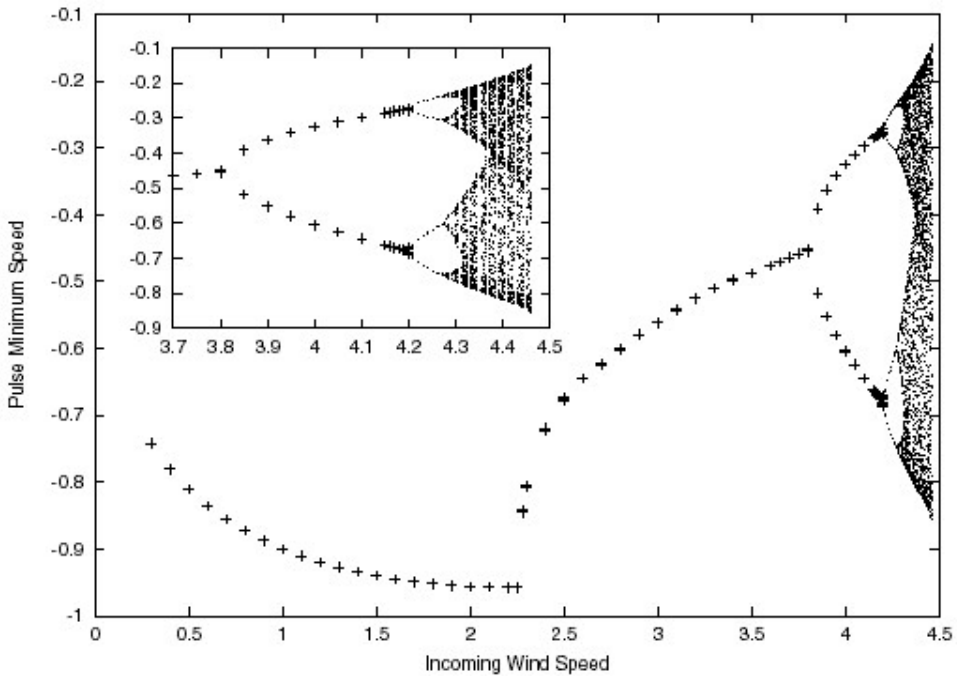

Figure 2.1: Bifurcation diagram of burning speed versus incoming gas speed showing the typical period doubling cascade. Reproduced with permission from Decker and Schult (2004), IOP Publishing.

Kelley and Schult (2006) studied the role of multi-reaction mechanisms in the prediction of extinction of opposed smolder waves due to over-blowing. They

considered a 2-step mechanism; virgin fuel oxidizes to char, and char oxidizes to ash. Their model suggests that oxygen depletion is caused by the char oxidation while extinction is driven by the virgin fuel oxidation. They concluded that under oxygen depleted conditions, a one-step mechanism cannot predict extinction of opposed smolder and thus advocate for multi-reaction mechanism to be developed and included in models of smoldering. The reported results use the kinetic parameters for PU from Rein *et al.* (2005) (the same work as the 3-step mechanism presented in chapter 3 of this thesis) but their conclusions seem to hold for a broad range of parameter values.

2.4 Smoldering Combustion in the Absence of Gravity

Summerfield and Messina (1981) assessed for the first time the feasibility of conducting experiments in space-based facilities on smoldering combustion, attempting to identify the critical components of such experiments and conceptually designing them. After reviewing the state of the art in smoldering at that time, the authors proposed the used of a space-based experimental apparatus able to artificially create gravitational accelerations of varied magnitude. These experiments as specified in their study were never conducted.

Donsanjh and Pagni (1986) were among the first to conduct theoretical and normal-gravity experimental studies to determine the effect of buoyancy on the rate of spread of a smolder reaction. Varying the ambient pressure inside the experimental chamber and thus changing the density difference, they controlled

the buoyant forces without changing the gravity acceleration. The experiments were carried out in porous cellulose. Opposed smoldering was studied in natural downward propagation for ambient pressures ranging from 0.5 to 1.2 atm. They showed that the smolder velocity is proportional to the ambient pressure squared. Based on these results, it was concluded that transport by diffusion cannot by itself provide the oxidizer needed to support the spread of a smolder reaction. Qualitative agreement was found between their theoretical predictions and the experimental results.

Newhall *et al.* (1989) continued the above study by Donsanjh and Pagni (1986) by including the effect of forced airflow on opposed smoldering. The results showed that the reaction was limited by oxygen transport and that buoyancy plays a role in cellulose smoldering combustion, particularly at low flow velocities. The chemical reactions taking place in the smoldering cellulose were shown to be weakly dependent on pressure.

Cantwell and Fernandez-Pello (1990) report on the first experiments of smoldering in microgravity. Their polyurethane samples were ignited in 1-g gravity and then put in free-fall inside the NASA Glenn drop tower, which provided 2.2 s of microgravity. This microgravity time was known to be too short to provide meaningful insights of the process but nonetheless these early experiments pointed out the importance of the buoyancy-induced mass-flux of oxidizer at low forced flows.

Torero *et al.* studied the effects of buoyancy on opposed (Torero *et al.* 1993) and forward (Torero and Fernandez-Pello 1996) configurations by conducting a series of forced-flow and natural convection (Torero and Fernandez-Pello 1995)

experiments in normal gravity smoldering and comparing upward and downward propagation. The fuel used was polyurethane flexible foam. These studies provided further understanding of the controlling mechanism of smoldering combustion and solid verification of theoretical models of the process. In forced flow, buoyancy was observed to affect the propagation at low mass-fluxes and when the smolder front approached the end of the sample. Their results showed that the gas mass-flux to the front flown by natural convection depends on the sample length, as a consequence of the pressure drop along the porous sample (this observation was again later confirmed in Bar-Ilan *et al.* (2004b). For their test conditions and without forced flow, buoyant flows seemed to provide enough oxidizer flux to ignite and propagate the reaction, although as the sample length was increased the ignition time increased.

Experiments conducted in aircrafts following parabolic trajectories (Torero *et al.* 1994) allowed studying the effect of gravity changes in smoldering. Each parabola provided up to 25 s of microgravity, immediately followed by a short period of high gravity (2g). Although the variable-gravity periods were too short to study smolder propagation, they allowed the observation of trends in the smolder reaction temperature. The measurements showed that gravity plays a significant role in the competition between the supply of oxidizer and the transfer of heat to and from the reaction zone. (Fig. 2.2).

Stocker *et al.* (1996) reported the results of the microgravity experiments conducted aboard the Space Shuttle. They represent the first smolder experiments ever conducted under extended periods of microgravity. Inside the polyurethane foam small-samples, smolder did not propagate in a quiescent

environment of air. These results confirmed the conclusions from the previous experiments of Donsanjh and Pagni (1986). In the forced-flow experiments, smolder did not propagate away from the igniter-assisted region. This observation can be linked to the effect of the sample size in smoldering. For such a small sample (Fig. 2.3), the heat generated at the reaction zone by consumption of the oxidizer forced-flow was relatively too small to overcome the heat losses to the environment. This interpretation was later reinforced by the analytical study of Bar-Ilan *et al.* (2005). While the material thermally degraded, it produced carbon monoxide at a level up to 300 times that observed in similar experiments on Earth. This observation, together with available studies of transport and pulmonary deposition of airborne contaminants inside space facilities (Todd *et al.* 1994, Irons *et al.* 1994), highlight the associated increase in the toxic hazard of smolder in spacecrafts.

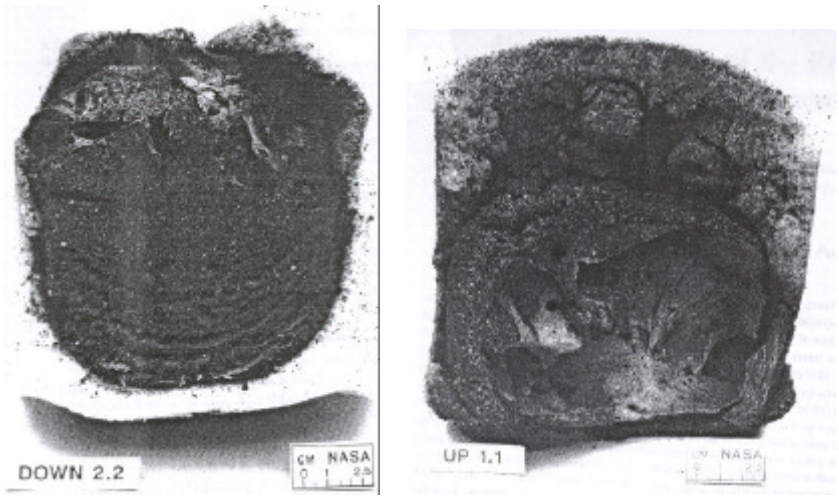

Figure 2.2: Photographs showing cut polyurethane samples burnt in smoldering experiments during parabolic flights. Left) downward smoldering; Right) upward smoldering. Photographs from Torero *et al.* (1994).

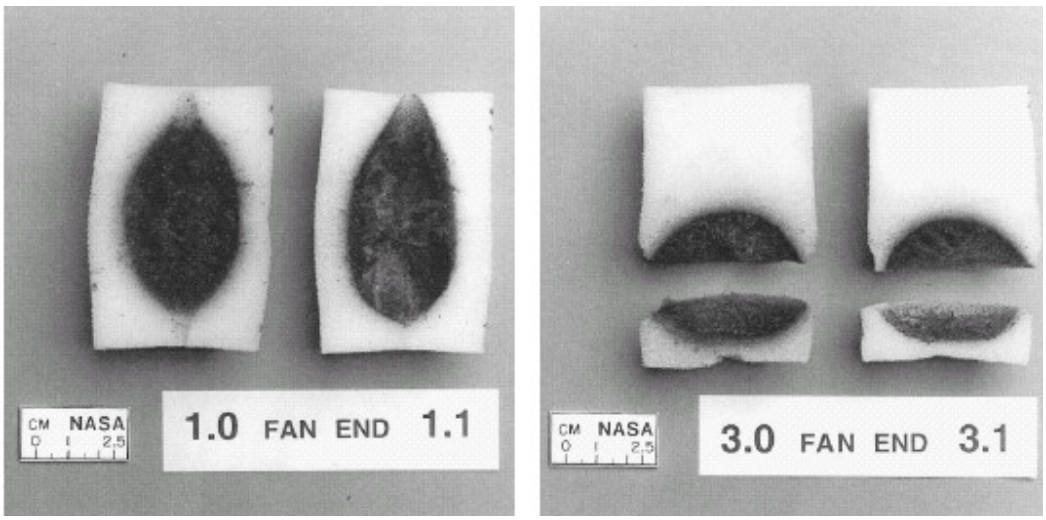

Figure 2.3: Photographs showing cut polyurethane samples burnt in smoldering experiments in microgravity. USML-1 mission of the Space Shuttle, 1992. Photographs courtesy of Dr. Stoker (Stoker *et al.* 1996).

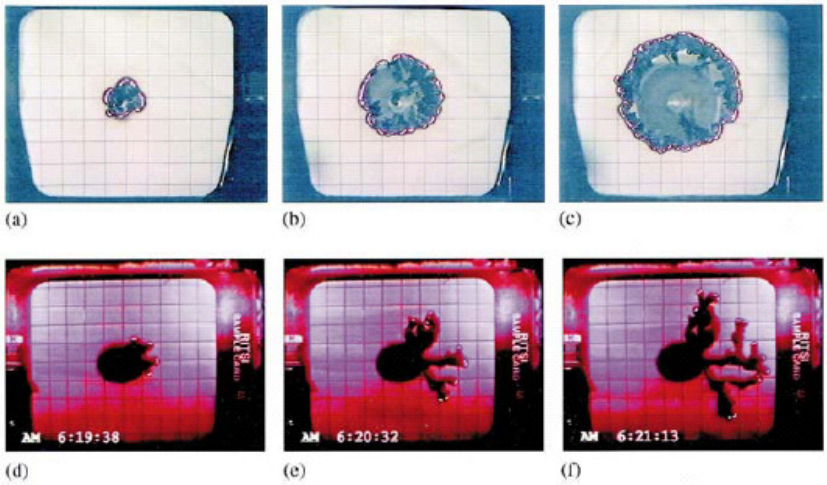

Figure 2.4: Time sequence showing the development of smoldering patterns in normal gravity (a–c) and in microgravity (d–f). STS-75 mission of the Space Shuttle, 1996. Photographs courtesy of Dr. Olson (Olson *et al.* 1998).

Olson *et al.* (1998) conducted experiments of smoldering in very thin fuel (filter paper) aboard the Space Shuttle. After ignition, a series of complex finger-shaped bifurcations propagating radial outward were observed in microgravity (Fig. 2.4), while in normal gravity the smolder front propagated with a circular geometry nearly uniform and continuous. The authors proposed that the low local oxygen-flux restricts the size of the smolder front, and suppresses smolder adjacent to it by local depletion of the oxygen.

The experiments conducted aboard the NASA Space Shuttles (Walther *et al.* 1999, Bar-Ilan *et al.* 2004a, Bar-Ilan *et al.* 2004b) are the most comprehensive experimental studies on the topic available to date. Together with the previous research results, these studies have confirmed and quantified the prevalent effect of gravity in smoldering ignition and propagation. Walther *et al.* (1999), investigated the propagation of smolder through a polyurethane foam sample in microgravity, under both diffusion driven and opposed forced flow smoldering. The experiments were carried out aboard the Space Shuttle. The forced flow test were the first experiments of smolder combustion in microgravity in sample sizes large enough to allow the self propagation of the smolder reaction throughout the sample length (Fig. 2.5). Results in microgravity were compared with normal-gravity. It was found that the microgravity opposed flow smolder temperatures, propagation velocities, toxic compound production and reaction extent laid between those of normal-gravity upward and downward tests. Neither of the two quiescent, microgravity cases resulted in self-sustained smolder propagation, whereas the normal-gravity downward cases propagated vigorously. The difference in these results shows that gravity has a significant

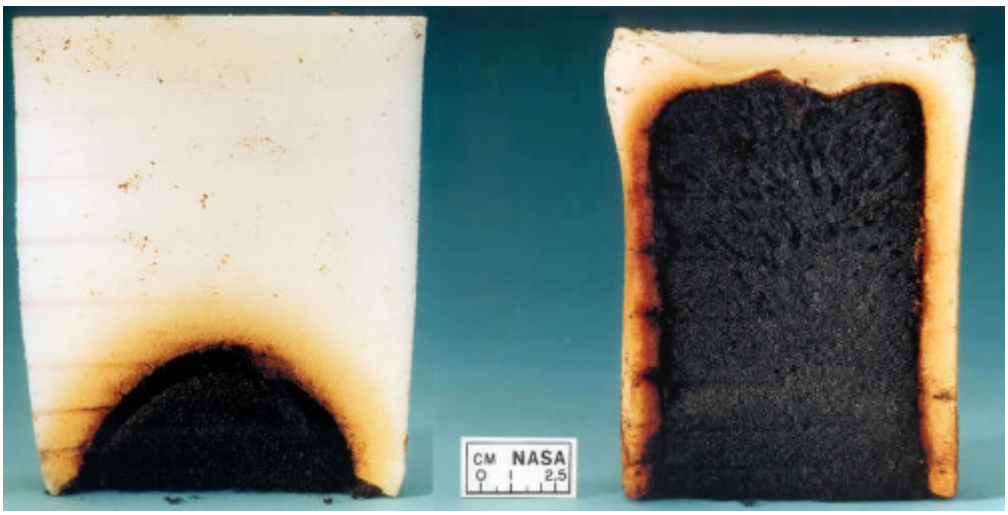

Figure 2.5: Photographs showing cut polyurethane samples burnt in smoldering experiments in microgravity. STS-69 mission of the Space Shuttle, 1995. Left) quiescent environment with 0.35 O_2 volume fraction; Right) opposed flow of air at 5 mm/s. Photographs from Walther *et al.* (1999).

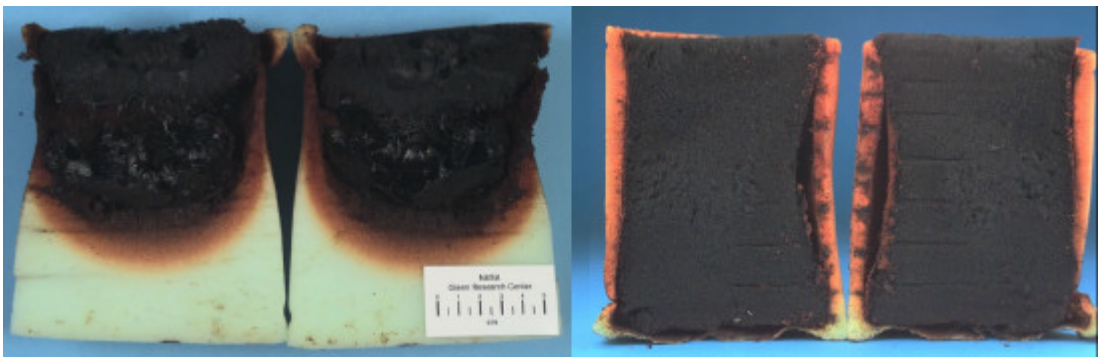

Figure 2.6: Photographs showing cut polyurethane samples burnt in smoldering experiments in microgravity. STS-105 mission of the Space Shuttle, 2001. Left) forward flow of air at 3 mm/s (Bar-Ilan *et al.* 2004a); Right) opposed flow of air at 3 mm/s (Bar-Ilan *et al.* 2004b).

effect on smolder combustion. Post-flight thermogravimetric analysis showed little effect of gravity on the chemical composition of the char left. The comparison of the tests conducted in microgravity and normal gravity in the forward configuration of Bar-Ilan *et al.* (2004a) indicates that smolder propagation velocities are higher in microgravity than in normal gravity, and that there is a greater tendency for a transition to flame in microgravity than in normal gravity (Fig. 2.6). These differences were attributed to the reduced heat losses in the microgravity environment, leading to increased char oxidation. The experiments in forced-flow smoldering in opposed configuration of Bar-Ilan *et al.* (2004b) allowed comparison of the results in microgravity to those in normal gravity. Bar-Ilan and coworkers also conducted experiments at varied ambient pressure. The experimental results and theoretical analysis suggest than the removal of buoyancy-induced heat losses in microgravity allows for self-sustained propagation at an oxidizer mass-flux below the critical value observed in normal-gravity (0.30 g/m^{2}s is required in microgravity whereas 0.5 to 0.8 g/m^{2}s is required in normal gravity). The methodology to analytically calculate heat losses to the surroundings presented in chapter 4 (section 4.3) of this thesis were applied in Bar-Ilan *et al.*(2004b) to microgravity and normal gravity environments (Fig. 2.6). It showed that the heat losses in the smoldering experiments were up to seven times higher in normal gravity than in microgravity environments. The pressure effect on the chemical kinetics were shown to be small (of the order of $P^{0.33}$). These experiments also showed that in quiescent environments the smoldering front can only propagate in regions assisted by the heat of the igniter, but the reaction propagated further

and further as the oxidizer concentration is increased. This further confirmed the importance of oxidizer availability and heat losses as the controlling factors in smoldering.

2.5 Transition from Smoldering to Flaming Combustion

While considerable work has been conducted to understand the smoldering combustion of solid fuels, there has been considerably less research done on the transition from smoldering to flaming. The topic has been approached mainly from an experimental point of view and little work has been done on the mathematical modeling of the process. Nonetheless, there are phenomenological theories/models capable of explaining the transition from smoldering to flaming. For example, a mathematical heat-balance analysis of the process is used in Bar-Ilan *et al.* (2005) to predict the conditions for the onset of the transition.

Palmer's work (Palmer 1957) is one of the first studies on smoldering and to report on its transition to flaming combustion. Palmer investigated smoldering of horizontal piles of sawdust. He observed that the transition from smoldering to flaming combustion occurred only in the forward configuration and at external airflows higher than 0.1 m/s. He also noted that transition occurred at lower air velocities as the diameter of the granulated fuel was increased.

Ortiz-Molina *et al.* (1979) studied the relative smoldering tendency of different flexible PU foams by varying the ambient oxygen concentration. They

reported that transition occurred at high oxygen concentrations (about 0.37 oxygen mass fraction) and only for samples of large size (50 x 120 x 450 mm). Their samples in the form of small cylinders (18 mm in diameter) did not transition. In Rogers and Ohlemiller (1980) experiments on the smolder characteristics of PU foam, the authors studied opposed smolder propagation in 100 x 115 mm cylinders and they reported that transition to flaming occurred only at oxygen mass fractions above 0.6.

Babrauskas (1985) conducted a more practical investigation of the transition from smoldering to flaming as it applies to fire safety in upholstered furniture. He observed the behavior of upholstered armchairs, set smoldering by a lit cigarette. The results showed that in still air conditions, flaming can commence after an hour or more. It was proposed that the mechanism involved the establishment of smoldering in the crevice between the seat and the back, where good insulation allowed vigorous smoldering to develop.

Alexopoulos and Drysdale (1988) carried out an experimental study of the transition from smoldering to flaming combustion in insulated chimneys made of fiber insulation board. The chimneys' cross-sections varied from squared, to rectangular and slot shapes. Smoldering was initiated at the bottom of the apparatus and allowed propagating in natural convection until flaming occurred. The study noted the difficulty to obtain reproducible results. Times to transition were in the range from 7 to 25 min (average of 18 min) depending on the shape and size of the cross-section. The authors pointed out that heat balance is the controlling mechanism rather than availability of oxygen. They ventured to suggest that glowing char is not the source of ignition, favoring

more the spontaneous ignition mechanism as the responsible for the onset of flaming of the vapors. The authors proposed a mechanism for the transition to flaming in upholstered furniture: a funnel effect triggers the transition when cushion is burned to the bottom and additional flow of air is established by buoyancy (this mechanism was later commented in Drysdale (1999), and it is represented in Fig. 2.7).

Ohlemiller's (1990) work with cellulose examined smoldering of thick, horizontal beds of permeable cellulosic insulations in the presence of air flowing over its top surface. Ohlemiller found that while opposed smoldering combustion responded only weakly to an increased air flow with no transition to flaming at flow velocities up to 5 m/s, forward smoldering responded strongly to increased air flows and yielded transition to flaming at about 2 m/s. The author argued that the convective heat-transfer effects in the forward configuration intensify the smolder in the reaction zone, causing the development of cavities, which act as flame initiation regions and flame holder. Chen *et al.* (1990) examined the behavior of smolder combustion of cellulosic materials (grain, wood shavings and shredded paper) at external air stream velocities up to 6 m/s. In his experiments, no transition to flaming was observed for the smoldering of grain samples, while for wood shavings smolder combustion with subsequent transition to flaming occurred at a wide range of air velocities (1.2 to 3 m/s). For shredded paper without forced airflow, as the depth of the sample was increased, the time to transition to flaming decreased. The authors concluded that the controlling mechanisms are the internal and external heat transfers, and the availability of oxidizer.

Torero and Fernandez-Pello (1995) concluded that the transition to flaming combustion is generated when the char oxidation reaction is vigorous and, shortly after, it extinguishes due to oxygen depletion. They noted that during this extinction period, the fuel continues to be pyrolyzed, and when the oxygen is again replenished to levels where a flammable mixture is present in the gas phase, ignition occurs.

The work of Tse *et al.* (1996) on transition to flaming is one of the most important studies on the matter to date. They investigated the transition to flaming of two-dimensional, forced flow smolder propagation in polyurethane foam. The configuration involved a vertically oriented polyurethane slab with forced air over its outer surface, and inner flow during the ignition period. Three sides and the top of the sample were insulated. Tse *et al.* developed a novel ultrasonic imaging technique to examine the evolution of the reactions through the interior of porous combustible material. This technique provided information about the location of a propagating smolder front, as well as any permeability variations of the char left behind by the propagating smolder reaction. The authors reported two types of reactions within the sample, one of smolder propagation and initial char oxidation, and another of intense secondary char oxidation where transition occurs. Their experiments revealed that the transition to flaming occurs inside the hot char region below the smoldering zone, after which the flames propagate outward to the interface and engulf the entire sample. They observed that localized high temperatures in the char region precede observation of flaming at the interface. Tse *et al.* proposed the explanation that a well-insulated, exothermic surface reaction proceeds

within the oxygen-limited char until a sudden influx of oxidizer, brought to this location by void formation within the char region, triggers the transition to flaming. This mechanism is not different from that reported by Ohlemiller (1990).

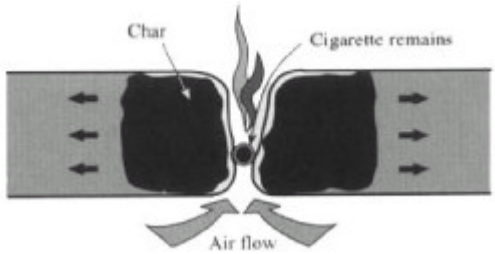

Figure 2.7: Representation of incipient transition from smoldering to flaming in a burn-through of polyurethane foam cushions. Figure courtesy of Dr. Ogle (Ogle and Schumacher 1997).

Ogle and Schumacher (1997) experimentally studied the patterns left when an upholstered sofa smolders and compared them with the patterns left when it flames, including the transition to flaming. They established a forensic correlation between the burn-patterns left and the stage of the fire so as to aid fire investigators in the determination of fire cause, *i.e.* if the fire started as smoldering or as flaming, or if it transitioned. They pointed at the Drysdale's funnel-effect (Alexopoulos and Drysdale 1988, Drysdale 1999) as a consistent explanation of their experimental observations in transition to flaming (Fig 2.7).

Babrauskas and Krasny (1997) conducted a survey of literature on experiments involving the transition from smoldering to flaming in upholstered furniture items. They found six well-documented experimental studies of the subject. Summarizing the results of all the experiments, they reported a total of 102 upholstered items that smoldered, out of which 65 of them transitioned to

flaming. The time to transition range from 22 to 206 min with an average time of 88 min. The authors noted that the sparse existing data did not permit firm conclusions.

Chao and Wang (2001b) experimentally studied the mechanisms of transition from smoldering to flaming combustion with natural convection. These authors concluded that oxidation of the residual char initiates the transition to flaming in the interior of the foam (as Ohlemiller (1990) and Tse *et al.* (1996) concluded). They identified a minimum fuel sample length (on the order of 200 mm) below which transition did not occur in their experiments. This minimum length was shorter for flame-retarded foams than non flame-retarded foams, and shorter for foams with lower moister contents.

The last published papers addressing the fundamentals of the topic (Bar-Ilan *et al.* 2005, Putzeys *et al.* 2005) focused on the transition to flaming for small samples of polyurethane foam (see Fig. 1.1 in chapter 1 of thesis). The sample size was too small to sustain a propagating reaction without heat assistance. Thus, their samples (50 x 50 x 120 mm) were heated from the lateral sides by guard-heaters and from the free-surface side by a radiant heater. The effect of oxygen concentration, external airflow velocity and radiant heating were studied. Ultrasound imaging of the process was also used in Putzeys *et al.* (2005). The two papers show the heavy dependence of smoldering propagation and its transition to flaming combustion on heat losses and oxygen concentration, and the importance of the sample size. Their experiments further confirmed the finding of Ohlemiller (1990) and Tse *et al.* (1996).

Chapter 3

Determination of Polyurethane Foam Kinetics using Genetic Algorithms

"so easy it seemed, Once found, which yet unfound most would have thought Impossible!"

John Milton (1608-1674).

3.1 Introduction

In addition to the thermophysical aspects of smoldering, inclusion of the chemical reactions occurring on the solid fuel is important when modeling smolder combustion. Chemical kinetics governs the front structure and dictates the global heat-released rate by smoldering. Proper computation of the reaction rates is particularly essential for the kinetically controlled regimes of ignition, extinction, and the transition to flaming. Thus, smoldering models need

quantitative information on the heterogeneous reactions taking place in the thermally degrading solid. However, it is difficult to establish and quantify the kinetic mechanism of solid decomposition with certainty, especially for materials with complex kinetics like polymers.

Most of the studies on polyurethane (PU) foam thermal-decomposition do not provide all the information needed for models of smoldering combustion. They either provide a kinetic scheme of thermal degradation not complete for oxidative environments (Ravey and Pearce 1997, Font *et al.* 2001, Auerbach 1989) or provide kinetic parameters that are not appropriate for numerical models (Bilbao *et al.* 1996, Chao and Wang 2001a). Some authors modelling smolder of PU had to use the kinetic parameters of other polymeric fuels (Leach 1997, Leach 2000) and use calibration procedures to extract some unknown parameters (Leach 2000, and see Chapter 4 of this thesis). Furthermore, conventional mechanisms of PU foam do not describe well smoldering in its different propagation modes, and as a consequence different mechanisms are used for each propagation mode (Dosanjh *et al.* 1987, Dosanjh and Pagni 1987).

In this work, the kinetic behavior of PU is explored using thermogravimetric (TG) data and as a result, a comprehensive and quantified kinetic-mechanism is proposed. This mechanism is valid to model smoldering behavior in both opposed and forward propagation. First the established reduced mechanism of Ohlemiller (1985) is studied and applied to PU foam. Then an improved mechanism for PU with five reactions is proposed based on experimental TG analysis. A mathematical model of solid mass-loss is used with the reduced mechanism to simulate the TG experiments. A genetic algorithm is used to find the set of

kinetic and stoichiometric parameters that provide the best agreement between the model predictions and the experimental data. The mechanism and the parameters are then used to model the propagation of a smoldering front to verify its predictive capabilities. Here, the methodology is tested with cellulose pyrolysis and applied to PU oxidative and thermal decomposition, but it is applicable to any solid material.

3.2 Thermogravimetry and Kinetics Mechanisms

PU is a class of versatile polymers produced by the reaction of a polyol with an isocyanate plus catalysts, surfactants, and water. In the form of foam, it is used in a wide range of industrial applications with worldwide consumption in the order of millions of kilograms per year. The aeronautics, automobile, construction and furniture industrial sectors use it for thermal insulation, upholstery, shock absorbing, and soundproofing. PU foam is a major fire-safety concern due to its relatively low ignition resistance, being a common fire-ignition source through smoldering and transition to flaming (Hall 2004, Levchik and Weil 2004, Brereton and Laing 1992).

The degradation of polymers in general, and of PU in particular, involves complex pathways to chemical and physical changes. These pathways are not yet fully understood. An example of the changes in the microscale morphology of PU as it smolders can be seen Fig. 3.1, which shows scanning electron microscopy (SEM) images. The virgin foam (Fig. 3.1a) has a well-organized distribution of hollow pores of polygonal faces, which are formed by fibers of near-uniform

thickness. When the foam pyrolyzes at temperatures between 250 and 300 °C (Fig. 3.1b), the distribution of pores changes and the fibers' edges deform toward membraned shapes. The char remaining after smoldering at temperatures between 400 and 450 °C (Fig. 3.1c) is comprised of needle-like fibers and no longer has a uniform structure. The loss of mass compared to the virgin foam is evident.

The analysis of the chemical reactivity of a solid material as it is heated can be done experimentally through thermogravimetric (TG) analysis. TG is a testing procedure in which changes in the weight of a solid specimen are recorded as it is heated in a temperature- and composition-controlled gaseous atmosphere. It provides information regarding the different reactions taking place in the solid material and is widely used in the study of thermal degradation. The estimation of the corresponding kinetic parameters from TG experimental data is a well-established methodology and a wide variety of techniques (Conesa *et al.* 2001, Grønli *et al.* 1999) are available in the literature. For one-step mechanisms, the simplest analytical method consists on fitting experimental data with a linear expression between the logarithm of the reaction rate and the inverse of the temperature (Kissinger 1997).

The thermogravimetry results in inert atmosphere (usually 100% nitrogen or helium) are used to study the pyrolysis of the solid, and in the air atmosphere to study its oxidation. Two kinds of curves are obtained from each TG experiment as a function of temperature. One curve is the mass (or weight) of solid remaining; the other curve is the mass-loss (or weight-loss) rate. Different curves are obtained at different heating rates but similar shapes are seen for each kind.

The TG experiments of Chao and Wang (2001a) for non fire-retarded PU foam in inert atmosphere show two peaks in the mass-loss rate (Fig. 3.2). In air atmosphere, the mass-loss rate (Fig. 3.3) shows three peaks. In spite of PU's complex kinetic-behaviour, experimental evidence suggests that it can be approximated by a reduced mechanism consisting of only a few global reactions, which capture the most significant behavior.

A chemical kinetics mechanism can be as simple as being composed of only one global reaction or it could include dozens of reactions. For solid kinetics, it is more frequent to see mechanisms with just a few reactions (in the field of gas kinetics the number of reactions is significantly higher). These reduced mechanisms seek to understand the controlling factors in the propagation process with the ultimate goal of describing smoldering tendencies. Thus, it is sufficient to include a reasonably accurate description of the major chemical and heat effects (global kinetics). In the following sections, two different reduced mechanisms for PU are explored.

3.2.1. Ohlemiller's 3-step mechanism

A mechanism that has been frequently used to describe smoldering of a polymeric fuel is the 3-step chemical-reaction scheme proposed by Ohlemiller (1985). Ohlemiller's 3-step mechanism is composed of: foam-pyrolysis (Eq. 3.1); foam oxidation (Eq. 3.3); and char oxidation (Eq. 3.4), accounting for three solid species: foam, char and ash, and two gas species; oxygen and smoldering products.

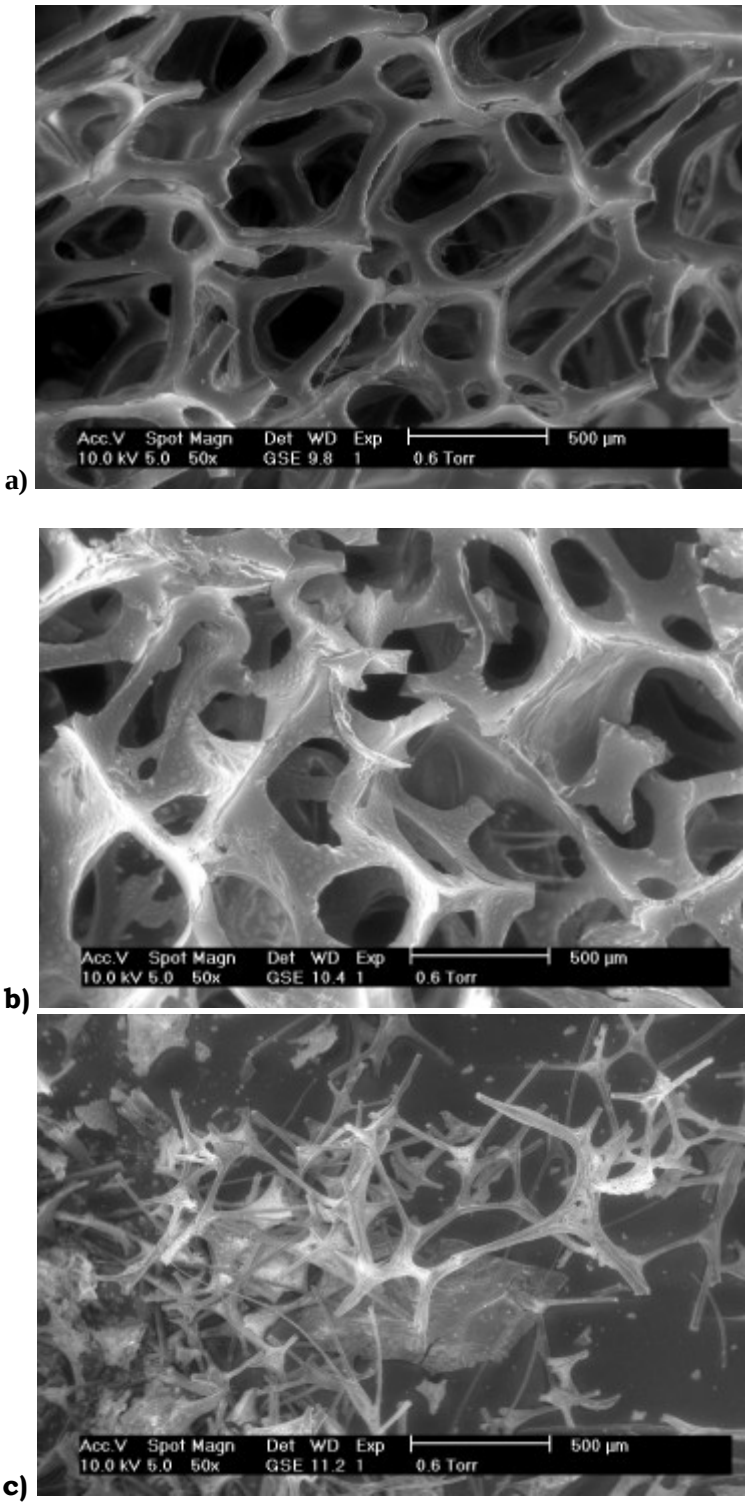

Figure 3.1. Scan Electron Microscopy imaging of polyurethane foam: (a) virgin foam; (b) pyrolyzed foam; and (c) smoldered char. (Photographs courtesy of Mikofski 2005).

$$Foam \rightarrow \nu_{c,p}\ Char + \nu_{g,p}\ Gas \quad (3.1)$$

$$Foam + \nu_{O_2,o}\ O_2 \rightarrow \nu_{c,o}\ Char + \nu_{g,o}\ Gas \quad (3.2)$$

$$Char + \nu_{O_2,c}\ O_2 \rightarrow \nu_{a,c}\ Ash + \nu_{g,c}\ Gas \quad (3.3)$$

This mechanism was based on the well-know decomposition of cellulose, and many papers used it together with kinetic-parameters for cellulose derived by Kashiwagi and Nambu (1992). The main setback of this mechanism when applied to PU is that it only considers one pyrolysis reaction, and thus cannot capture the double-peak behaviour of PU foam decomposition in inert atmosphere observed by Chao and Wang (2001a) (Fig. 3.2).

3.2.2. New 5-step mechanism

The TG experiments of Chao and Wang (2001a) for PU flexible foam indicate that a mechanism with a minimum of five steps is needed to describe the thermal decomposition. In their tests, Chao and Wang used a flexible PU foam, non-fire retarded and commercially available. The tests were conducted at heating rates of 5, 10, and 20 °C/min. Analyzing the experiments in a nitrogen atmosphere to explore the pyrolysis paths (Fig. 3.2), it can be seen that two reactions are taking place instead of one. Other TG analyses also confirm that PU pyrolysis occurs in two stages (Ravey and Pearce 1997, Rogers and Ohlemiller 1981, Mahajan et al. 2000, Dick *et al.* 2000). Thus, the three-step mechanism referred to above will be improved with an additional pyrolysis path and with the consideration of an extra solid species, referred to here as β-foam. The inclusion of the β-foam implies the addition of its subsequent oxidation to char. The TG

experiments in air atmosphere (Fig. 3.3) show three peaks in the solid mass-loss rate between 25 and 400 °C. The mechanism then suggests that each peak is the mass-loss of a corresponding solid species by competing pyrolysis and oxidation pathways. This way, the first peak would be the mass-loss of the virgin foam, the second that of the β-foam, and the third one that of the char. To account for the small mass left at 450 °C, a fourth solid species has to be included: residue.

Thus, a five-step mechanism is proposed here that is composed of: two foam-pyrolysis (Eqs. 3.4 and 3.5); two foam oxidations (Eqs. 3.6 and 3.7); and one char oxidation (Eq. 3.8), accounting for four solid species: foam, β-foam, char and residue, and two gas species; oxygen and smoldering product.

$$Foam \rightarrow \nu_{\beta,p}\ \beta\text{-}foam + \nu_{gp,p}\ Gas \tag{3.4}$$

$$\beta\text{-}foam \rightarrow \nu_{c,p\beta}\ Char + \nu_{gp,p\beta}\ Gas \tag{3.5}$$

$$Foam + \nu_{O_2,o}\ O_2 \rightarrow \nu_{c,o}\ Char + \nu_{gp,o}\ Gas \tag{3.6}$$

$$\beta\text{-}foam + \nu_{O_2,o\beta}\ O_2 \rightarrow \nu_{c,o\beta}\ Char + \nu_{gp,o\beta}\ Gas \tag{3.7}$$

$$Char + \nu_{O_2,c}\ O_2 \rightarrow \nu_{r,c}\ Residue + \nu_{gp,c}\ Gas \tag{3.8}$$

The two main chemical constituents of PU are isocyanate and polyol. The major breakdown mechanism in PU is the scission of the polyol-isocyanate bond. The isocyanate vaporizes and the polyol remains to further decompose (Ravey and Pearce 1997, Beyler and Hirschler 2001). Consequently, in the above the scission of the polyol-isocyanate bond, and the β-foam corresponds to the less-volatile polyol left behind. The polyol further pyrolyzes by the consecutive reaction in Eq. (3.5). To keep the mechanism as simple as possible but still comprehensive, the oxidation reactions of virgin PU and β-foam (Eq. 3.6) are

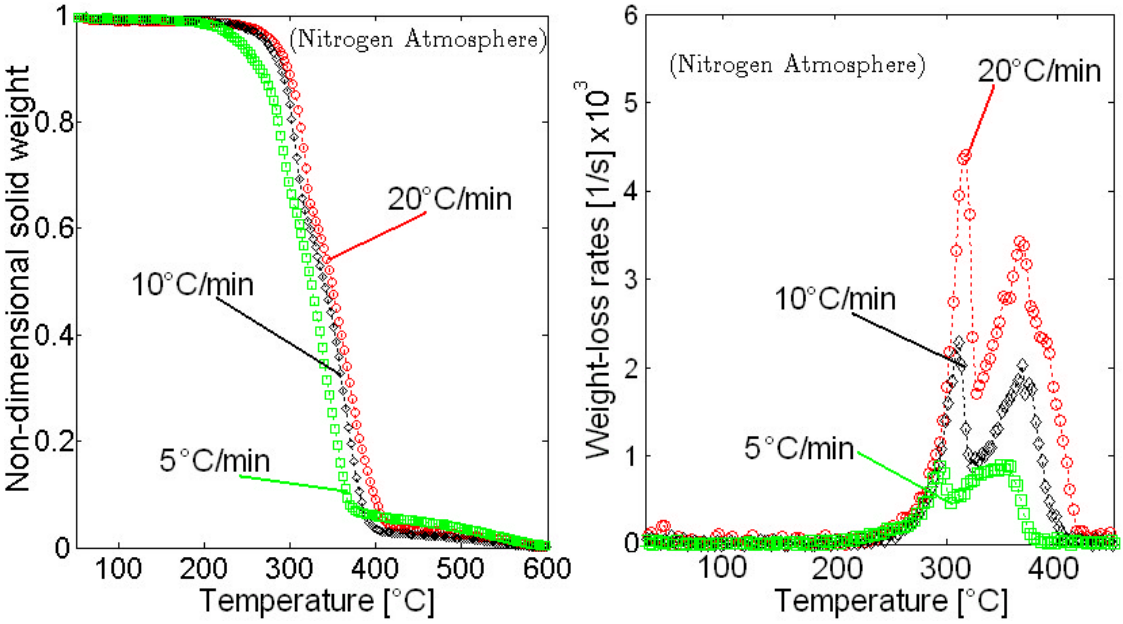

Figure 3.2. Polyurethane-foam thermogravimetric results in nitrogen as a function of temperature for three heating rates; left) solid mass; right) mass-loss rate. Experiments of Chao and Wang (2001a).

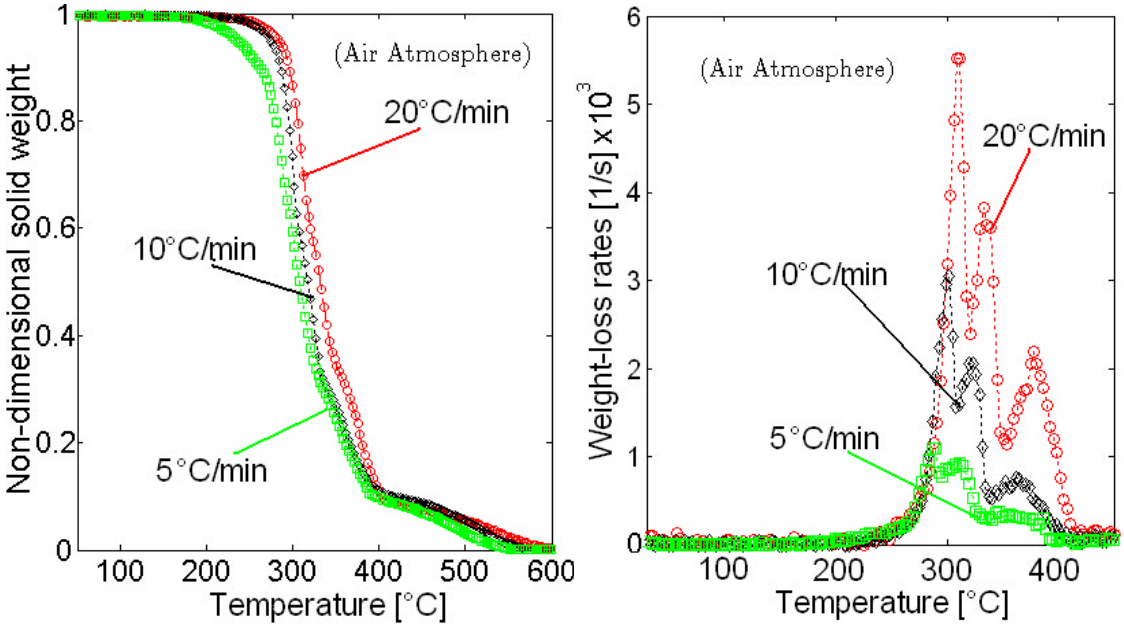

Figure 3.3. Polyurethane-foam thermogravimetric results in air as a function of temperature for three heating rates; left) solid mass; right) mass-loss rate. Experiments of Chao and Wang (2001a).

assumed to have the same kinetic parameters as a simplification. Also for simplicity the produced char in Eq. (3.6) is assumed to be the same species as the char produced by foam oxidation in Eq. (3.5). The solid product from the char oxidation is referred to as residue and not as ash because it can still react at higher temperatures (ash, as in Ohlemiller's mechanism, would imply no further reactivity). This residue oxidizes at temperatures between 450 and 600 °C, but this reaction was not included in the mechanism because it occurs at higher temperatures and is of little consequence to smolder propagation (Rogers and Ohlemiller 1980, Chao and Wang 2001b).

3.3 Mass-Loss Model and Kinetic Parameters

In order to implement the aforementioned mechanisms (3-step, Eqs. 3.1-3.3; and 5-step, Eqs. 3.4-3.7) in numerical models of smoldering, it is necessary to compute the reaction rates and thus requires obtaining the kinetic parameters of each reaction in a suitable form. These parameters are be different for each mechanism.

With multiple-reaction mechanisms such as the ones mentioned here for PU, the analytical methods to obtain kinetic parameters become inefficient or impossible to apply. Hence, a more general method is implemented in this section that can be applied to any mass-loss mechanism expressible in mathematical terms. The method consists in developing a mathematical model of mass-loss kinetics to simulate the decomposition of PU when heated. The results

are then compared with the experimental TG data until the kinetic parameters that provide the best agreement between predictions and experimental data are found. This methodology is efficient and simple, proving good results (Branca *et al.* 2003, Mamleev *et al.* 2000).

In TG experiments, the sample weight is very small, on the order of a few milligrams, and the flow rate of gases (*i.e.* nitrogen or air) into the chamber is high compared to the release rate of gaseous products from the degrading solid. Thus, transport effects can be neglected and oxygen concentration be assumed constant and uniform. With these assumptions, the equation governing the solid mass-loss rate can be expressed as:

$$\frac{d}{dt}\left(\frac{m}{m_0}\right) = \frac{dw}{dt} = \frac{dw_f}{dt} + \frac{dw_\beta}{dt} + \frac{dw_c}{dt} + \frac{dw_r}{dt} = \\ = (\nu_{\beta,p} - 1)\dot{\omega}_p + (\nu_{c,p\beta} - 1)\dot{\omega}_{p\beta} + (\nu_{c,o} - 1)\left(\dot{\omega}_o + \dot{\omega}_{o\beta}\right) + (\nu_{r,c} - 1)\dot{\omega}_c \tag{3.9}$$

Each one of the reaction paths described above is assumed to have an Arrhenius-type reaction rate of the form:

$$\dot{\omega}_i = A_i e^{-\frac{E_i}{RT}} w_i^{n_i} y_{O_2}^{\delta} \tag{3.10}$$

The TG experiments used here (Chao and Wang 2001a) only report results in either nitrogen or air, so there is not enough information to derive the oxygen reaction-order δ in Eq. (3.10). Consequently, the coefficient δ is set to 1 for oxidation reactions (*i.e.* first order reaction) and set to 0 in pyrolysis reactions (*i.e.* independence of oxygen).

The initial conditions for Eq. (3.9) are:

$$\begin{aligned} &w_f(0) = 1 \\ &w_\beta(0) = w_c(0) = w_r(0) = 0 \\ &T(0) = T_0 \end{aligned} \tag{3.11}$$

The temperature rise and the oxygen fraction are set equal to those in the experiments, and the expressions are:

$$\begin{aligned} &\frac{dT}{dt} = hr \equiv constant \\ &y_{O_2} = 0\ (N_2\ atm.)\ \ or\ \ y_{O_2} = 0.23\ (air\ atm.) \end{aligned} \tag{3.12}$$

The time integration of the mass-loss rate (Eq. 3.9) with the set conditions (Eqs 3.11 and 3.12) gives the solid mass w at any given time. The solution to this ODE requires a numerical stiff solver. When these equations are considered together with any mechanisms, they contain a number of kinetic parameters that need to be provided. It is proposed here that when not available in the literature, these parameters could be determined solving an inverse problem. The inverse problem consist in combining together the mass-loss model and an optimization technique to identify the set of kinetic parameters that best reproduces the mass-loss in the TG experiments. There are two different criteria to quantify the mass-loss disparity between the TG experimental measurements and the calculations for a given kinetic mechanism: one is to compare the solid-mass curve (left of Figs. 3.2 and 3.3), which offers accuracy for the stoichiometric yields and an overall description of the kinetic behaviour. The other criterion is to compare the mass-loss rate curve (right of Figs. 3.2 and 3.3), which offers more accuracy for the Arrhenius parameters (since it describes the location and intensity of each peak) and an overall description of the stoichiometric yields. The best technique would be to combine both criteria.

3.3.1. Trial-and-Error with the 3-step mechanism

The inverse problem is easier to solve when the simpler 3-step mechanism is used, and a straightforward method like trial-and-error can be applied. When Eq. (3.9) is solved with the 3-step mechanism in Eqs. (3.1-3.3), there are ten unknown kinetic-parameters: three activation energies E_i, three pre-exponential factors A_i, one reaction-order coefficient n_p, and three stoichiometric yields $\nu_{j,i}$ (see Table 3.1 for a list of all). In order to further reduce the dimensionality of the problem, the reaction-order coefficients n_c and n_o have been set equal to 1. The trial-and-error method consists on the variation one by one of the value of each parameter and compare the mass-loss result with the experiments until a reasonable agreement is achieved. The value of each parameter is varied within a range of reasonable values. First the best pyrolysis parameters are found using the TG curves in nitrogen atmosphere. Then these are fixed and the oxidation parameters are found using the TG curves in air atmosphere.

The TG measurements of Chao and Wang (2001a) for flexible PU foam at 10°C/min heating-rate are used to obtain the set of kinetic parameters. Only the solid-mass curve (w) is used determining the kinetic set. The resulting curves with the final parameters for the 3-step mechanism are presented in Fig. 3.4 for nitrogen atmosphere and Fig 3.5 for air atmosphere. It is seen that the mechanism is able to capture the overall TG behavior. The mechanism does not capture the mass-loss in air at temperatures between 450 and 600 °C, because

the ash is assumed inert and its oxidation was not included. Numerical values of all the kinetic parameters extracted are given in Table 3.1.

Table 3.1. Estimated kinetic and stoichiometric parameters for PU foam 3-step mechanism using trial-and-error.

Parameter	Value	Units
E_p	200	kJ/mol
$\log_{10}(A_p)$	15.7	$\log_{10}$(1/s)
n_p	3	-
$\nu_{c,p}$	0.05	kg/kg
E_o	155	kJ/mol
$\log_{10}(A_o)$	12.3	$\log_{10}$(1/s)
$\nu_{c,o}$	0.4	kg/kg
E_c	185	kJ/mol
$\log_{10}(A_c)$	13.6	$\log_{10}$(1/s)
ν_{ac}	0.3	kg/kg

These kinetic parameters provide solid-mass curves that are also in agreement with other TG experiments (Bilbao *et al.* 1996). In addition, integration of Eq. (3.8) with the kinetic values given by Rogers and Ohlemiller (1980) for air atmosphere results in a similar mass-loss curve as that presented by Chao and Wang (2001a) (Fig. 3.3, left). However, these authors combined foam pyrolysis and foam oxidation in one reaction path.

The 3-step mechanism with these kinetic parameters for PU has been found to give fairly good results when modeling smoldering propagation (Kelley and Schult 2006, and chapter 4 of this thesis). However, due to the consideration of a single pyrolysis-step, the mechanism predicts excessive mass-loss and performs poorly at different heating rates. The trial-and-error technique allows finding reasonably

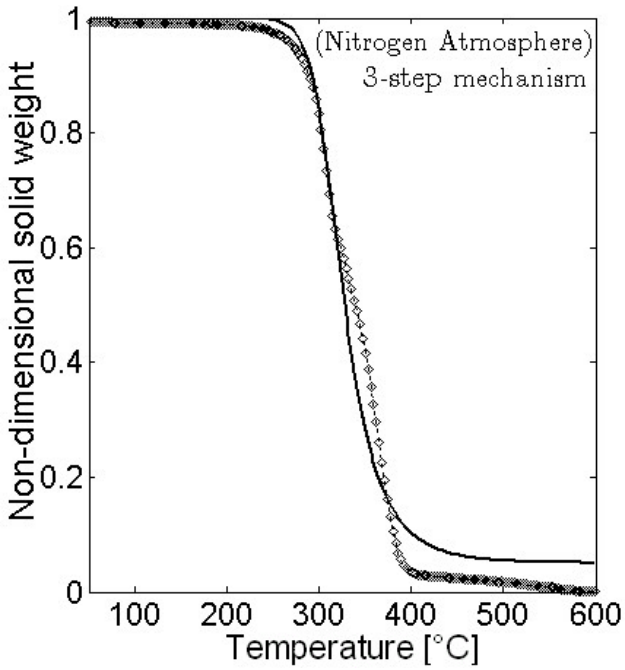

Figure 3.4. Polyurethane foam solid-mass in nitrogen as a function of temperature for the heating rates of 10°C/min. Line: 3-step mechanism calculations; Marks: experimental (Chao and Wang 2001a).

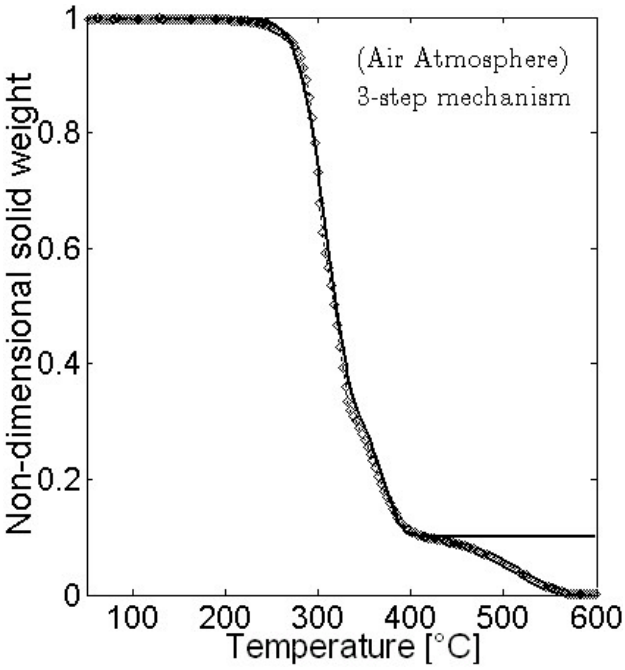

Figure 3.5. Polyurethane foam solid-mass in air as a function of temperature for the heating rates of 10°C/min. Line: 3-step mechanism calculations; Marks: experimental (Chao and Wang 2001a).

good parameters for the kinetics, but the process is time consuming and not efficient. Moreover, it is difficult to verify if the solution found is a global optimum.

3.3.2. Full Optimization with the 5-step mechanism

The 5-step mechanism is a significant improvement over the 3-step for the modeling of the kinetics and thus its performance must be explored in detail. The main setback with the 5-step mechanism is that the task to find good kinetic parameters becomes an important challenge. When Eq. (3.9) is solved with the 5-step mechanism in Eqs. (3.4-3.8) and it is assumed the same parameters for the foam and the β-foam oxidations, there are sixteen kinetic parameters: four activation energies E_i, four pre-exponential factors A_i, four reaction-order coefficients n_i, and four stoichiometric yields $\nu_{j,i}$ (see complete list in Table 3.3).

The solution to this inverse problem becomes too large a task, even for classical optimization tools. The high dimensionality of the problem produces a large search-space and very complicated landscapes for the optimization target, with numerous local maxima and minima. Furthermore, the inverse problem is ill-posed by its own nature. That is, uniqueness of the solution (the kinetic parameters set) is not guaranteed because very complex physical processes are being simulated with a quite simple kinetic model. For these reasons, a powerful and efficient multidimensional-optimization technique for non-linear problems, such as Genetic Algorithms, is needed.

3.4 Genetic Algorithms

A genetic algorithm (GA) is a heuristic search method that imitates the principles of biological adaptation (Goldberg 1989, Foster 2001). Its simple and robust mechanism of optimization is based upon the mechanics of the Darwinian theory of survival-of-the-fittest. GAs are a particular class of evolutionary algorithms developed in the 1970s which became widely used in many different fields only after large computer power became readily available in the 1980s. GAs have been applied to combustion chemical-kinetics with emphasis on homogeneous gas-reactions (Alander *et al.* 1994, Polifke *et al.* 1998, Elliott *et al.* 2004). Related to the present work, some papers have been published in heterogeneous reactions: catalytic reactions (Wolf and Moros 1997) and polymer curing (Garcia 1999).

In GAs, the candidate solutions represent the individuals in a population that evolves within a determined environment. In the particular application here to mass-loss kinetics, a candidate solution or individual will be a set of values of the kinetic parameters, and the environment will be the mathematical model and the experimental TG results. The procedure is the following. An initial population of individuals is randomly generated, then the population undergoes a process of selection such that only those giving the best description of the TG results (the fittest) of every generation are selected and survive. Children for the next generation are bred by reproduction from the parameter-set pool of the parents, plus random mutations. In general, the fittest individuals of any population tend

to reproduce and survive to the next generation, thus improving successive generations. GAs explore most of the search space and exponentially exploit promising regions through mutation, crossover and selection operations applied to individuals in the population. The method has a stochastic component to ensure wide exploration and to avoid getting trapped in local extrema.

Contrary to classical optimization methods for non-linear problems (trial and error, linearization, gradient method, Monte Carlo simulation and solution mapping), GAs can handle high multidimensionality, intricate or non-continuous objective-landscapes, multiple local optima, and noise in the data. Its primary advantages are: resistance to becoming trapped in local optima, efficient exploration of the parameter space, and no need to evaluate jacobian matrices. Its disadvantages are: heuristic in nature, inefficiency for small problems, and maybe not be the fastest method. GAs are capable of quickly finding promising regions of the search space but may take a relatively long time to reach a fine localized solution.

In this paper, the GA code used is GAOT (Houck *et al.* 1995) in a real-number implementation. Population sizes between 100 and 500 are used. In general, the higher the population is, the larger the explored search-space and convergence occurs in less generations but the computer time per generation increases. The adaptation of each parameter-set is measured with a fitness function which is defined here as the inverse of the error between the calculations and the experimental measurement:

$$\Phi = \left(\int \left| \frac{dW^{calc}}{dt} - \frac{dW^{exp}}{dt} \right| dT \right)^{-1} + \gamma \left(\int \left| W^{calc} - W^{exp} \right| dT \right)^{-1} \qquad (3.13)$$

The fitness accounts for errors both in the solid mass-loss rate dw/dt and in the solid mass w. The constant γ represents the relative influence on the fitness of the error in the mass over the influence of the error in the mass-loss rate. Its value is chosen by the user's convenience and set in this application to 50 for scaling of both fitness terms. The integrals in Eq. (3.13) are numerically evaluated in the range of temperature of the TG experiments (typically from room temperature to around 600 °C or higher). In principle the perfect solution would have an infinite fitness, but in this particular application, and due to noise in the data plus the imperfect fitting, the magnitude of the fitness is around 100. The algorithm is stopped when no further improvement of the fitness occurs after some hundreds of generations. Typically, convergence was achieved in less than 1000 generations, yielding a total computer time of about 10 hours on a year-2003 3.0-GHz standard PC.

3.5 Testing the Methodology against a Benchmark

Before the above methodology is applied to PU, the effectiveness of the method is tested by applying it to a specific problem. The thermal degradation of cellulose is chosen as the benchmark because it has simpler and well-known kinetics (Grønli *et al.* 1999). TG results for cellulose at a heating rate of 5 °C/min in nitrogen atmosphere (Fig. 3.8) were chosen as the best available data to be used in the test. The data are taken from the work by Grønli *et al.* 1999 (curve #7) on cellulose pyrolysis, which is a round-robin study where different

laboratories provided TG data and estimated kinetic-parameters of the same material (Avicel-PH105).

The mathematical mass-loss model presented above was modified to fit the cellulose pyrolysis scheme, which is fairly well described by a single-step, first order, pyrolysis reaction:

$$\frac{d}{dt}\left(\frac{W}{W_0}\right)=\frac{d}{dt}\left(\frac{W_{cell}}{W_0}\right)+\frac{d}{dt}\left(\frac{W_c}{W_0}\right)=(\nu_{c,p}-1)\dot{\omega}_p \tag{3.10}$$

$$\dot{\omega}_p = A_p e^{-\frac{E_p}{RT}} \frac{W_{cell}}{W_0} \tag{3.11}$$

The results from applying the methodology to this problem can be used to illustrate an exemplar application. Evolution of the best fitness (*i.e.* performance of the best parameter-set found at each generation) in one of the runs is presented as an example in Fig. 3.6, which shows that the improvement is very fast at the beginning and tends toward convergence in the long term. Fig. 3.7 shows the performance of all the individuals attempted by the GA during a typical search in the mass-loss/temperature space. This figure illustrates how initial individuals perform poorly, but as generations proceed, new individuals provide improved mass-loss curves that eventually converge to the experimental results.

The optimized parameters and the results are shown in Table 3.2 and Fig. 3.8. It is seen that the simulated TG curve fits the experimental curve over the entire temperature range. Moreover, the parameters estimated are in excellent agreement with those reported in the benchmark (Grønli *et al.* 1999) which were determined using an analytical method.

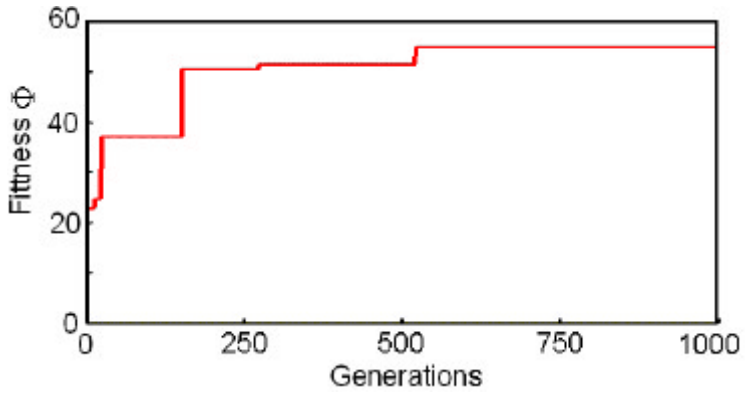

Figure 3.6. Evolution with generations of the best fitness found by the genetic algorithm during a typical search for cellulose kinetics.

Table 3.2. Kinetic and stoichiometric parameters for cellulose and comparison with TG benchmark (curve #7 in Grønli *et al.* 1999).

Parameter	GA	TG Benchmark	TG Scatter	GA-TG Difference	Units
E_p	236	241	12 %	2 %	kJ/mol
$\log_{10}(A_p)$	18.4	18.8	17 %	2 %	$\log_{10}(1/s)$
$\nu_{c,p}$	0.050	0.052	90 %	4 %	-

Grønli *et al.* (1999) reported significant scatter among the measured mass-loss curves provided by the different laboratories due to experimental errors in sample size, heating rate, thermal lag and the instruments used. This experimental scatter subsequently induced variations in the kinetic parameters

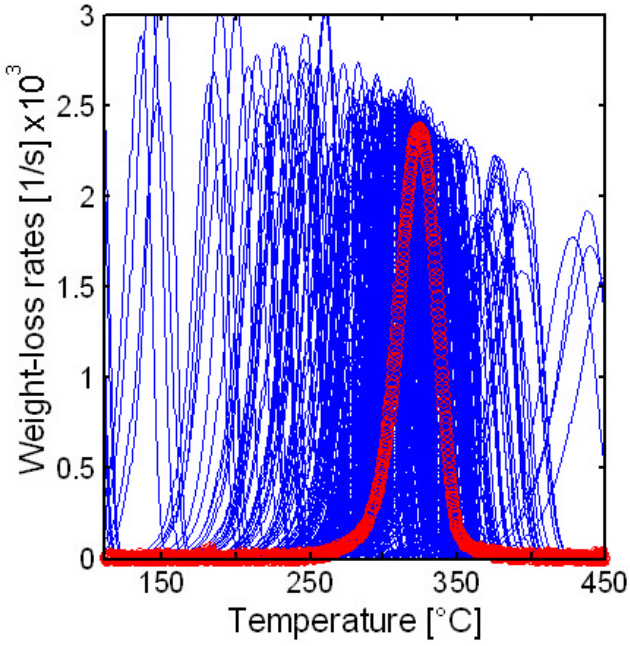

Figure 3.7. Mass-loss behavior of all the individuals attempted by the genetic algorithm during a typical search for cellulose kinetics. Circles are the TG experimental results of Grønli *et al.* (1999) (curve #7).

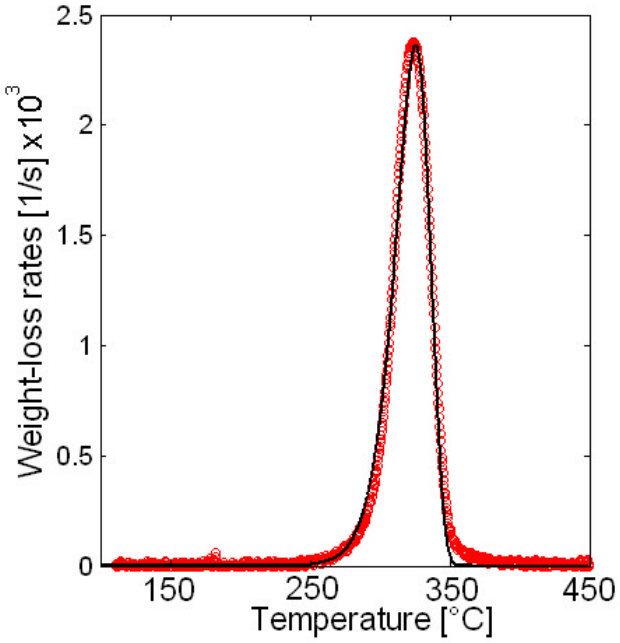

Figure 3.8. Cellulose mass-loss rate in nitrogen as a function of temperature for a heating rate of 5 ℃/min. Marks are experiments (Grønli *et al.* 1999, curve #7); Lines are numerical.

they estimated. These variations are reported in Table 3.2 as TG scatter. The differences between the benchmark values and the GA-estimated values are also presented in Table 3.2. It is seen that these differences are significantly lower than the induced variations due to TG scatter. This comparison suggests that with respect to the analytically based method used in the benchmark, the difference introduced by the application of GAs is significantly lower than the associated experimental error in TG.

3.6 Application to the 5-step mechanism of Polyurethane Foam

In this section, the proposed methodology is applied to determine the kinetic parameters of PU thermal-decomposition using the 5-step mechanism in Eqs. (3.4-3.8). The TG measurements of Chao and Wang (2001a) for flexible PU foam are used. Test in nitrogen give information on the pyrolysis paths only (Fig. 3.2), and in air on the pyrolysis and oxidation paths together (Fig. 3.3).

Analysis of available experimental data on the smoldering of PU (Bar-Ilan *et al.* 2004a) shows that the temperature variation rate (*i.e.* heating rate) of the virgin foam produced by the propagating front ranges between 1 and 150 °C/min, with an average about 50 °C/min. For this reason, the heating rate of 20 °C/min (the highest available from the TG data) was chosen to obtain the kinetic parameters. The other two heating rates (5 and 10 °C/min) were used as blind predictions for validation and to test the suitability of the parameters for extrapolation to different heating rates.

The results of applying the genetic algorithms methodology to predict the TG results of PU are presented in Figs. 3.9 and 3.10. It is seen that the 5-reaction mechanism is able to capture the position and magnitude of the peaks in the mass-loss rate curves, demonstrating its capabilities at different heating rates and gas atmospheres. Numerical values of all the kinetic parameters extracted are given in Table 3.3.

Table 3.3. Estimated kinetic and stoichiometric parameters for PU foam 5-step mechanism using genetic algorithms.

Parameter	Best	Range	Units
E_p	148	[136, 160]	kJ/mol
$\log_{10}(A_p)$	11.3	[10.4, 12.5]	$\log_{10}$(1/s)
n_p	0.21	[0.13, 0.31]	-
$\nu_{\beta,p}$	0.70	[0.69, 0.71]	kg/kg
$E_{p\beta}$	124	[121, 127]	kJ/mol
$\log_{10}(A_{p\beta})$	8.2	[7.8, 8.5]	$\log_{10}$(1/s)
$n_{p\beta}$	1.14	[1.12, 1.18]	-
$\nu_{c,p\beta}$	0.05	[0.04, 0.06]	kg/kg
E_o	194	[161, 220]	kJ/mol
$\mathrm{Log}_{10}(A_o)$	15.4	[12.6, 16.7]	$\log_{10}$(1/s)
n_o	0.52	[0.47, 0.69]	-
$\nu_{c,o}$	0.57	[0.55, 0.57]	kg/kg
$E_{o\beta}$	194	[161, 220]	kJ/mol
$\mathrm{Log}_{10}(A_{o\beta})$	15.4	[12.6, 16.7]	$\log_{10}$(1/s)
$n_{o\beta}$	0.52	[0.47, 0.69]	-
$\nu_{c,o\beta}$	0.57	[0.55, 0.57]	kg/kg
E_c	201	[193, 220]	kJ/mol
$\log_{10}(A_c)$	15.2	[14.5, 16.7]	$\log_{10}$(1/s)
n_c	1.23	[1.10, 1.49]	-
$\nu_{r,c}$	0.23	[0.21, 0.25]	kg/kg

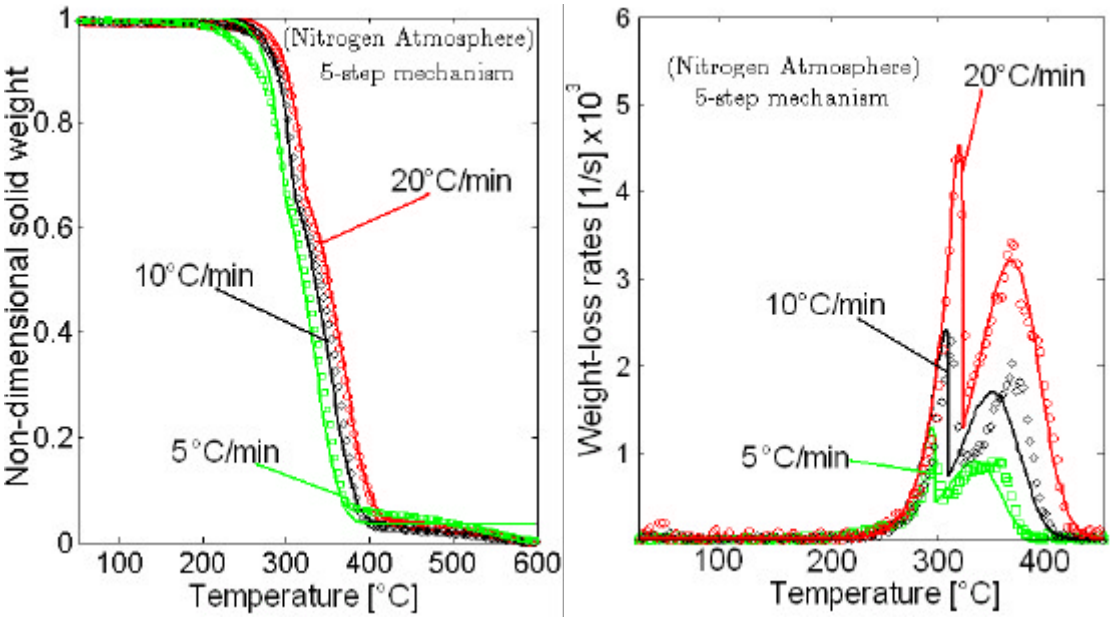

Figure 3.9. Polyurethane-foam kinetic behavior in nitrogen as a function of temperature for three heating rates, left) solid mass; right) mass-loss rate. Lines: 5-step mechanism calculations; Marks: experimental (Chao and Wang 2001a).

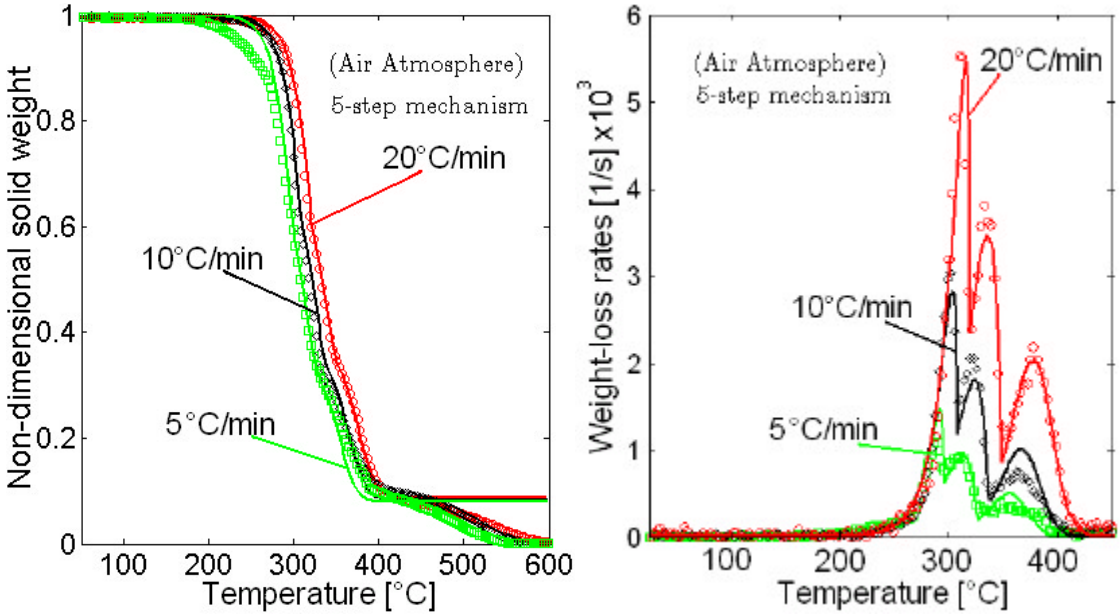

Figure 3.10. Polyurethane-foam kinetic behavior in air as a function of temperature for three heating rates, left) solid mass; right) mass-loss rate. Lines: 5-step mechanism calculations; Marks: experimental (Chao and Wang 2001a).

The effects of each reaction in the mechanism (Eqs. 3.4-3.8) on the simulated TG results are explored in Figs. 3.11 and 3.12, which show the calculated reaction rates $\dot{\omega}_i$ at a heating rate of 20 °C/min. In nitrogen atmosphere (Fig. 3.11), the virgin foam pyrolysis produces the first peak in the TG mass-loss shown in Fig. 3.9, and the β-foam pyrolysis produces the second peak. There is some overlap of the pyrolysis paths between 290 and 320 °C/min. Evidently, no oxidation takes place in nitrogen atmosphere. In air (Fig. 3.12), the competing reactions of pyrolysis and oxidation of the virgin foam overlap completely, producing the first peak in the TG mass-loss rate shown in Fig. 3.8 between 200 and 330 °C. In air most of the virgin foam is pyrolyzed rather than oxidized and β-foam pyrolysis has low intensity. In a similar way, the competing reactions of pyrolysis and oxidation of the β-foam overlap completely too producing the second peak in the TG mass-loss rate shown in Fig. 3.8 between 270 and 350 °C. Fig. 3.12 shows that in air, most of the virgin foam is pyrolyzed rather than oxidized, whereas most of the β-foam is oxidized rather than pyrolyzed. The oxidation of the char takes place between 300 °C and 420 °C.

Values of the stoichiometric parameters in Table 3.3 can also be used to interpret the mass-yields of species and gases. Pyrolysis of the virgin foam would yield roughly one-third as gas, whereas pyrolysis of the β-foam would yield little char and thus most of it becomes gas. Foam and β-foam oxidation both would yield roughly half gas and haft char, whereas char oxidation would have a very small yield of solid residue.

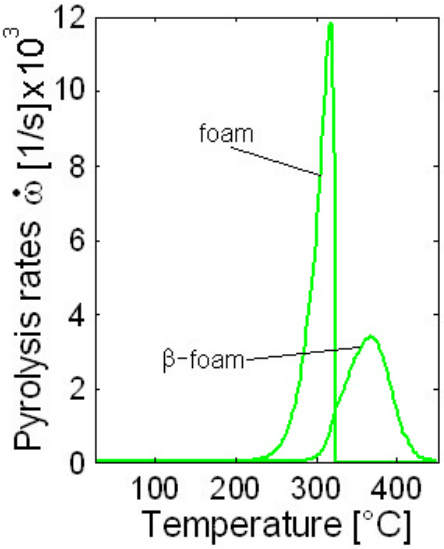

Figure 3.11. 5-step mechanism simulated polyurethane mass-loss pyrolysis reaction-rates $\dot{\omega}_i$ in nitrogen atmosphere, as a function of temperature for 20 ℃/min heating-rate.

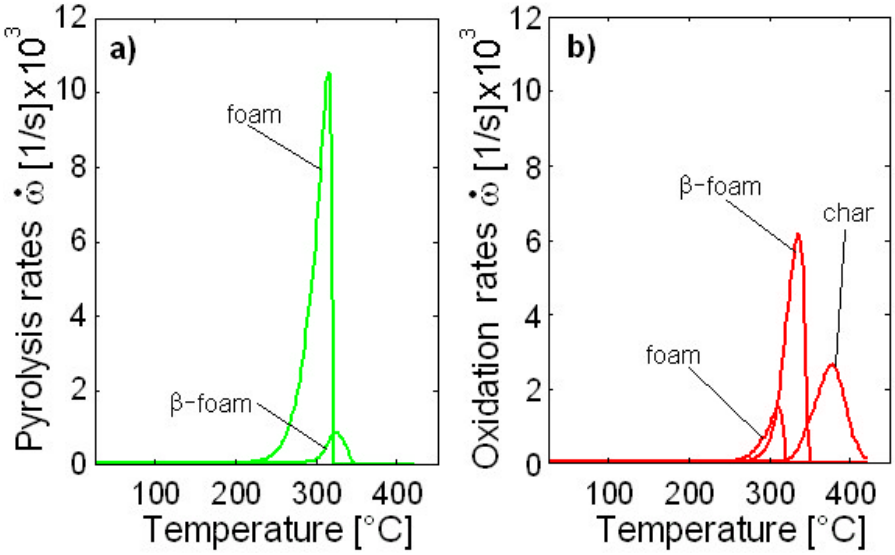

Figure 3.12. 5-step mechanism simulated polyurethane mass-loss reaction-rates $\dot{\omega}_i$ in air atmosphere for; a) pyrolysis; and b) oxidations, as a function of temperature for 20 ℃/min heating-rate.

The uniqueness of the solution (uniqueness of the kinetic-parameter set) is always a concern in inverse problems. To resolve the issue, two approaches are followed; one is to verify the predictions at the other two heating rates (blind predictions); and the other is to determine confidence limits by expressing the solution for each parameter as the value of the fittest individual accompanied by the range of values of other well-fitted individuals (top 10% of the end population). The estimated values for the pre-exponential factors and the activation energies are considerably sensitive to the optimization conditions, and thus their wide confidence limits. This sensitivity is expected (Grønli *et al.* 1999), but it is found that significant differences in the values of the kinetic parameters yield small differences in the simulated TG curves. Also, the parameters show interdependence; the upper bound for the pre-exponentials correspond to the upper bound of the activation energies, and so do the lower bounds. Lower values of the pre-exponential factor are compensated for by slightly lower values of the activation energy. The results show that the interdependence is particularly strong and linear ($R^2 > 0.97$) in the cases of the foam pyrolysis and the char oxidation. Their respective trends inside the ranges shown in Table 3.3 are in the form of:

$$\log_{10}(A_p) = -2.40 + 0.093E_p \tag{3.14}$$

$$\log_{10}(A_c) = -1.56 + 0.083E_c \tag{3.15}$$

Where A_i is expressed in [1/s] and E_i in [kJ/mol]. This interdependence of the values is called “kinetic compensation effect” and has been long-observed to occur in the estimation of kinetic parameters from TG experiments (Chornet

and Roy 1980, Koga 1995). This linear interdependence results from the interaction between the mathematical nature of the Arrhenius-reaction rates and some physicochemical and experimental factors (Koga 1995).

This mechanism does not capture the small mass-loss that occurs in air at temperatures between 450 and 600 °C. As mentioned before, this secondary oxidation reaction was not included because it is of little consequence to smolder propagation (Rogers and Ohlemiller 1980). Moreover, this secondary oxidation consumes one-order of magnitude higher oxygen mass per reactant mass than the first oxidation (Chao and Wang 2001b) so the reaction might be controlled by oxygen transport rather than by chemical kinetics, in which case it would not be applicable in the mathematical kinetic-model (Eq. 3.9 and 3.10).

3.7 Application of the Kinetics to Model Smoldering Structure

To determine the capabilities of the 5-step mechanism and the obtained parameters to predict the characteristics of a smolder reaction, a propagating smolder-front is modeled to study the predicted structure of the different species in the vicinity of the front, and the role of each of the reactions in this structure.

As mention in Chapter 1 of this thesis, one-dimensional propagation of smoldering is classified as either forward or opposed (Fig. 1.3). These propagation modes differentiate from each other by the heat and mass transfer

characteristics and thus have essential differences in the role played by each reaction (Ohlemiller and Lucca 1983). Conventional models of PU smoldering use different kinetic schemes depending on the propagation mode. Forward smolder is generally described as having both the pyrolysis and oxidation reactions independently included in the mechanism (Dosanjh and Pagni 1987, Schult *et al.* 1996, Buckmaster and Lozinski 1996, Torero and Fernandez-Pello 1996), whereas in opposed they are lumped together in a global single reaction (Ohlemiller *et al.* 1979, Dosanjh *et al.* 1987, Torero *et al.* 1993, Schult *et al.* 1995, Lozinski and Buckmaster 1995). By considering a 5-reaction mechanism a smolder model should be able to simulate the smolder behavior in both forward and opposed configurations.

In order to verify this, a smolder front is modeled to study the role of each reaction in the PU smolder process. The model is one-dimensional and steady state, and only solves the species equations since they incorporate directly the reaction rates. The energy equation is replaced with a prescribed temperature distribution ahead of and behind the propagating smolder front. The former is obtained fitting the theoretical temperature distribution from Decker and Schult (2004) with previous experimental results for both opposed and forward smolder propagation. Behind the smolder front the temperature is set constant to the maximum smolder temperature in the experiments, because of the assumption of no heat losses. A constant gas velocity is considered to flow through the porous material and it is assumed that the gas and solid phases are in thermal equilibrium. The corresponding boundary value problem is given in nondimensional form by the following system of ODEs.

Mass fraction of oxygen in the gas phase:

$$\frac{dy_{O_2}}{d\xi} = \frac{\rho_s}{\rho_g}\frac{L}{\tau(u_{sml}+u_g)}\sum_i \nu_{O_2,i}\dot{\theta}_i = \frac{\rho_s}{\rho_g}\frac{1}{Da_g}\left(\nu_{O_2,o}\dot{\theta}_o + \nu_{O_2,o\beta}\dot{\theta}_{o\beta} + \nu_{O_2,c}\dot{\theta}_c\right) \quad (3.16)$$

Mass fraction of solid species j:

$$\frac{d}{d\xi}\left(\frac{W_j}{W_0}\right) = \frac{L}{\tau u_{sml}}\sum_i \nu_{j,i}\dot{\theta}_i = \frac{1}{Da_s}\sum_i \nu_{j,i}\dot{\theta}_i \quad (3.17)$$

Where u_{sml} is the smolder-front propagation velocity, u_g the gas velocity and $\dot{\theta}_i = \tau A_i e^{-\frac{E_i}{RT}}\left(\frac{W_i}{W_0}\right)^{n_i} y_{O_2}^{\delta}$ is the non-dimensional reaction-rate. The characteristic time τ is defined by scaling the order of magnitude of $\dot{\theta}_i$.

The boundary conditions and the temperature profile for each propagation mode are set following conditions illustrated in Fig. 3.13. For forward propagation:

$$\begin{aligned} &y_{O_2}(\xi=-\infty) = 0.23 \\ &\frac{W_f}{W_0}(\xi=\infty) = 1 \\ &\frac{W_\beta}{W_0}(\xi=\infty) = \frac{W_c}{W_0}(\xi=\infty) = \frac{W_r}{W_0}(\xi=\infty) = 0 \end{aligned} \quad (3.18)$$

$$\Pi_{fwd} = \begin{cases} 1 & \xi \le 0 \\ \exp(-\alpha_{fwd}\xi) & \xi > 0 \end{cases} \quad (3.19)$$

and for opposed:

$$\begin{aligned} &y_{O_2}(\xi=-\infty) = 0.23 \\ &\frac{W_f}{W_0}(\xi=-\infty) = 1 \\ &\frac{W_\beta}{W_0}(\xi=-\infty) = \frac{W_c}{W_0}(\xi=-\infty) = \frac{W_r}{W_0}(\xi=-\infty) = 0 \end{aligned} \quad (3.20)$$

$$\Pi_{opp} = \begin{cases} \exp(\alpha_{opp}\xi) & \xi < 0 \\ 1 & \xi \geq 0 \end{cases} \quad (3.20)$$

Where the nondimensional temperature is defined as $\Pi = (T - 300)/(T_{sml} - 300)$, and $\alpha = L/L_t$ is the ratio of the smolder-front characteristic-thickness to the thermal characteristic-thickness.

Table 3.4. Scale variables for the smoldering propagation model

Parameter	Value	Units	Reference
u_g	3	mm/s	(Bar-Ilan *et al.* 2004)
T_{sml} (forward)	680	K	(Bar-Ilan *et al.* 2004b)
u_{sml} (forward)	-0.15	mm/s	(Bar-Ilan *et al.* 2004b)
α_{fwd}	1.25	-	(Bar-Ilan *et al.* 2004b)
T_{sml} (opposed)	690	K	(Bar-Ilan *et al.* 2004a)
u_{sml} (opposed)	0.19	mm/s	(Bar-Ilan *et al.* 2004a)
α_{opp}	0.71	-	(Bar-Ilan *et al.* 2004a)
$\nu_{O_2,o}$ and $\nu_{O_2,o\beta}$	0.08	-	based on results
$\nu_{O_2,c}$	0.30	-	based on results
ρ_s	26.4	kg/m^3	(Chao and Wang 2001)
τ	10.9	s	scaling
L	20	mm	scaling

To apply Eq. (3.16) it is needed to know first the mass consumptions of oxygen for the oxidation reactions in Eqs. (3.6-3.8), namely $\nu_{O_2,o}$, $\nu_{O_2,o\beta}$ and $\nu_{O_2,c}$. These values are not available in the literature and thus the results of the model were used to determine them. First, it is assumed than $\nu_{O_2,o}$ and $\nu_{O_2,o\beta}$ are equal. Based on the numerical predictions, the chosen values were those resulting in the oxidation reactions occurring near the location of the peak temperature. These values (Table 3.4) are in the same order of magnitude that

the reported values in the numerical model of smoldering with the 3-step mechanism in Chapter 4 of this thesis. The other parameters used in the model, given also in Table 3.4, are either extracted from previous studies of PU smoldering in microgravity, or selected from proper scaling.

3.8 Results and Discussion

Results of the spatial profiles for the reaction rates and species mass-fractions in the smolder front can be seen in Fig. 3.15 (forward) and Fig. 3.16 (opposed). It is seen that the model predicts that both fronts consume all the incoming oxygen as observed experimentally (Ohlemiller 1985, Bar-Ilan *et al.* 2004a, Torero and Fernandez-Pello 1996, Torero *et al.* 1993). Considerable differences can be observed in the smolder front structure for the two propagation modes.

In forward smolder (Fig. 3.15), the oxidation and the pyrolysis reactions form two distinct propagating fronts: the pyrolysis front moving ahead and the oxidation front moving behind. This result is in agreement with experimental observation of forward smolder (Bar-Ilan *et al.* 2004b, Torero and Fernandez-Pello 1996). Forward smolder results in virtually no oxidation of the virgin foam, as all of it is converted to β-foam. The β-foam is subsequently consumed by pyrolysis and oxidation. Also, there is a small fraction of char left behind the front. This is because the assumption of no heat-loss produces an upstream region of high temperature where oxygen concentration is also high, so the char oxidation step is vigorous, and all the char is converted to solid residue. This mechanism is

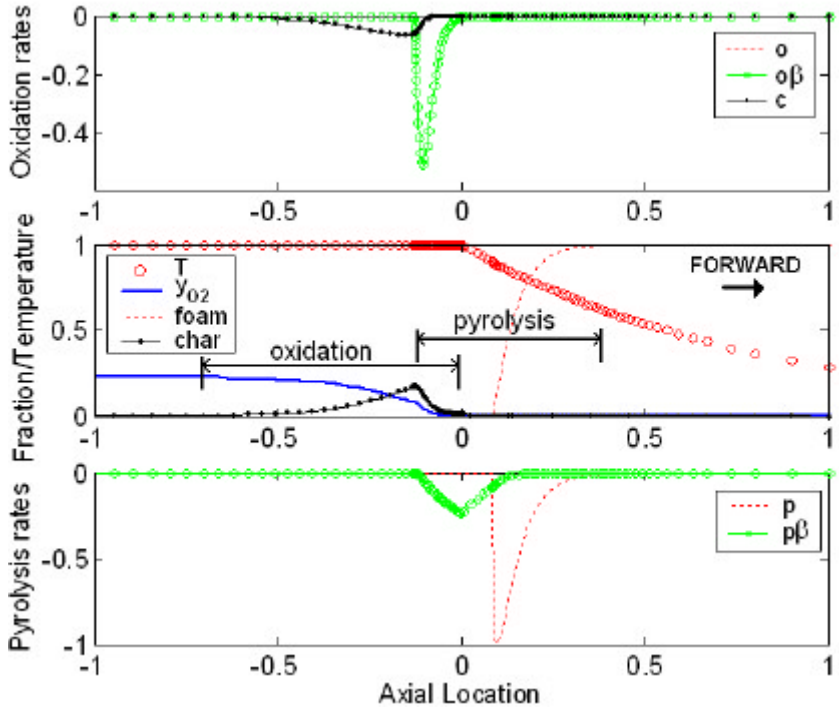

Figure 3.15. Results for the front structure of forward smolder in polyurethane foam.

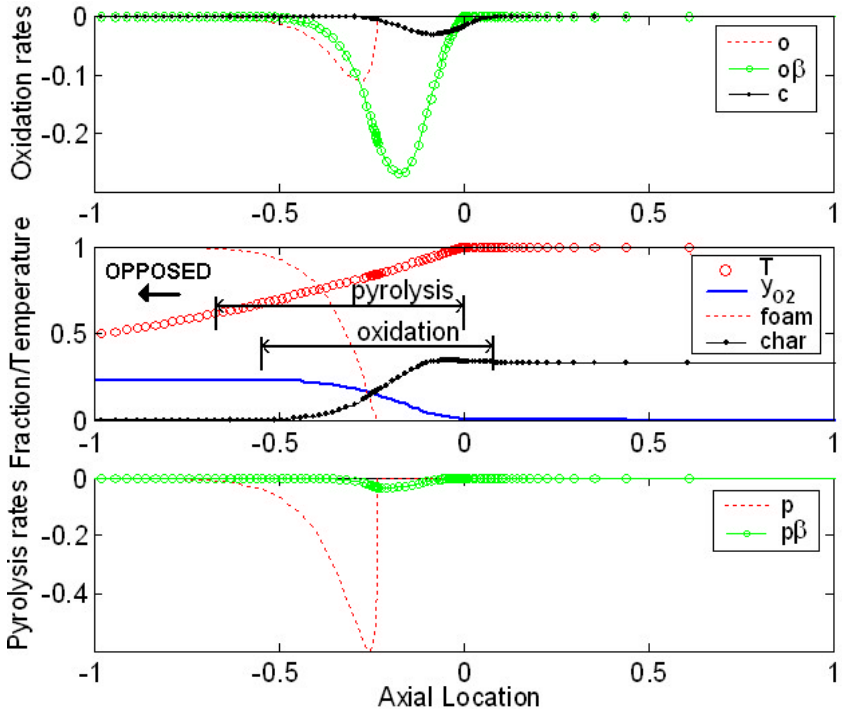

Figure 3.16. Results for the front structure of opposed smolder in polyurethane foam.

potentially coupled to the transition from smoldering to flaming, since transition has strong links with the highly exothermic char-oxidation and residue (secondary char) oxidation reactions. In contrast, in opposed smolder (Fig. 3.16) the oxidation and the pyrolysis reactions overlap to form one single front. This result is also in agreement with experimental observations, where the propagation front appears as one single smolder-front (Bar-Ilan *et al.* 2004a, Torero *et al.* 1993). The degradation of the virgin foam occurs via both pyrolysis and oxidation reactions but is dominated by the former. The β-foam is mainly consumed by the oxidation path rather than by its competing pyrolysis path. In opposed smolder, there is a higher char fraction left behind the front than in forward smolder, which is also in agreement with experimental observations (Bar-Ilan *et al.* 2004a, Torero *et al.* 1993). This is due to the starvation of oxygen occurring before the char oxidation is complete.

3.9 Conclusions

The determination of solid-phase pyrolysis and oxidative kinetics by correlating a reaction mechanism of thermal and oxidative degradation with thermogravimetric data has been demonstrated. With the simple trial-and-error technique, it was possible to find fairly good kinetic parameters for the 3-step mechanism proposed by Ohlemiller. Together with the powerful optimization technique of genetic algorithms, it is found that the new 5-step mechanism proposed here and the calculated kinetic-parameters work very well for the

prediction of thermogravimetric data at different heating rates and gas atmospheres. Moreover, the mechanism and its parameters are able to model smolder propagation.

Using the proposed 5-step mechanism in a simplified model of smolder propagation shows that it is possible to predict at least phenomenologically the experimental observations of the species distributions in both opposed and forward smolder. This result could be very useful in the development of numerical models of smoldering combustion, especially in multidimensional simulations where distinction between forward and opposed modes is no longer rigorous.

The validity of the application of TG-estimated parameters outside the realm of TG presents some controversies (Schneider 1992, Galwey 2004). These controversies arose from the significant discrepancies encountered in the kinetic parameters derived from different studies of the same material. In spite of this, TG remains the experimental technique offering the most reliable data to estimate kinetic parameters (Grønli *et al.* 1999).

The methodology proposed here can be applied to other solid materials, or to estimate other not easily available material-properties, such as enthalpies of reaction from calorimetry experiments. In addition to the application to smoldering combustion, the kinetic mechanisms developed here are applicable to study the disposal of PU wastes by thermal degradation; pyrolysis or incineration (Kaminsky 1985).

Chapter 4

Model of Forward Smoldering Combustion with 3-step Kinetics

"things should be made as simple as possible, but not any simpler"

Albert Einstein (1879-1955).

4.1. Introduction

Smoldering combustion is controlled by strong interactions between heat, mass and momentum transports and heterogeneous chemical reactions in porous media. Numerical models of the ignition and propagation of smoldering combustion provide means of identifying and quantifying the smolder-controlling mechanisms and are especially useful to understand experimental observations. In addition, they are a cost-effective complement to experimentation, in particular under special circumstances as it is the case in microgravity environments. Space-based smoldering experiments are scarce and unique

because of their high cost and consequently it is of great importance to use modeling approaches to extend the limited microgravity data to different configurations, thermal and flow conditions, and fuels. Moreover, under microgravity conditions, there is no transport by buoyancy and thus the flow field is simplified and easier to model.

Transient one-dimensional models, while using a simplified representation of the spatial domain, are able to reproduce the interactions between these phenomena with accuracy and to provide useful insights of the process if the main physical mechanisms are modeled. Leach *et al.* (2000) developed a one-dimensional numerical model of forward smoldering with a 3-step kinetic mechanism. This model was an extension of an early version of opposed smoldering (Leach *et al.* 1997, Leach *et al.* 1998). The model in Leach *et al.* (2000) performed relatively well but left some room for improvements. For example, they used the kinetics parameters of cellulose and did not include buoyancy, but the model was calibrated with PU (polyurethane) normal-gravity experiments. Some improvements of their model are addressed here with the inclusion of PU kinetic parameters and the effect of heat losses in the perpendicular direction. The results of the model are calibrated and then compared to the only microgravity experimental data available. These microgravity experiments (Bar-Ilan *et al.* 2004a) were conducted aboard the NASA Space Shuttle missions STS-105 and STS-108.

4.2. Numerical Model

The model solves the one-dimensional time-dependent conservation equations for the solid and the gas. The computational domain follows the forward configuration; forced airflow and ignition are imposed at the same boundary. As a result the reaction front moves in the same direction as the airflow (from right to left). The computational domain and boundary conditions are shown in Fig. 4.1.

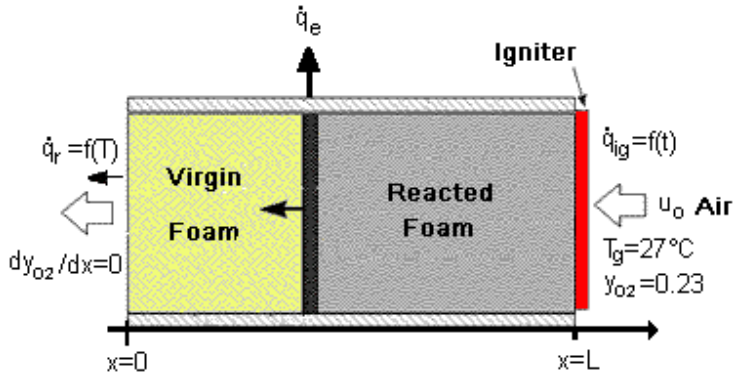

Figure 4.1: Computational domain and boundary conditions imitating the experimental setup in Bar-Ilan *et al.* (2004a). The reaction front moves in the same direction as the oxidizer flow.

The conservation equations solved are; solid-phase energy Eq. (4.1), solid-phase species Eqs. (4.2)-(4.4), gas-phase energy Eq. (4.5), gas-phase continuity Eq. (4.6), oxygen in the bulk gas Eq. (4.7) and oxygen at the surface Eq. (4.8). Radiative heat transfer inside the porous media is included into the conductivity k_s assuming the optically thick limit. Heat and oxygen transport from the solid surface to the bulk gas is taken into account so that the gas and the solid phases are not assumed to be in thermal or chemical equilibrium. Radial heat losses to the surrounding environment are modeled through a volumetric heat transfer

coefficient U_e. The chemical reactivity of the solid is modeled with a 3-step chemical mechanism with the kinetic parameters for PU (see section 4.4). The properties of the solid-phase are weight averaged for the three solid species considered; foam, char and ash. Buoyant-induced flows are not modeled, so the simulations are in microgravity conditions. More details of the computational model are available in Leach *et al.* (2000).

$$\rho_s c_s \frac{\partial T_s}{\partial t} = \frac{\partial}{\partial x}\left(k_s \frac{\partial T_s}{\partial x}\right) - \dot{\omega}_o \rho_f \Delta h_o - \dot{\omega}_p \rho_f \Delta h_p - \dot{\omega}_c \rho_c \Delta h_c + \\ + h_{gs} \frac{A_{gs}}{V}\left(T_g - T_s\right) + U_e \frac{A_L}{V}\left(T_0 - T_s\right) \tag{4.1}$$

$$\frac{\partial w_f}{\partial t} = -\dot{\omega}_p - \dot{\omega}_o \tag{4.2}$$

$$\frac{\partial w_c}{\partial t} = \nu_{c,p}\dot{\omega}_p + \nu_{c,o}\dot{\omega}_o - \dot{\omega}_c \tag{4.3}$$

$$\frac{\partial w_a}{\partial t} = \nu_{a,c}\dot{\omega}_c \tag{4.4}$$

$$\phi \rho_g c_{pg}\left(\frac{\partial T_g}{\partial t} + u\frac{\partial T_g}{\partial x}\right) = \phi k_g \frac{\partial^2 T_g}{\partial x^2} + h_{gs}\frac{A_{gs}}{V}\left(T_s - T_g\right) \tag{4.5}$$

$$\frac{\partial}{\partial t}(\rho_g \phi) + \frac{\partial}{\partial x}(\rho_g \phi u) = \phi\left[\dot{\omega}_p \rho_f \nu_{g,p} + \dot{\omega}_o \rho_f (\nu_{g,o} - \nu_{O_2,o}) + \dot{\omega}_c \rho_c (\nu_{g,c} - \nu_{O_2,c})\right] \tag{4.6}$$

$$\frac{\partial}{\partial t}\left(\rho_g \phi y_{O_2}\right)_b + \frac{\partial}{\partial x}\left(\rho_g \phi u y_{O_2}\right)_b + \frac{\partial}{\partial x}\left(\rho_g \phi y_{O_2} V_{O_2}\right)_b = \\ = -h_m \frac{A_{gs}}{V}\left(y_{O2} - y_{O_2,su}\right) \tag{4.7}$$

$$\frac{\partial}{\partial t}\left(\rho_g \phi y_{O_2}\right)_{su} + \frac{\partial}{\partial x}\left(\rho_g \phi y_{O_2} V_{O_2}\right)_{su} = \\ = -\dot{\omega}_o \rho_f \nu_{O_2,o} - \dot{\omega}_c \rho_c \nu_{O_2,c} + h_m \frac{A_{gs}}{V}\left(y_{O_2} - y_{O_2,su}\right) \tag{4.8}$$

The computational domain and the boundary conditions imitate those described in the microgravity experiments of Bar-Ilan *et al.* (2004a). At $t = 0$, the entire fuel bed is unreacted and the temperature of the solid and the gas is 27 °C. The ignition protocol of the sample is applied to the right boundary ($x = L$) by imposing at that location a constant heat flux during 400 s. The imposed heat flux is such that the temperature rise with time at the igniter location is the same as in the experiments. The thermal boundary condition after the ignition protocol is that heat is lost to the ambient through a heat-loss coefficient h_L. During the ignition, the inlet flow velocity at $x = L$ is 0.01 mm/s. After ignition, the inlet flow velocity is set to the corresponding nominal value (always significantly higher than 0.01 mm/s) and kept constant thereafter. Inlet gas temperature and composition at $x = L$ are kept constant at all times. At the left boundary ($x = 0$), the by-product gases exit the computational domain and the thermal boundary condition is that heat is lost to the surrounding through a heat-loss coefficient h_0. The equations are discretized in the space domain using finite differences and solved with time using the stiff integrator VODE (Brown *et al.* 1989).

4.3. Analytical Calculation of the Radial Heat Losses

Heat losses from the reaction front have been identified as one the controlling mechanism of smolder propagation (Ohlemiller 1985, Bar-Ilan *et al.* 2004a). The convective heat losses from the solid to the flowing gas were included in the

model of Leach *et al.* (2000), but not the heat losses in the radial (perpendicular) direction. In this work, the radial heat-losses to the surrounding environment have been analytically calculated and included into the model. The methodology of these calculations applies to any geometry in general, but the numerical values derived apply only to the experimental apparatus used in the microgravity test of Bar-Ilan *et al.* (2004a).

The accurate calculation of the radial heat losses is a complex problem and requires numerically solving the complete two-dimensional process. However, a simplified steady state analysis can be used to approximately calculate them if the characteristic time for smolder propagation is considerably greater than the characteristic time for radial thermal-diffusion. The characteristic time for smolder propagation is approximately given by the ratio of the smolder-front length δ to the smolder velocity u_{sml}. The smolder-front is defined here as the region where the foam temperature rises from ambient to the smolder temperature (approximately a length of 40 mm in the experiments of Bar-Ilan *et al.* 2004a). The smolder velocity is of the order of 0.1 mm/s. Thus, the characteristic time for smolder propagation is for these experiments on the order of 400 s. Since convection is the dominant mode of radial heat transfer through the foam (as will be proven later); with a calculated heat transfer coefficient of 6 W/m^2s, an estimated thermal layer near the sample holder wall of 10 mm (from the pictures that show an unburnt region of approximately this width) and the foam thermal properties shown in Table 4.1, the characteristic time for thermal diffusion is 14 s. Thus the smolder-propagation characteristic-time is over one

order of magnitude larger than the thermal-wave characteristic-time, which justifies the validity of a steady state analysis of the heat losses from the smolder reaction to the surrounding environment.

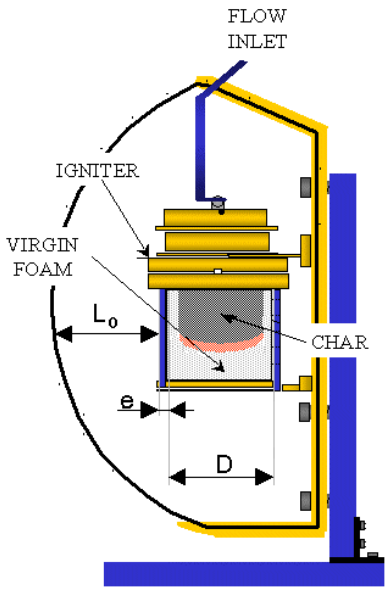

Figure 4.2: Schematic of the experimental apparatus; chamber, holder and sample (Bar-Ilan *et al.* 2004a).

Under the steady-state assumption, the radial transfer of heat from the smolder reaction to the environment can be calculated by equating the heat fluxes through the foam, the sample-holder wall and the outside environment (see Fig. 4.2). Under forced flow conditions, convection is the dominant mode of heat transfer through the foam to the wall. Conduction is the only heat-transfer mechanism across the sample-holder wall, whereas heat transfer to the surrounding air occurs primarily by conduction in microgravity. Thus the radial heat losses can be approximately calculated from the expressions:

$$\dot{Q}''_{loss} = \frac{T_m - T_0}{\frac{1}{h_{in}} + \frac{e}{k_w} + \frac{L_0}{k_0}} \qquad (4.9)$$

Where k_w is the convective heat transfer inside the foam, k_w is the conductivity of the wall, k_0 is the conductivity of the air surrounding the holder, L_0 is the average distance from the holder to the inner side of the chamber (see Fig. 4.2), e is the of thickness of the holder wall, and T_m is defined as:

$$T_m = (T_{sml} + T_0)/2 \tag{4.10}$$

For forced convection inside a porous media, it is found that under not-fully developed flow the Nusselt number is given by the following experimental correlation (Nield and Bejan 1992, and Incropera and DeWitt 1996):

$$Nu_D = \frac{h_{in} D}{k_{eff}} = 5.856 + \frac{\dfrac{0.1069}{\lambda}}{\left(1 + \dfrac{0.04}{\lambda^{2/3}}\right)} \tag{4.11}$$

Where $\lambda = \dfrac{\delta}{D\,Re\,Pr}$ is the Graetz number. The sample holder wall is made of Vespel and its thickness e is 4 mm. In microgravity, heat transfer across the quiescent air surrounding the sample holder is primarily by conduction. In-flight experimental measurements allow determining that the chamber outer-wall temperature is maintained constant temperature T_0 during the tests.

The radial heat losses predicted by Eq. (4.9) are calculated using the properties in Table 4.1, and converted to an equivalent heat-transfer coefficient U_e of 0.3 W/m^{2}K. Kallman (2005) derived a heat-transfer coefficient of 0.45 W/m^{2}K comparing her numerical predictions to the microgravity experiments of opposed smolder (Walther *et al.* 1999). The agreement between the two values is excellent taking into account how different the two approaches are. The same

methodology to the one presented here but for normal-gravity conditions was applied in Bar-Ilan *et al.* 2004b, giving a heat-transfer coefficient seven times larger than in microgravity conditions.

The heat-loss coefficient to the surroundings together with the lateral area to volume ratio is applied into Eq. (4.1), assuming that external heat losses are considered uniform along the sample. The lateral area to volume ratio depends on the geometry of the sample used. For the cylindrical samples of diameter D used in the experiments, this ratio is given by:

$$\frac{A_L}{V} = \frac{4}{D} \tag{4.12}$$

Table 4.1: Parameters and properties from Bar-Ilan *et al.* (2004a) used for the calculation of radial heat loss

Parameter	Value	Units
T_{sml}	400	°C
T_0	27	°C
L_0	0.046	m
D	0.12	m
e	0.004	m
δ	0.04	m
k_{eff}	0.06	W/mK
k_w	0.56	W/mK

4.4. 3-step Chemical Kinetics

The 3-step global mechanism used is the same as the one discussed in section 3.3.1 of this thesis, and it is repeated here for reading convenience:

$$Foam \rightarrow \nu_{c,p}\ Char + \nu_{g,p}\ Gas \tag{3.1}$$

$$Foam + \nu_{O_2,o}\ O_2 \rightarrow \nu_{c,o}\ Char + \nu_{g,o}\ Gas \tag{3.2}$$

$$Char + \nu_{O_2,c}\ O_2 \rightarrow \nu_{a,c}\ Ash + \nu_{g,c}\ Gas \tag{3.3}$$

The corresponding reaction rates are computed assuming Arrhenius type. For the endothermic foam pyrolysis the expression is:

$$\dot{\omega}_p = A_p e^{-\frac{E_{ap}}{RT_s}} w_f^{n_p} \tag{4.13}$$

For the exothermic foam oxidation the expression is:

$$\dot{\omega}_o = A_o e^{-\frac{E_{ao}}{RT_s}} w_f y_{O_2} \tag{4.14}$$

And for the exothermic char oxidation the expression is:

$$\dot{\omega}_c = A_c e^{-\frac{E_{ac}}{RT_s}} w_c y_{O_2} \tag{4.15}$$

The fuel of the smoldering test in microgravity (Bar-Ilan *et al.* 2004a) was PU and thus the numerical model needs these fuel's kinetic parameters. Using thermogravimetric (TG) data, section 3.3.1 of this thesis derives the pre-exponential factors, the activation energies and the stoichiometric coefficients for the PU 3-step mechanism. These kinetic parameters are shown in Table 3.1 and are used in the model to compute the Arrhenius-type reaction rates expressed in Eqs. (4.13)-(4.15).

4.5. Thermochemistry and Model Calibration

Suitable thermochemistry values for solid fuels like PU are rarely available in the literature. Previous chemical studies of flexible PU foam have mainly focused on pyrolysis degradation. As a consequence, there is little valid experimental information on the oxidation reactions and the oxygen species. This precludes the determination of reliable oxygen consumptions and consistent heats of reaction as applied to the global reactions in PU. Rogers and Ohlemiller (1980) presented an early study of the thermochemistry of PU foam. They experimentally determined the heat of pyrolysis and the heat of char oxidation, which are used in this model. Since the heat of foam oxidation that they reported includes the heat of pyrolysis, it is not suited for our kinetics scheme. Therefore calibration of the model results to the microgravity data is used to determine the values of these unknown parameters: oxygen consumptions for both foam and char oxidation reactions and heat of foam oxidation. These three parameters, however, are not independent if it is assumed that the heat release per mass of oxygen consumed is a constant value for the oxidation reactions (Ohlemiller *et al.* 1979). Consequently, Eq. (4.15) is imposed.

$$\frac{\nu_{O2,c}}{\nu_{O2,o}} = \frac{\Delta h_c}{\Delta h_o} \tag{4.15}$$

Given this assumption and using data from Rogers and Ohlemiller (1980), the only two parameters left for calibration of the model are Δh_0 and $\nu_{O_2,c}$. The values determined after calibration are shown in Table 4.2. These values are of

the same order as those derived by Ohlemiller *et al.* (1979) with their numerical model for smolder and in overall agreement too with the experimental estimations for the overall smolder process (Rogers and Ohlemiller 1980).

Table 4.2. Thermochemistry parameters used in the model.

Parameter	Value	Units	Reference
Δh_p	775	J/g	Rogers and Ohlemiller (1980)
Δh_o	-900	J/g	Calibrated
$\nu_{O_2,o}$	0.12	g-O_2/g-f	Eq. 4.15
Δh_c	-4600	J/g	Rogers and Ohlemiller (1980)
$\nu_{O_2,c}$	0.62	g-O_2/g-c	Calibrated

4.6. Results and Discussion

The solid-temperature profiles obtained from the numerical model are shown in Figs. 4.3 and 4.4. The airflow velocities at the inlet for these two cases are the same as for the microgravity experiments: 5 mm/s (Fig. 4.3) and 3 mm/s (Fig. 4.4). It is observed that whereas the smoldering front in the 5 mm/s case propagated all through the PU sample, the smoldering front in the 3 mm/s case was quenched at about half way. For the 5 mm/s case, the smolder peak temperature corresponds to that of self-propagation and is 430 °C with a velocity of 0.26 mm/s, in agreement with the experiments. The smoldering peak temperature for the 3 mm/s case is 480 °C at 12 cm, and the initial propagation velocity is around 0.11 mm/s in agreement with the experiments. At $t = 800$ s, the reaction has weakened and it extinguishes.

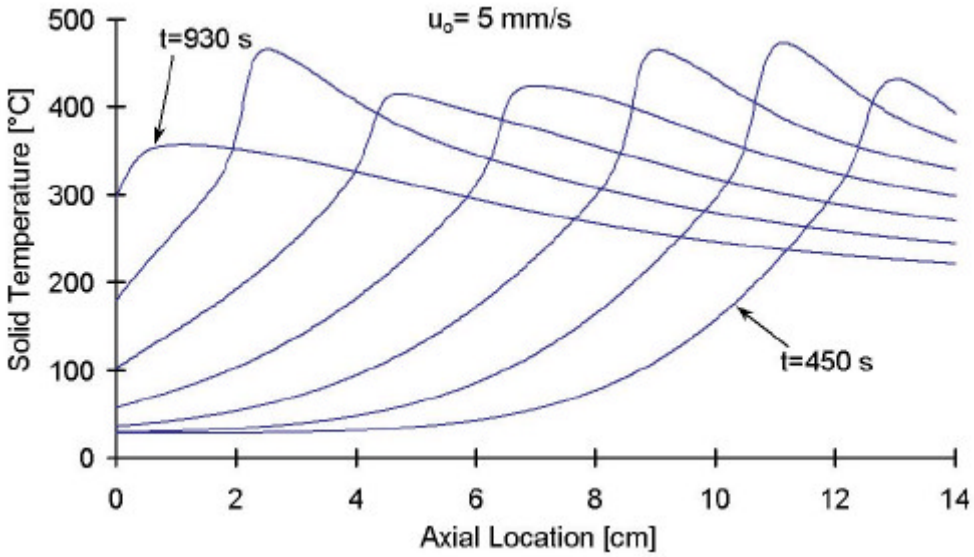

Figure 4.3: Solid temperature vs. distance for an air inlet velocity of 5 mm/s. Each line is a different time, starting at 450s and in steps of 80s.

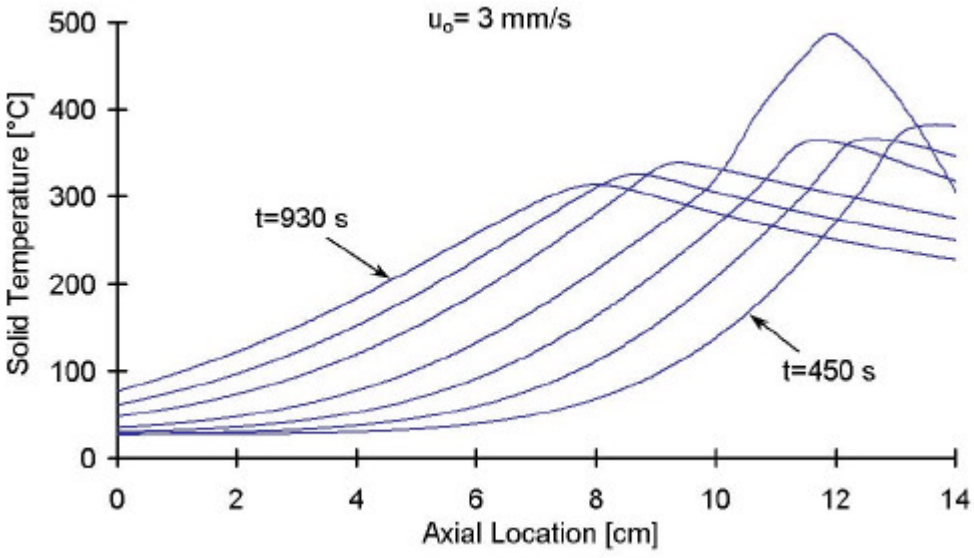

Figure 4.4: Solid temperature vs. distance for an air inlet velocity of 3 mm/s. Each line is a different time, starting at 450s and in steps of 80s.

The results of the model shows that most of the oxygen in the bulk gas is consumed during self-propagation. The pyrolysis front is predicted to move a few mm ahead of the foam oxidation front, in the region where oxygen is depleted. The char oxidation reaction is predicted to move with the foam oxidation but a few mm behind it, in the region where there is sufficient char and oxygen to sustain the char oxidation. These three observations are in agreement with experimental observations (Ohlemiller 1985, Torero and Fernandez-Pello 1996, Ohlemiller 2002, Bar-Ilan *et al.* 2004b).

A direct comparison of the model results with the experimental temperature profiles vs. time for different locations is shown in Fig. 4.5 for 5 mm/s and in Fig. 4.6 for 3 mm/s inlet airflows. In the experiments, the thermocouples measuring the temperature were placed in the center of the sample along the x-axis. In both cases, the faster temperature-increase at $t = 400$ s is due to the effect of turning from low airflow during the ignition to the nominal airflow. When directly comparing the temperature profiles with experiments, it can be seen that the model predicts well the overall characteristics at high temperatures, while the accuracy is lower at low temperatures, especially during the initial heating/ignition period. The present comparisons, despite the obvious inaccuracies, reproduce most of the important features of the process and this is a major improvement. Plateaus can be seen in the thermocouple traces of both experiments (Fig. 4.5 and 4.6) at about 75 °C. These plateaus, which behave as a wave propagating downstream, have been investigated via numerical modeling by Sui-Hang (2005) and attributed to water evaporation driven by the preheating of the

foam. The preheating of the solid fuel and the plateaus ahead of the smolder wave is typical of the forward configuration (Torero and Fernandez-Pello 1996, Walther *et al.* 1999). The numerical model presented here does not include water evaporation and thus early heating rates are expected to be different between experiments and numerical results.

For the 5 mm/s airflow case, Fig. 4.5 shows that ignition and self-propagation of smolder is achieved. The bottom of Fig. 4.5 shows the comparison for only two mid-sample locations to avoid the confusion when the eight locations are shown. The model calculates the smolder velocity and the peak temperatures accurately. However, the model predicts more vigorous propagation at the end of the sample that in microgravity where the end-effect weakens the reaction at the last centimeters. It is observed that in the model, the igniter region reaches a lower temperature than in the experiments. It is the opinion of the author that this increase in temperature in the experiments is due to localized char oxidation that raises the solid temperature to a range where secondary char-oxidation becomes significant. This secondary char-oxidation reaction is not implemented into the model and therefore, the predicted peak-temperatures are lower near the igniter. As seen in Fig. 4.5, the solution for the temperature profiles contains some small pulsations that are generated by char oxidation. Mathematically, the pulsating behavior may be originated from a bifurcation of the solution (Bayliss and Matkowsky 1990, Decker and Schult 2004), although no information on this issue has been reported for forward smoldering with multiple reactions included.

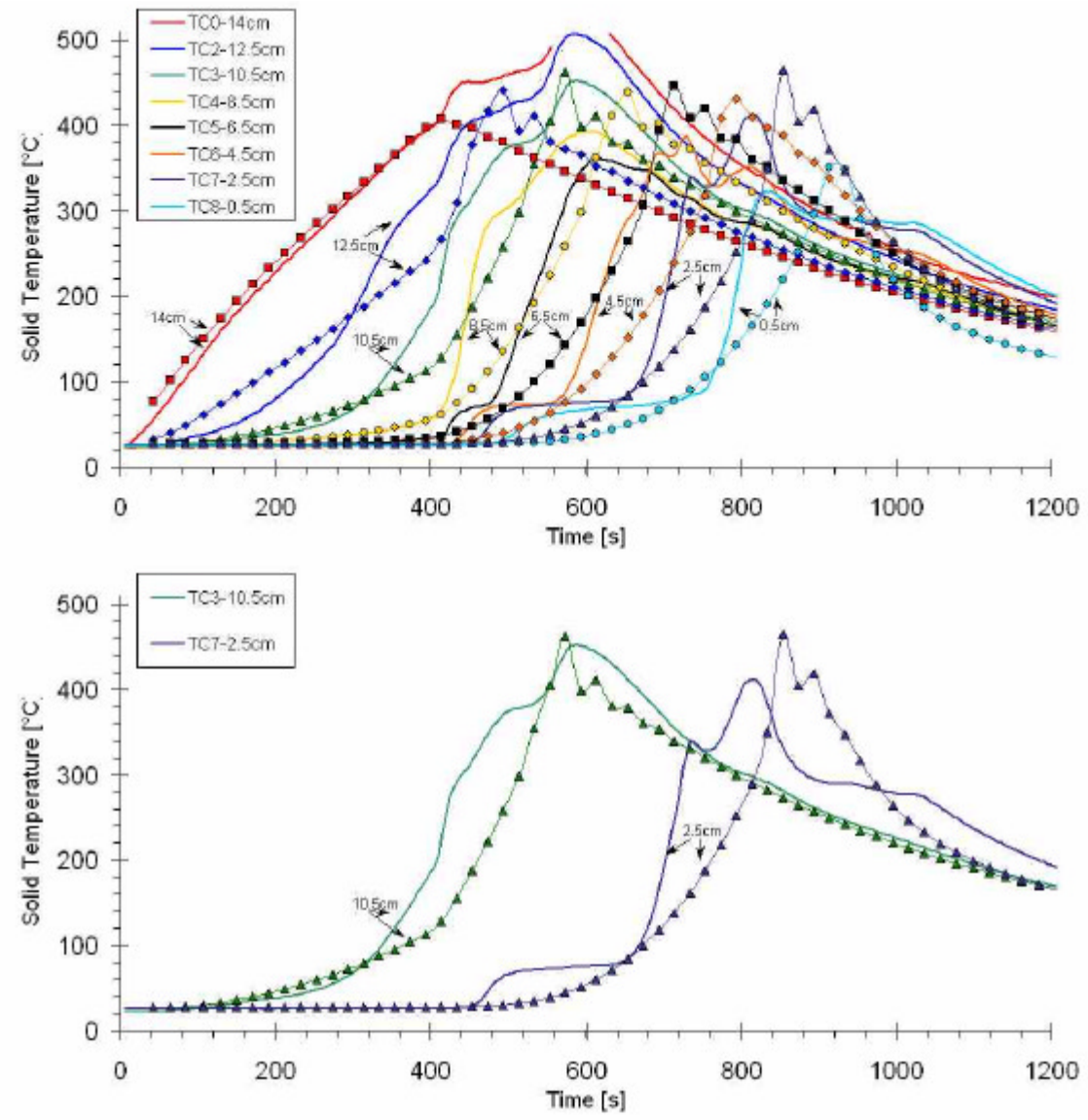

Figure 4.5: Solid temperature vs. time at different locations for inlet airflow of 5mm/s. Comparison of model results (lines with symbols) and experimental measurements (lines) from Bar-Ilan *et al.* (2004a). Top: all thermocouples traces; Bottom: two selected thermocouple traces.

For the 3 mm/s airflow case, Fig. 4.6 shows that ignition of smolder is achieved but not propagation away from the igniter. The bottom of Fig. 4.6 shows the comparison for only two mid-sample locations to avoid the confusion when the eight locations are shown. The peak temperature at approximately 650 s is due to a stronger and more localized char-oxidation that ultimately quenches the smolder propagation. Since char oxidation has five times higher heat of reaction and oxygen consumption than foam oxidation, its influence in the smolder process is greater and leads to both significant temperatures rises and higher oxygen depletion. With limited oxygen supply (*i.e.* low inlet air velocities), char oxidation consumes most of the oxygen in some locations and produces a higher heat-release rate, which causes the localized higher temperature-peak. The gas exiting the char oxidation region is depleted of oxygen and thus the foam oxidation reaction is oxygen-starved. This oxygen starvation, together with the higher heat-losses as the front is moving further from the hot igniter-assisted region, ultimately quenches the smolder. This role of the char oxidation reaction is in accordance with the experimental interpretations of Bar-Ilan *et al.* (2004a), who state that at 3 mm/s airflow, the char oxidation mechanism effectively quenched the smolder reaction leaving the last third of the sample unreacted. Also Torero and Fernandez-Pello (1995) reported experimentally observing that the onset of oxidation reactions on the char left behind depleted the oxygen from the gas flow. This quenching mechanism can be observed in more detail in Fig. 4.7, which shows that the extinction of the smolder wave is caused by the char-oxidation depletion of oxygen shortly after the ignition. This mechanism is effectively captured in the

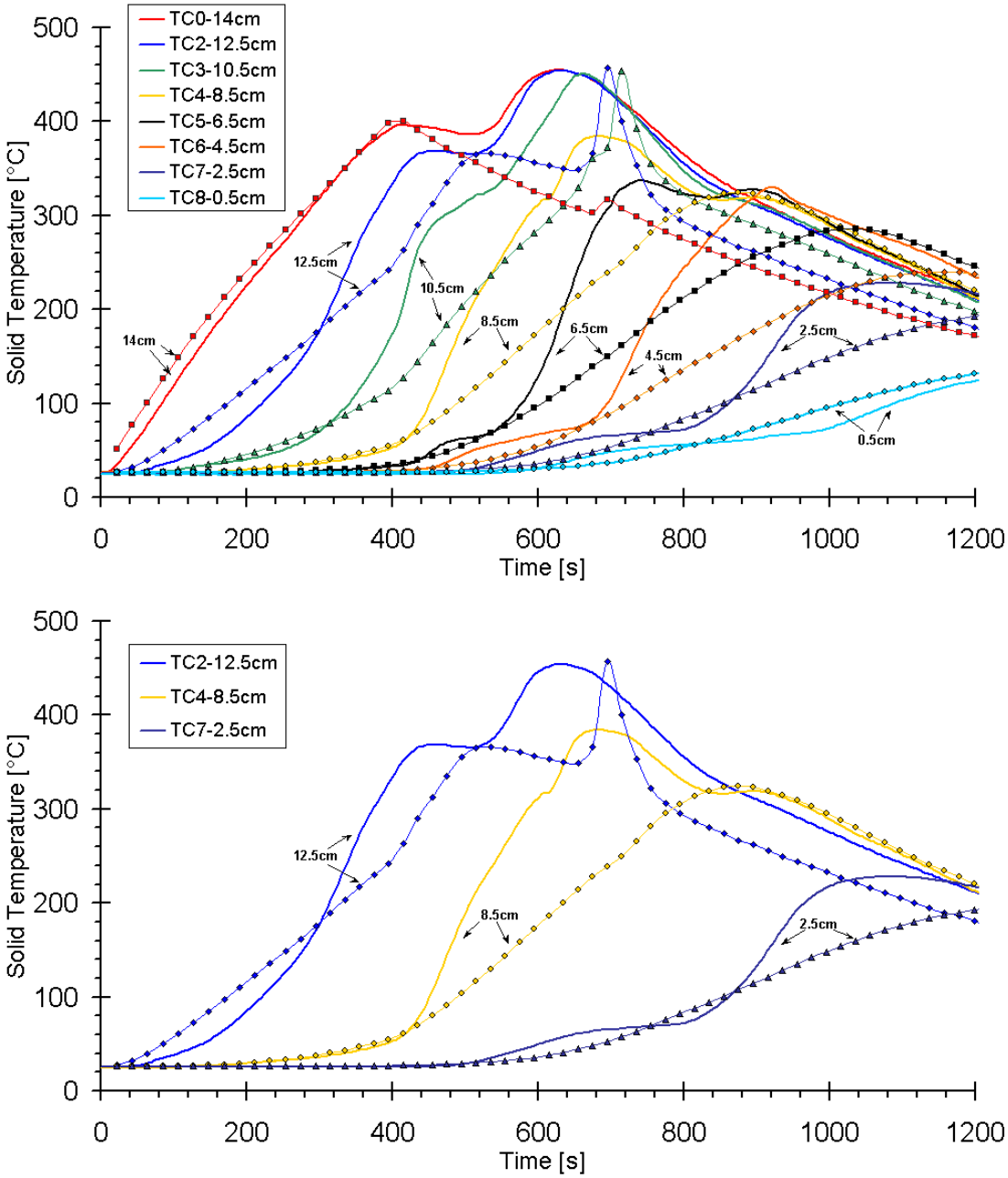

Figure 4.6: Solid temperature vs. time at different locations for inlet airflow of 3mm/s. Comparison of model results (lines with symbols) and experimental measurements (lines) from Bar-Ilan *et al.* (2004a). Top: all thermocouples traces; Bottom: two selected thermocouple traces.

computational model although the predicted time and location of occurrence is not entirely accurate.

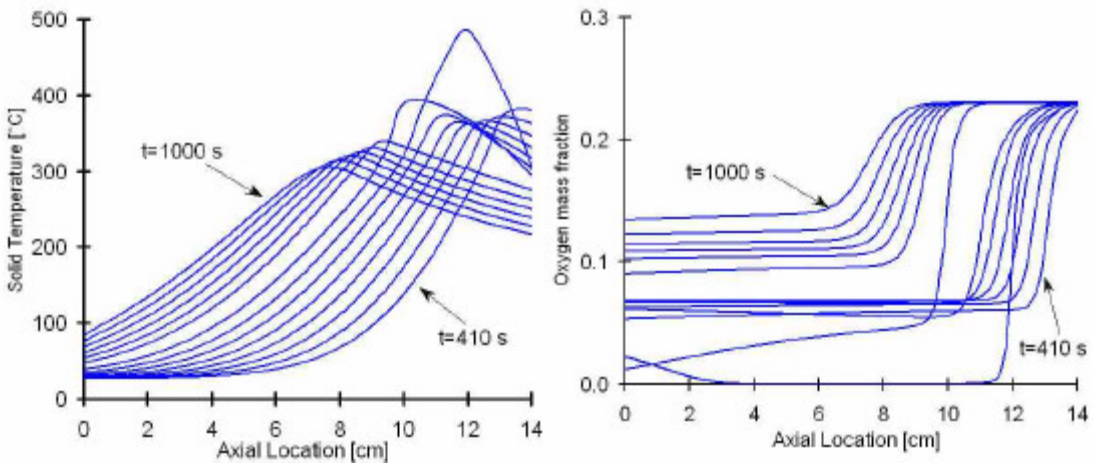

Figure 4.7: Temperature and gas oxygen concentration vs. distance at different times for the inlet airflow of 3 mm/s. Each line is a different time, starting at 410s and in steps of 45s. These figures show that the extinction of the smolder wave is caused by the char-oxidation depletion of oxygen between 635 and 770 s.

Numerical results of the smolder self-propagation velocity as a function of the inlet-air velocity are presented in Fig. 4.8. Comparison to experimentally measured smolder velocities allows the conclusion that the numerical model describes the experimental data qualitatively, and after calibration in a quantitative manner too. The model predicts no smolder-ignition for air velocities below 2.9 mm/s. For airflows close to 2.9 mm/s but higher, the model predicts smolder-ignition but no self-propagation since the reaction quenches half way along of the sample. For these cases, Fig. 4.8 reports the initial propagation velocity. It should be pointed out that the location of this no ignition limit is affected by the particular ignition and that the minimum airflow velocity predicted here is for the ignition protocol implemented in the experiments. Away from the no ignition limit, in the self-propagation regime,

the smolder velocity is shown to be linear with the airflow as predicted for oxygen-limited smolder propagation.

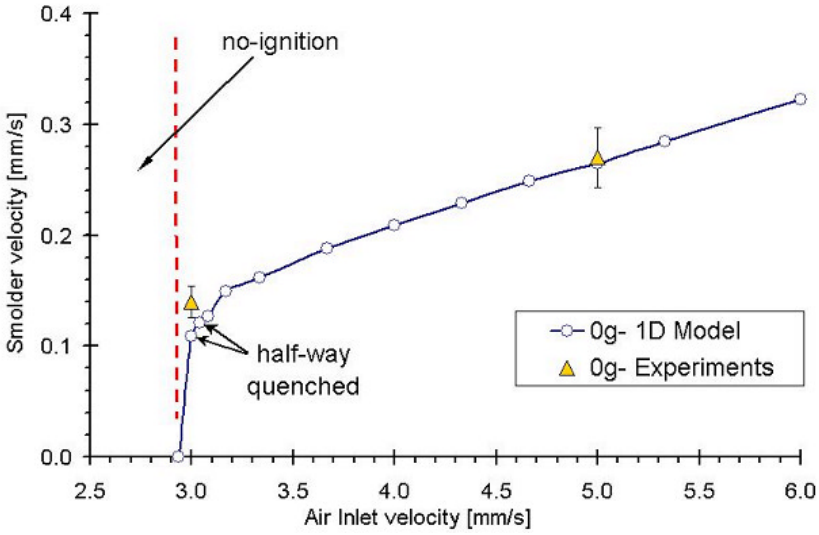

Figure 4.8: Numerical results of smolder propagation velocity as a function of the inlet-air velocity, and comparison to experimental results from Bar-Ilan *et al.* (2004a). Experimental data points include error bars.

The inclusion of the external heat loss to the exterior makes a significant difference in the predicted smolder characteristics. With no external heat loss, the char oxidation reaction dominates and engulfs the porous sample, resulting in solid temperatures up to 900 °C. This points out to a possible application of the model; to calculate the onset of flaming combustion in the gas phase (if the corresponding gas-phase reaction is included) and consequently predict the transition to flaming.

A major disagreement between the experiments and the numerical model is the predicted total loss of mass. While a typical smolder sample loses about half of its weight during smolder propagation in the core of the sample, the

numerical model indicates weight losses up to 90 %. This produces the simulations of smoldering to be solid-fuel depleted in some situations where it should be oxygen depleted. The main reason for these differences appears to be the inclusion of only one pyrolysis reaction in the attempt to describe what seems to be in reality a process with two consecutive reaction-paths. This approximation causes the pyrolysis yield of char, $\nu_{c,p}$, to be significantly underestimated.

4.7. Conclusions

Results of one-dimensional transient simulations of forward smoldering were compared to the only available microgravity data. In order to do this, the already published core of the model was improved with the derivation and inclusion of PU kinetics, the inclusion of external heat losses and the extraction (through calibration) of thermochemistry parameters of PU. The propagation velocity in microgravity has been used to calibrate the model and extract the heat of foam oxidation and the oxygen consumption for char oxidation of polyurethane foam. The model predicts the role of air velocity and char oxidation in accordance with experimental observations in microgravity. Comparison of the temperature profiles to experiments shows that while the accuracy is low at low temperature, the model predicts well the high temperatures and the propagation and extinction mechanisms. The present

comparisons, despite the obvious inaccuracies, reproduce most of the important features of the process and this is a major improvement.

The effect of inlet gas velocity was examined and a minimum airflow for ignition was identified. The model captures the experimentally observed quenching-mechanism produced by oxygen depletion at low inlet velocities. It is remarkable that this one-dimensional model with simplified kinetics is capable of predicting cases of smolder ignition with no self-propagation for airflows close to the minimum for ignition. The numerical model describes qualitatively well the experimental data and after calibration good quantitative agreement is achieved.

The only two microgravity-experiments ever conducted in forward propagation have been used here for comparison and calibration. Space-based experiments are difficult to conduct because of their elevated cost, and consequently the number of tests is generally limited, making numerical modeling a very important tool for the prediction of smoldering behavior in the absence of gravity. The model is used to extend microgravity data to different airflows and for better understanding of the controlling mechanisms of smolder for the purpose of fire safety, both in microgravity and normal gravity.

Chapter 5

Model of Opposed and Forward Smoldering Combustion with 5-step Kinetics

"God give me a restlessness whereby I may neither sleep nor accept praise till my observed results equal my calculated results or in pious glee I discover and assault my error. God give me strength not to trust to God!"

Arrowsmith, Sinclair Lewis (1885-1951).

5.1 Introduction

As mention in chapter 2, to date, no study has attempted to simulate both forward and opposed smoldering with the same kinetic mechanism and same kinetic parameters. Since there are no fundamental kinetic differences between opposed and forward smoldering combustion, the same appropriate kinetic scheme should describe adequately both forms.

The 5-step mechanism for PU developed in chapter 3 was shown to be able to predict phenomenologically the reaction structure in both opposed and forward configurations. This 5-step mechanism is implemented here into a detailed model of forward and opposed smoldering ignition and propagation. The results from previously reported microgravity experiments in (Bar-Ilan *et al.* (2004b) and (2004a)) with PU as fuel are used for calibration and testing of the numerical results.

5.2 Governing Equations

The computational domain is shown in Fig. 4.1, which reproduces the setup in the microgravity experiments as reported by (Bar-Ilan *et al.* (2004b) and (2004a)). The ignition is attempted at the boundary $x = 0$. Air is forced at one boundary and then flows through the domain. For opposed propagation, air is forced at the boundary $x = L$, while for forward propagation air is forced at the boundary $x = 0$.

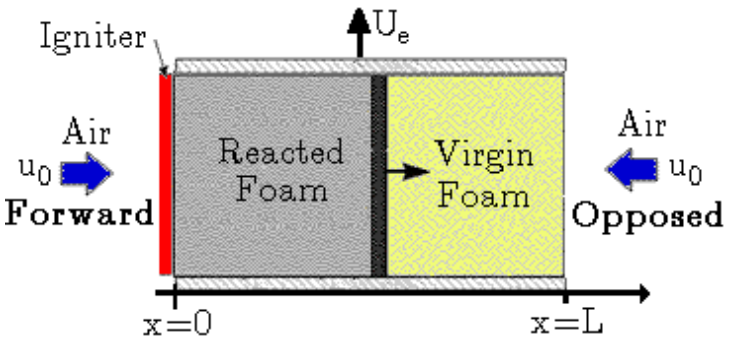

Figure 5.1: Computational domain for opposed and forward smoldering combustion.

The model solves the one-dimensional transient governing equations for the solid and gas. These equations are developed combining the models by Ohlemiller *et al.* (1979), Leach *et al.* (2000) and Di Blasi (1995), plus some novel contributions. The FORTRAN computer code can be consulted in the appendix of this thesis. The mathematical expressions for the reaction rates of the 5-step mechanism are presented in the subsection (5.2.1). In the subsection (5.2.2), the general equation for conservation of energy is developed for a given phase. The subsequent subsections developed the conservation equations for: energy of the solid (5.2.3), solid species (5.2.4), energy of the gas (5.2.5), continuity of the gas (5.2.6) and gas species (5.2.7).

5.2.1. Chemical Kinetics

The 5-step mechanism for PU was presented in chapter 3 of this thesis but it is briefly repeated here for reading convenience. It consists of: two foam-pyrolysis reactions; two foam oxidation reactions; and one char oxidation reaction, accounting for four solid species: foam, β-foam, char and residue, and two gas species; oxygen and product of smoldering.

$$Foam \rightarrow \nu_{\beta,p}\ \beta\text{-}foam + \nu_{gp,p}\ Gas \tag{3.4}$$

$$\beta\text{-}foam \rightarrow \nu_{c,p\beta}\ Char + \nu_{gp,p\beta}\ Gas \tag{3.5}$$

$$Foam + \nu_{O_2,o}\ O_2 \rightarrow \nu_{c,o}\ Char + \nu_{gp,o}\ Gas \tag{3.6}$$

$$\beta\text{-}foam + \nu_{O_2,o\beta}\ O_2 \rightarrow \nu_{c,o\beta}\ Char + \nu_{gp,o\beta}\ Gas \tag{3.7}$$

$$Char + \nu_{O_2,c}\ O_2 \rightarrow \nu_{r,c}\ Residue + \nu_{gp,c}\ Gas \tag{3.8}$$

The kinetic parameters (A_i, E_i, n_i and $\nu_{i,j}$) for each one of the reaction paths described above have been obtained in chapter 3 (Table 3.3) assuming Arrhenius-type reaction rates. For the pyrolysis reactions, the reaction rate is in the form of:

$$\dot{\omega}_i = A_i e^{-\frac{E_i}{RT}} w_i^{n_i}, \tag{5.1}$$

and for the oxidation reactions:

$$\dot{\omega}_i = A_i e^{-\frac{E_i}{RT}} w_i^{n_i} y_{O_2}, \tag{5.2}$$

where $w_i = m_i/m_0$, m_0 is the initial mass of the virgin fuel, and $\dot{\omega}_i$ gives the mass loss rate of solid per initial mass of the virgin fuel due to reaction i (expressed in units of [1/s]). The reaction rates are assumed to be independent of the specific surface area of the solid.

5.2.2. General Energy Conservation

The general, one-dimensional equation for conservation of energy in any phase is given by:

$$\frac{\partial h'''}{\partial t} = \frac{\partial}{\partial x}\left(\frac{A_{cd}}{A} k \frac{\partial T}{\partial x}\right) - \frac{\partial}{\partial x}\left(\dot{m}'' \frac{A_{cv}}{A} c_p (T - T_0)\right) \pm h_{gs} \frac{A_{gs}}{V}(T_g - T_s) - \sum_i \dot{m}_i''' \Delta h_i - U_e \frac{A_L}{V}(T_s - T_0) \tag{5.3}$$

Where h''' is the enthalpy per unit volume. This equation implies that the controlled volume has a geometrical cross-sectional area A, that the heat

exchange by conduction is through an effective area A_{cd}, and that the convective flow occurs thought an effective area A_{cv}. Each of the terms is explained here.

Heat by conduction:

$$\dot{q}'''_{cd} = \frac{\partial}{\partial x}\left(\frac{A_{cd}}{A} k \frac{\partial T}{\partial x}\right) \tag{5.4}$$

Heat by convection:

$$\dot{q}'''_{cv} = -\frac{\partial}{\partial x}\left(\dot{m}'' \frac{A_{cv}}{A} c_p (T - T_0)\right) \tag{5.5}$$

Heat transferred between gas and solid:

$$\dot{q}'''_{gs} = \pm h_{gs} \frac{A_{gs}}{V}(T_g - T_s) \tag{5.6}$$

Heat released by chemical reactions:

$$\dot{q}'''_{ge} = -\rho_0 \sum_i \dot{\omega}_i \Delta h_i \tag{5.7}$$

Heat losses to the external environment:

$$\dot{q}'''_{e} = -U_e \frac{A_L}{V}(T_s - T_0) \tag{5.8}$$

5.2.3. Solid Energy Conservation

The solid is not moving and thus the conservation of the energy in the solid has no contribution from convection and Eq. (5.3) is expressed as:

$$\frac{\partial h'''_s}{\partial t} = \frac{\partial}{\partial x}\left(k_{eff,s} \frac{\partial T}{\partial x}\right) + h_{gs} \frac{A_{gs}}{V}(T_g - T_s) - U_e \frac{A_L}{V}(T_s - T_0) - \rho_0 \left[\dot{\omega}_p \Delta h_p + \dot{\omega}_{p\beta} \Delta h_{p\beta} + \dot{\omega}_o \Delta h_o + \dot{\omega}_{o\beta} \Delta h_{o\beta} + \dot{\omega}_c \Delta h_c\right] \tag{5.9}$$

where the conductivity of the solid is given by:

$$k_{eff,s} = k_s + k_r \tag{5.10}$$

The conductivity includes the term $k_r = \frac{3}{16} l_m \sigma T_s^3$, which is the radiative conductivity in the optically thick limit (Siegel and Howell 2001). According to electron-microscopy photographs of PU foam (see Figure 3.1 in chapter 3 of this thesis), the mean penetration distance l_m is approximately three times the pore diameter d_p. One setback of one-dimensional simulations is that they cannot directly model heat losses in the perpendicular direction to the external environment, as occurs in actual experiments. However, the effect of these heat losses can be included in an approximate way in the form of a volumetric heat-loss coefficient U_e. This coefficient has been analytically calculated in chapter 4 of this thesis to be 0.3 W/m²K in the particular setup used in the microgravity experiments. The lateral area to volume ratio for the cylindrical samples used in the experiments is given by $A_L/V = 4/D$ (Eq. 4.12).

Assuming that the specific heats of the different solid species are similar to the specific heat of the virgin foam, and expressing the bulk solid density as $\rho_s = \rho_0 \sum_i w_i$ (see Eq. 5.30 below), the temperature of the solid can be calculated from the enthalpy as:

$$T_s = \frac{h_s'''}{c_s \rho_0 \sum_i w_i} + T_0 \tag{5.11}$$

5.2.4. Solid species conservation

Conservation of the solid species according to the 5-step mechanism in Eqs. (3.4-3.8), using the reaction rates in Eqs.(5.1 and 5.2) yields:

$$\dot{w}_f = -\dot{\omega}_p - \dot{\omega}_o \tag{5.12}$$

$$\dot{w}_{\beta f} = \nu_{\beta,p}\dot{\omega}_p - \dot{\omega}_{\beta p} - \dot{\omega}_{o\beta} \tag{5.13}$$

$$\dot{w}_c = \nu_{c,p\beta}\dot{\omega}_{p\beta} + \nu_{c,o}\dot{\omega}_o + \nu_{c,o\beta}\dot{\omega}_{o\beta} - \dot{\omega}_c \tag{5.14}$$

$$\dot{w}_r = \nu_{r,c}\dot{\omega}_c \tag{5.15}$$

Where $\dot{w}_i = \frac{d(m_i/m_0)}{dt}$, and m_0 is the initial mass of the virgin fuel.

5.2.5. Gas Energy Conservation

Using Eq. (5.3), the conservation of the energy in the gas is expressed as:

$$\begin{aligned}\frac{\partial}{\partial t}\left(\phi h_g'''\right) &= \frac{\partial}{\partial x}\left(\phi k_g \frac{\partial T_g}{\partial x}\right) - \frac{\partial}{\partial x}\left(\dot{m}_g''\phi c_{pg}\left(T_g - T_0\right)\right) \\ &- h_{gs}\frac{A_{gs}}{V}\left(T_g - T_s\right) - c_{pg}\left(T_g - T_s\right)\rho_0\sum_i \dot{w}_i\nu_{g,i}\end{aligned} \tag{5.16}$$

where the porosity is defined as $\phi = \frac{V_g}{V}$, and it is assumed that $\phi \approx \frac{A_{cd}}{A} \approx \frac{A_{cv}}{A}$. There is an additional term in right hand side of Eq. (5.16) ($c_{pg}\left(T_g - T_s\right)\rho_0\sum_i \dot{w}_i\nu_{g,i}$). This term accounts for the energy transported by the solid vapors that go into the gas phase. The effect of this term in the results is only significant when the gas and the solid are far from thermal equilibrium.

Darcy's law is used as the equation for the conservation of momentum, Eq. (5.17), and computes the gas velocity as a linear function of the pressure gradient across the porous medium. It is assumed than the gases released from the degrading solid do not affect the gas velocity. Buoyancy-induced flows are not modeled into Eq. (5.17), and thus the simulations are in microgravity conditions.

$$u = -\frac{K}{\mu}\frac{\partial p}{\partial x} \tag{5.17}$$

Then the mass flux is given by $m_g'' = -\rho_g \frac{K}{\mu}\frac{\partial p}{\partial x}$, and the final form of the conservation of energy for the gas is:

$$\begin{aligned}\frac{\partial}{\partial t}\left(\phi h_g'''\right) &= \frac{\partial}{\partial x}\left(\phi k_g \frac{\partial T_g}{\partial x}\right) + \frac{\partial}{\partial x}\left(\phi \rho_g \frac{K}{\mu}\frac{\partial p}{\partial x} c_{pg}\left(T_g - T_0\right)\right) \\ &- h_{gs}\frac{A_{gs}}{V}\left(T_g - T_s\right) - c_{pg}\left(T_g - T_s\right)\rho_0 \sum_i \dot{w}_i \nu_{g,i}\end{aligned} \tag{5.18}$$

The temperature of the gas can be calculated from the enthalpy as:

$$T_g = \frac{h_g'''}{c_{pg}\rho_g} + T_0 \tag{5.19}$$

5.2.6. Gas Mass Conservation

Using Darcy's law (Eq. 5.17), the time derivative of the gas density is given by:

$$\begin{aligned}\frac{\partial}{\partial t}\left(\phi \rho_g\right) = \frac{\partial}{\partial x}\left(\phi \rho_g \frac{K}{\mu}\frac{\partial p}{\partial x}\right) + \rho_0 \left[\begin{array}{l}\dot{\omega}_p \nu_{g,p} + \dot{\omega}_{p\beta}\nu_{g,p\beta} + \dot{\omega}_o\left(\nu_{g,o} - \nu_{O_2,o}\right) \\ + \dot{\omega}_{o\beta}\left(\nu_{g,o\beta} - \nu_{O_2,o\beta}\right) + \dot{\omega}_c\left(\nu_{g,c} - \nu_{O_2,c}\right)\end{array}\right]\end{aligned} \tag{5.20}$$

The pressure of the gas is calculated using the ideal gas law Eq. (5.21).

$$P = \rho_g \frac{RT_g}{\overline{MW}} \tag{5.21}$$

5.2.7. Gas Species Conservation

The time rate of change of the mass density of the oxygen and the gas products is given respectably by:

$$\frac{\partial}{\partial t}\left(\phi\rho_g y_{O_2}\right) = \frac{\partial}{\partial x}\left(\phi\rho_g \frac{K_x}{\mu}\frac{\partial p}{\partial x} y_{O_2}\right) + \frac{\partial}{\partial x}\left(\phi\rho_g D_{diff}\frac{\partial y_{O_2}}{\partial x}\right) - \rho_0 \sum_i \dot{\omega}_i \nu_{O_2,i} \tag{5.22}$$

$$\frac{\partial}{\partial t}\left(\phi\rho_g y_{gp}\right) = \frac{\partial}{\partial x}\left(\phi\rho_g \frac{K_x}{\mu}\frac{\partial p}{\partial x} y_{gp}\right) + \frac{\partial}{\partial x}\left(\phi\rho_g D_{diff}\frac{\partial y_{gp}}{\partial x}\right) + \rho_0 \sum_i \dot{\omega}_i \nu_{gp,i} \tag{5.23}$$

Where the term containing the oxygen consumption by the oxidation reactions is:

$$\sum_i \dot{\omega}_i \nu_{O_2,i} = \dot{\omega}_o \nu_{O_2,o} + \dot{\omega}_{o\beta} \nu_{O_2,o\beta} + \dot{\omega}_c \nu_{O_2,c} \tag{5.24}$$

and the term containing the generation of gas products is:

$$\sum_i \dot{\omega}_i \nu_{O2,i} = \dot{\omega}_p \nu_{gp,p} + \dot{\omega}_o \nu_{gp,o} + \dot{\omega}_{p\beta} \nu_{gp,p\beta} + \dot{\omega}_{o\beta} \nu_{gp,o\beta} + \dot{\omega}_c \nu_{gp,c} \tag{5.25}$$

Since the gas density is solved in Eq. (5.20), it is convenient to convert Eqs. (5.22) and (5.23) to the time rate of change of the mass fractions. To do this, the chain rule theorem is applied, *i.e.* for the oxygen equation:

$$\frac{\partial}{\partial t}\left(\phi\rho_g y_{O_2}\right) = y_{O_2}\frac{\partial}{\partial t}\left(\phi\rho_g\right) + \phi\rho_g \frac{\partial y_{O_2}}{\partial t} \tag{5.26}$$

and the expression is substituted into Eq. (5.22) to obtain:

$$\frac{\partial y_{O_2}}{\partial t} = \frac{1}{\phi\rho_g}\left[\frac{\partial}{\partial x}\left(\phi\rho_{O_2}\frac{K_x}{\mu}\frac{\partial p}{\partial x}\right) - y_{O_2}\frac{\partial}{\partial t}\left(\phi\rho_g\right) + \frac{\partial}{\partial x}\left(\phi\rho_g D_{diff}\frac{\partial y_{O_2}}{\partial x}\right) - \rho_0 \sum_i \dot{\omega}_i \nu_{O_2,i}\right] \tag{5.27}$$

Similarly, for the gas products of smoldering combustion:

$$\frac{\partial y_{gp}}{\partial t} = \frac{1}{\phi\rho_g}\left[\frac{\partial}{\partial x}\left(\phi\rho_{gp}\frac{K}{\mu}\frac{\partial p}{\partial x}\right) - y_{gp}\frac{\partial}{\partial t}\left(\phi\rho_g\right) + \frac{\partial}{\partial x}\left(\phi\rho_g D_{diff}\frac{\partial y_{gp}}{\partial x}\right) + \rho_0\sum_i \dot{\omega}_i \nu_{gp,i}\right] \quad (5.28)$$

5.3 Other Physical Properties

The expressions linking the physical properties of the porous medium at any spatial location with those of the gas and solid species must be consistent with the structure of the medium and the governing equations shown above. In this subsection, the development of these expressions and the assumptions made are shown.

5.3.1. Solid Properties

The expressions for the porosity ϕ and density of the porous media ρ_s have to include the contribution from different solid species and the volume occupied by the gas. The total volume occupied by the porous medium V is the sum of V_g, the volume of the gas, and V_s, the volume of the solid. The latter is the sum of the volumes V_i occupied by each of the solid species. Then, assuming that the total spatial volume V does not change with time, we have:

$$\phi = \frac{V_g}{V} = 1 - \frac{V_s}{V} = 1 - \frac{\sum_i V_i}{V} = 1 - \sum_i \vartheta_i = 1 - \rho_0 \sum_i \frac{w_i}{\tilde{\rho}_i} \quad (5.29)$$

$$\rho_s = \frac{\sum_i m_i}{V} = \frac{m_0 \sum_i w_i}{V} = \rho_0 \sum_i w_i \tag{5.30}$$

Where $\vartheta_i = \frac{V_i}{V}$ is the specific volume of species, $\rho_0 = \frac{m_0}{V}$ is the initial bulk density and $\tilde{\rho}_i = \frac{m_i}{V_i} = \rho_0 \frac{w_i}{\vartheta_i}$ is the solid density of the species i, m_i is the mass of the species i. The species solid-densities $\tilde{\rho}_i$ are not well known, expect for the virgin foam $\tilde{\rho}_f$. Thus, it is assumed that the solid densities are equal to the density of the virgin foam ($\tilde{\rho}_i \approx \tilde{\rho}_f$) and so, Eq. (5.29) further simplifies to:

$$\phi = 1 - \rho_0 \sum_i \frac{w_i}{\tilde{\rho}_i} = 1 - \frac{\rho_0}{\tilde{\rho}_f} \sum_i w_i = 1 - (1 - \phi_0) \sum_i w_i \tag{5.31}$$

This equation expresses how the porosity of the medium changes at any spatial location as a function of the mass of each solid species. The expression is convenient since the relative masses w_i are directly solved for in Eqs. (5.12)-(5.15). The rest of the properties of the solid phase (d_p, d_f and K) are weight averaged for the four solid species considered, assuming that the β-foam has the same properties as the foam, and that the residue has the same properties as the char. Values for the most important parameters in the model are shown in Table 5.2.

5.3.2. Gas Properties

The molecular weight of the gas mixture is computed as a weighted average using the mass fractions:

$$\overline{MW} = \frac{1}{y_{O_2} / MW_{O_2} + y_{N_2} / MW_{N_2} + y_{gp} / MW_{gp}} \tag{5.32}$$

The concentration of nitrogen is calculated from the equation of total mass:

$$y_{N_2} = 1 - y_{O_2} - y_{gp} \tag{5.33}$$

The molecular weight of the smoldering gases, MW_{gp}, strongly depends on the reactivity history of the smoldering process. Walther *et al.* (1999) reported the composition of the gases collected during PU smoldering experiments. This composition is used to approximate the molecular weight of the products of smoldering with $MW_{gp} = 39\,g/mol$. The mass diffusivity D_{diff} is assumed to be that of O_2 in air (2.7 10^{-5} m^2/s). The rest of the properties of the gas phase (μ, c_{pg} and k_g) are approximated to those of air using temperature-dependent correlations at atmospheric pressure (Incropera and DeWitt 1996). Values for the most important parameters in the model are shown in Table 5.2.

5.3.3. Volumetric heat-transfer coefficient between gas and solid

The heat transfer between the gas phase and the solid phase is quantified by the multiplication of the heat-transfer coefficient h_{gs} and the exchange area to volume ratio A_{gs}/V. There is considerable controversy regarding the correct expression for both properties in a reacting porous-material like flexible PU. Florido *et al.* (1989) conducted an experimental study to measure the volumetric coefficient in insulating porous materials, but their results are only applicable to very low permeability materials. Leach *et al.* (1997) reported on

the effect of this coefficient on the propagation of a smoldering front in a porous media. They studied a very wide range of volumetric heat-transfer coefficients, from 10 to 10^5 W/m^{3}K. This wide range gives an idea of the difficulties to estimate its proper value. They reported that for values above 10^3 W/m^{3}K the results become independent of the coefficient in the range of air velocities of interest for smoldering combustion. This indicates that virtual thermal equilibrium is reached between the gas and the solid for h_{gs} values above that.

The electron-microscopy photographs of the foam presented in chapter 3 of this thesis (Fig. 3.1) provide a visual representation of the virgin foam and char microstructures, and measurements of the pore and fiber diameters. These measurements are presented in Table 5.1. A simple estimation of the order of magnitude of the volumetric coefficient can be done using these measurements and a rough model of the geometry of the pores. Assuming that the heat-transfer boundary-layer in the gas is of the order of magnitude of the pore diameter, the heat-transfer coefficient is given by:

$$h_{gs} = \frac{k_g}{\delta} \approx \frac{k_g}{d_p} \tag{5.34}$$

Table 5.1: Pore and fiber diameters measured from electron-microscopy photographs from chapter 3 of this thesis.

Foam	Pore d_p	Fiber d_f
Virgin (Fig. 3.1a)	500 µm	85 µm
Charred (Fig. 3.1c)	650 µm	50 µm

Approximating the pore geometry as hollow cube whose edges are the fibers (geometry also called a wire cage, see Fig. 5.2), the exchange surface to volume ratio is given by the exchange surface to volume ratio is given by:

$$\frac{A_{gs}}{V} \approx \frac{12 d_f}{d_p^2} \tag{5.35}$$

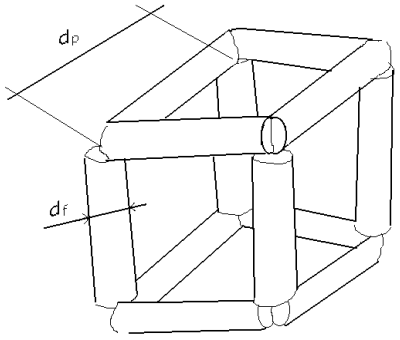

Figure 5.2: Sketch of the wire-cage representation of the foam microstructure. From Rein (1999).

When the geometry values in Table 5.1 are substituted into this expression, the exchange surface to volume ratio is 4100 1/m for the virgin foam. This value is inside the range from 4000 to 5000 1/m given by Rogers and Ohlemiller (1980) as an experimental estimation for PU. The order of magnitude of the volumetric heat-transfer coefficient with these expressions is 10^5 W/m^{3}K, which is high enough to imply virtual thermal equilibrium between the gas and the solid in the range of air velocities of interest for smoldering combustion (as the results confirm).

5.4 Initial and Boundary conditions

At $t = 0$, the entire fuel bed is unreacted and the solid and gas are at ambient temperature (27 °C). The heat-flux imposed by the igniter is such that the temperature rise with time at the igniter location is the same as in the experiments (ignition time of 600 s with a final igniter temperature of 480 °C for the opposed case (Bar-Ilan *et al.* 2004b), and ignition time of 400 s with a final temperature of 400 °C for the forward case (Bar-Ilan *et al.* 2004a). The thermal boundary condition after the ignition protocol is that heat is lost to the exterior resulting in the same cooling effect as seen in the experiments. As in the experiments, during the ignition, the inlet flow velocity is $u_{ig} = 0.01$ mm/s. After ignition, the inlet forced-flow velocity u_0 is set to the corresponding nominal value and kept constant at the boundary thereafter.

Initial conditions:

$$\begin{cases} T_s(x,0) = T_g(x,0) = T_0 \\ w_f(x,0) = 1 \\ w_\beta(x,0) = w_c(x,0) = w_r(x,0) = y_{gp}(x,0) = 0 \\ u(x,0) = u_{ig} \\ y_{O_2}(x,0) = 0.23 \end{cases} \tag{5.36}$$

Boundary conditions for opposed propagation:

$$\begin{aligned} \frac{\partial h_s'''}{\partial t}(0,t) &= \begin{cases} f_{ig}(t) & for\ t \le t_{ig} \\ -U_0\left(T_s(0,t) - T_0\right) & for\ t > t_{ig} \end{cases} \\ \frac{\partial T_s}{\partial x}(L,t) &= -h_L\left(T_s(0,t) - T_0\right) \end{aligned} \tag{5.37}$$

$$\frac{\partial T_g}{\partial x}(0,t) = 0 \qquad T_g(L,t) = T_0 \tag{5.38}$$

$$P(0,t) = P_0 \qquad u(L,t) = \begin{cases} u_{ig} & for\ t \le t_{ig} \\ u_0 & for\ t > t_{ig} \end{cases} \tag{5.39}$$

$$\frac{\partial y_{O_2}}{\partial x}(0,t) = 0 \qquad y_{O_2}(L,t) = 0.23 \tag{5.40}$$

$$\frac{\partial y_{gp}}{\partial x}(0,t) = 0 \qquad y_{gp}(L,t) = 0 \tag{5.41}$$

Boundary conditions for forward propagation:

$$\frac{\partial h_s'''}{\partial t}(0,t) = \begin{cases} f_{ig}(t) & for\ t \le t_{ig} \\ -U_0\left(T_s(0,t) - T_0\right) & for\ t > t_{ig} \end{cases} \qquad \frac{\partial T_s}{\partial x}(L,t) = -h_L\left(T_s(0,t) - T_0\right) \tag{5.42}$$

$$T_g(0,t) = T_s(0,t) \qquad \frac{\partial T_g}{\partial x}(L,t) = 0 \tag{5.43}$$

$$u(0,t) = \begin{cases} u_{ig} & for\ t \le t_{ig} \\ u_0 & for\ t > t_{ig} \end{cases} \qquad P(L,t) = P_0 \tag{5.44}$$

$$y_{O_2}(0,t) = 0.23 \qquad \frac{\partial y_{O_2}}{\partial x}(L,t) = 0 \tag{5.45}$$

$$\begin{aligned} y_{gp}(0,t) &= 0 \\ \frac{\partial y_{gp}}{\partial x}(L,t) &= 0 \end{aligned} \tag{5.46}$$

5.5 Numerics and Solution Method

The spatial partial derivatives in the governing equations are discretized using explicit finite-differences in a uniform grid whose nodes are Δx in length. The state variables are defined at the center of each node and the velocities at the edges of each node. For example, Darcy's law (Eq. 5.17) becomes:

$$u\Big|_t^{i+\frac{1}{2}} = -\frac{K}{\mu}\Big|_t^{i+\frac{1}{2}} \frac{P_t^{i+1} - P_t^i}{\Delta x} \tag{5.47}$$

which is substituted into the gas continuity (Eq 5.20) to give:

$$\frac{\partial}{\partial t}\left(\phi\rho_g\right)\Big|_{t+1} = \frac{\phi\rho_g \frac{K}{\mu}\Big]_t^{i+\frac{1}{2}} \frac{P_t^{i+1} - P_t^i}{\Delta x} - \phi\rho_g \frac{K}{\mu}\Big]_t^{i-\frac{1}{2}} \frac{P_t^i - P_t^{i-1}}{\Delta x}}{\Delta x} + \rho_0 \sum_i \dot{\omega}_i \nu_{g,i} \tag{5.48}$$

And so on with the other partial derivative in space. The resulting system of equations consists of nine ODEs per node, one for each of the variables: h_s''', h_g''', ρ_g, w_f, w_β, w_c, w_r, y_{O_2} and y_{gp}. This system is then solved in time using the stiff integrator VODE (Brown *et al.* 1989).

The grid-independence study is arguably the most reliable way to check if a numerical solution is accurate (Anderson 1995). Different solutions were computed for different-sized grids in order to find the relationship between the grid and the results. The error in the temperature profile computer with a given

grid is defined as the integral of the square of the difference respect to the solution with a grid of 2000 nodes (in opposed propagation with an airflow of 3 mm/s). The convergence of the results as the grid is increased is demonstrated (see Fig. 5.3). The study concludes that a grid of 500 nodes provides satisfactory accuracy.

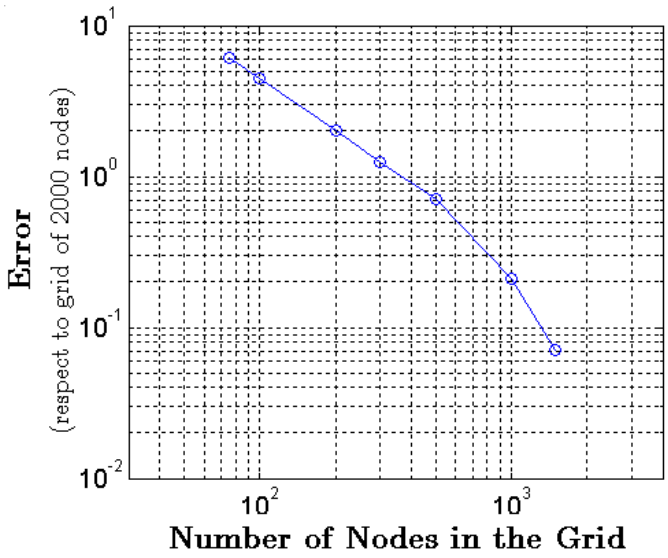

Figure 5.3: Results of the grid-independence study showing the convergence of the solution as the grid size increases. The results are for the temperature profile at $t = 900$ s in opposed propagation with an airflow of 3 mm/s. The error is calculated respect to the temperature profile with a grid of 2000 nodes.

5.6 Thermochemistry calibration

Suitable thermochemistry values for the smoldering combustion of PU are not available in the literature. Previous chemical studies of flexible PU foam have mainly focused on pyrolysis degradation. As a consequence, there is little

experimental information on oxygen consumptions and heats of reaction (Δh_p, $\Delta h_{p\beta}$, Δh_o, $\Delta h_{o\beta}$, Δh_c, $\nu_{O_2,o}$, $\nu_{O_2,o\beta}$ and $\nu_{O_2,c}$). For this reason, these unknown parameters are determined through comparison of the numerical results with two experiments in microgravity as shown below. The final values for the thermochemistry parameters are shown in Table 5.2.

Table 5.2: Value of the most important parameters used in the model.

Parameter	Value	Units	Reference
D	0.12	m	Bar-Ilan *et al.* (2004b) and (2004a)
L	0.14	m	Bar-Ilan *et al.* (2004b) and (2004a)
ρ_0	30	kg/m^3	Bar-Ilan *et al.* (2004b) and (2004a)
ϕ_0	0.97	-	Bar-Ilan *et al.* (2004b) and (2004a)
c_s	1760	J/kg	Bar-Ilan *et al.* (2004b) and (2004a)
K_f	5.2 10^{-9}	m^2	Putzeys *et al.* (2006)
K_c	3 10^{-8}	m^2	Putzeys *et al.* (2006)
k_s	3.4 10^{-2}	W/mK	Wu *et al.* (1999)
Δh_p	50	J/g-f	this study
$\Delta h_{p\beta}$	750	J/g-β	this study
Δh_o	-1600	J/g-f	this study
$\Delta h_{o\beta}$	-1500	J/g-β	this study
Δh_c	-3000	J/g-c	this study
$\nu_{O_2,o}$	0.08	g-O_2/g-f	this study
$\nu_{O_2,o\beta}$	0.3	g-O_2/g-β	this study
$\nu_{O_2,c}$	1.5	g-O_2/g-c	this study

5.7 Results and Discussion

Results for the temperature profiles of the solid and a direct comparison with the experiments are shown in Figs. 5.4 and 5.5. For the opposed case with an airflow of 3 mm/s case, the smoldering peak-temperature is 380 °C with a propagation velocity of 0.12 mm/s. The smoldering peak-temperature for the forward case with an airflow of 5 mm/s is 430 °C, and the propagation velocity is 0.21 mm/s. In forward propagation, the temperature profiles shows a dip moving ahead of the front that is caused by the endothermic pyrolysis. This dip is not present in the opposed propagation. It is seen that the model predicts successfully the experimental data in both opposed and forward propagation configurations.

While running different cases with the model, it was noted that modifications in the ignition protocol can have a significantly effect in the smoldering behaviour. In order to compare to the experiments it is important to match the thermal and flow boundary conditions. In the opposed case and only during ignition, the predicted temperatures between the second and third thermocouple (distance 15 and 60 mm from the igniter) are lower that in the experiments (left of Fig. 5.5). This is due to an under predicted heat-released rate at the very low flow velocity during the ignition protocol. The forward case is the most difficult to model because two phenomena that are not included into the model took place in the experiments. The first phenomenon is related to the plateaus at about 75 °C (right of Fig. 5.5), which are typical of forward propagation and have been attributed to water evaporation (Sui-Hang 2005, Torero and Fernandez-Pello

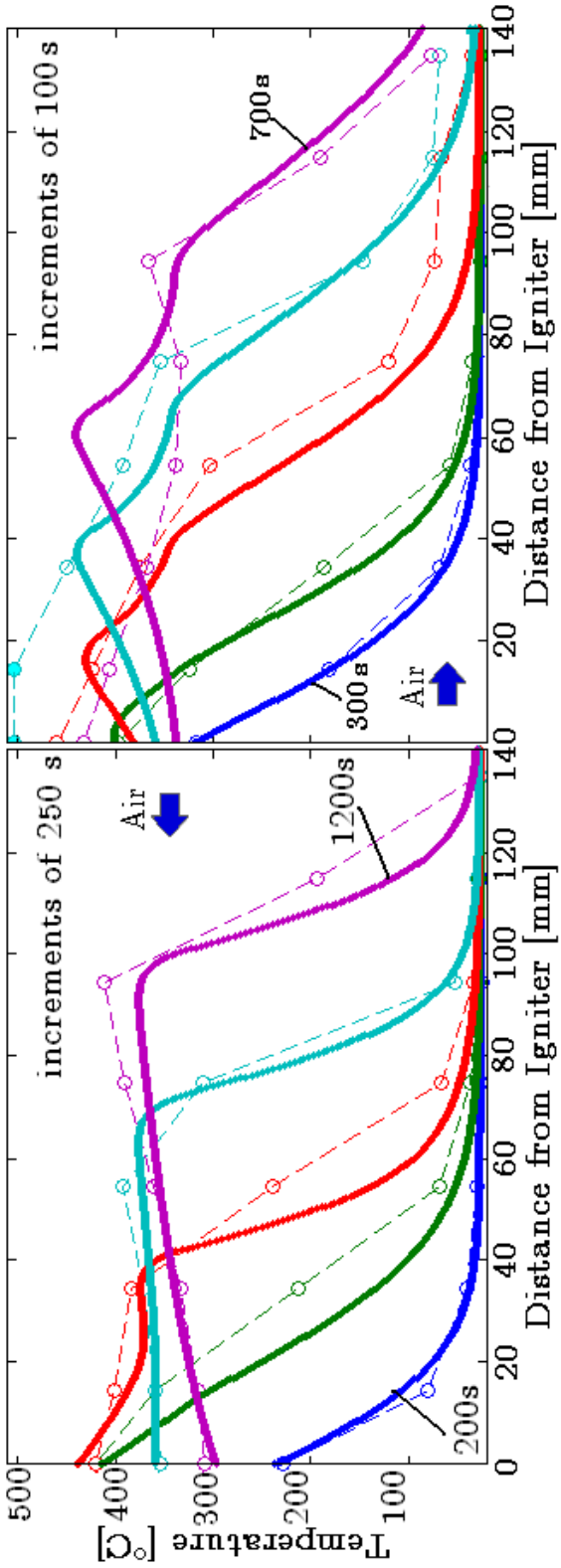

Figure 5.4: Temperature profiles of the solid vs. distance from igniter at different times; left) opposed smoldering with an inlet airflow of 3 mm/s; and right) forward smoldering with an inlet airflow of 5 mm/s. Comparison of numerical results (line) with experimental results (circle with dashed line) (Bar-Ilan et al. 2004b, Bar-Ilan et al. 2004a).

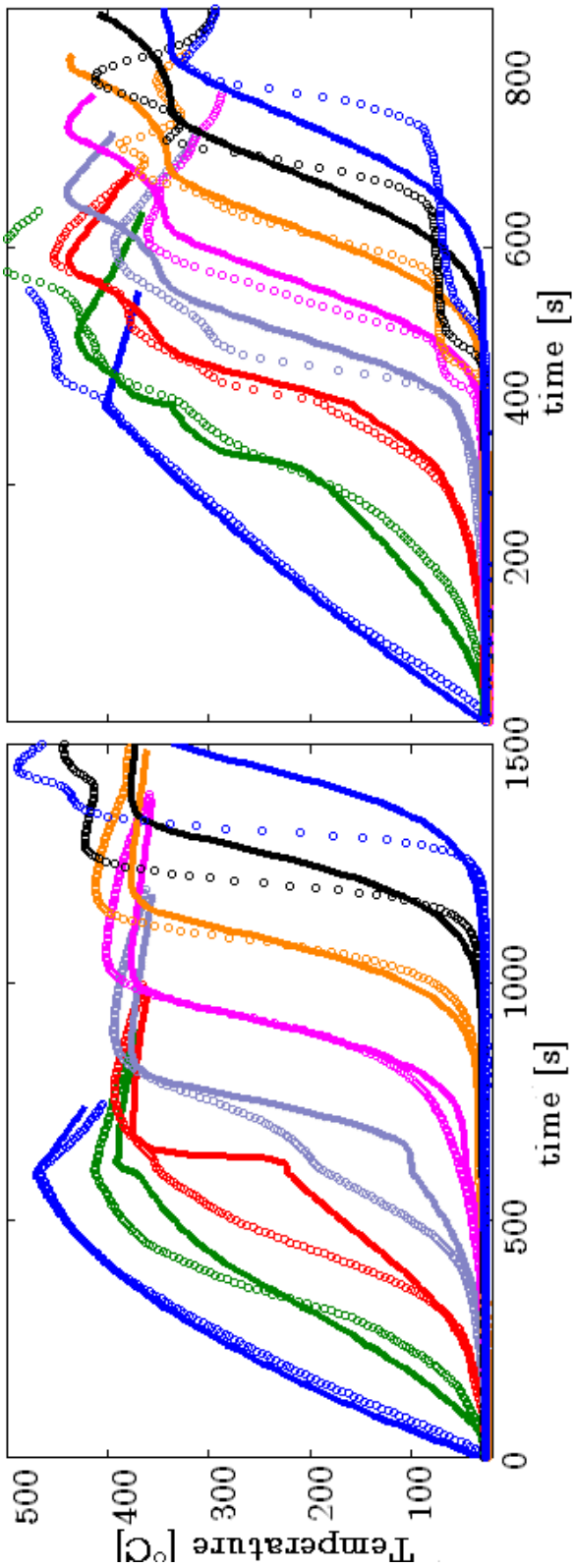

Figure 5.5: Temperature of the solid vs. time at different locations for; left) opposed smoldering with an inlet airflow of 3 mm/s; right) forward smoldering with an inlet airflow of 5 mm/s. Comparison of numerical (circles with line) with experimental results (line) (Bar-Ilan et al. 2004b, Bar-Ilan et al. 2004a).

1996). Because the numerical model does not include water evaporation, it cannot capture the ~100 s delay in the thermocouples away from the igniter. The other phenomenon is the on-set of secondary char-oxidation in the region around the second and third thermocouples at 600 s (Bar-Ilan *et al.* 2004a, and chapter 4 of this thesis), which produces higher temperatures and higher oxygen consumption. This reaction is not included in the 5-step mechanism and thus makes the model predict lower temperatures.

The temperature fields of the propagating waves can be also seen in Fig. 5.6 for opposed and forward propagations. These plots show the contour lines for the temperature of the solid as a function of time and space. The slope of each contour line gives the propagation velocity. In the opposed case (left of Fig. 5.6), the velocity is moderately constant in time and uniform in space after ignition. This indicates that the thickness of the smoldering front is constant during the process. In the forward case (right of Fig. 5.6), the velocity is moderately constant in time but it can be observed that the contour lines diverge in space after ignition. This indicates that in forward propagation the thickness of the smoldering front grows as the reaction progresses.

The time profiles of four variables are presented in Fig. 5.7 as an exemplar application in opposed smoldering combustion (airflow of 3 mm/s). The solid temperature profiles (Fig. 5.7a) show that the smoldering reaction is initiated at $t = 700$ s and that it propagates against the airflow from the igniter ($x = 0$) to the other end of the sample ($x = L$) in 900 s. The oxygen mass fraction profiles (Fig. 5.7b) show than during ignition, the transport of oxygen to the igniter is dominated by diffusion (straighter curves), whereas after ignition the higher

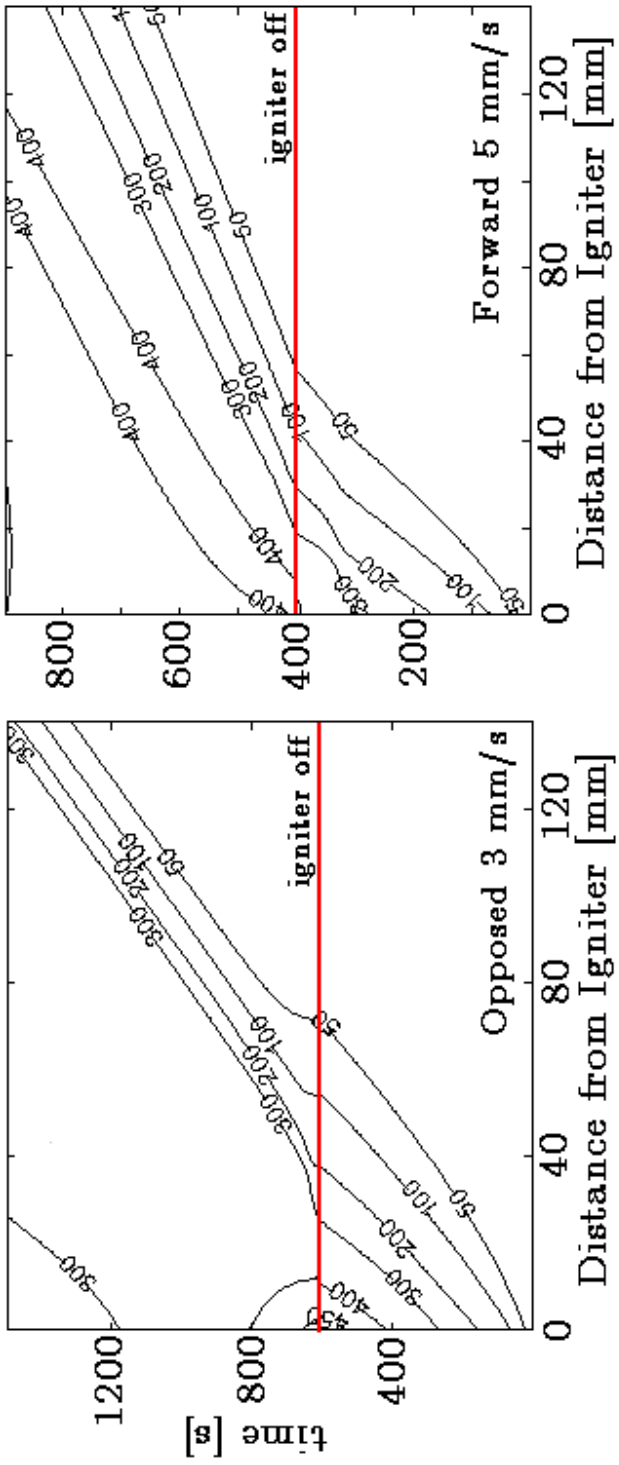

Figure 5.6. Numerical results for temperature contours lines as a function of time and space; left] opposed smoldering with an inlet airflow of 3 mm/s; and right] forward smoldering with an inlet airflow of 5 mm/s. The slope of each contour line gives the propagation velocity.

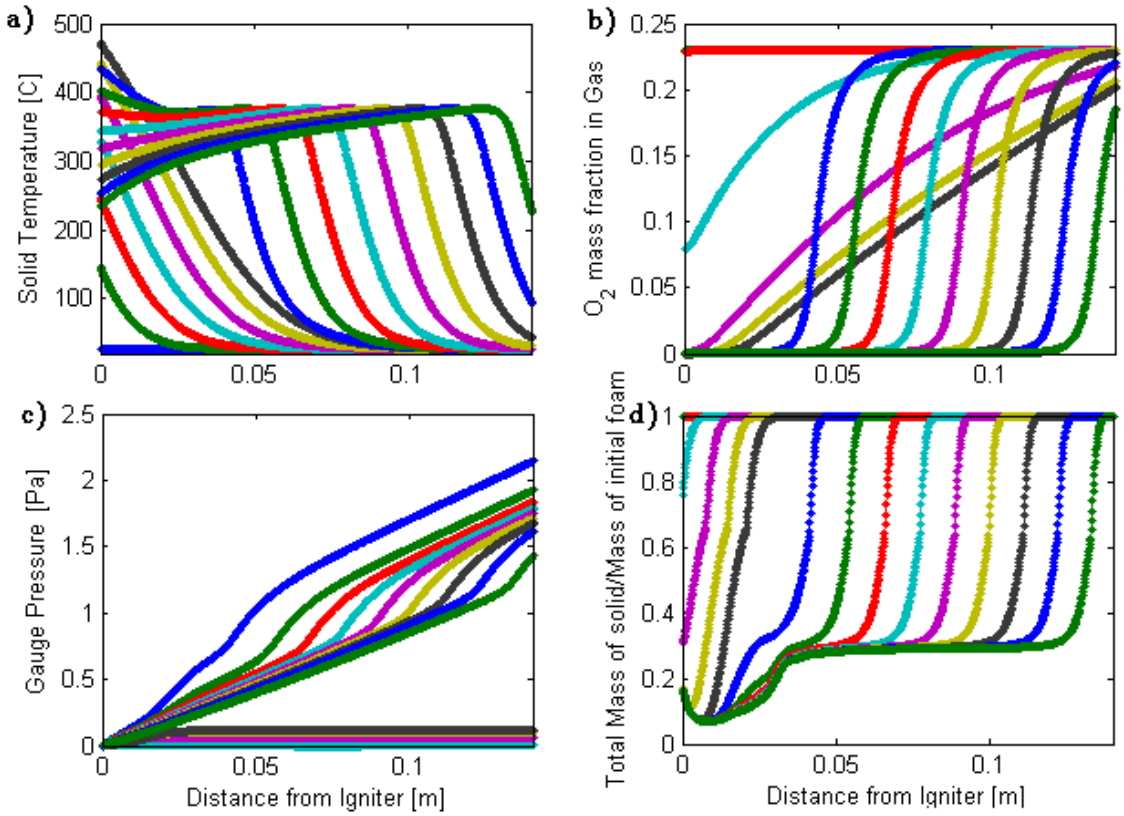

Figure 5.7: Numerical results for opposed smoldering with an airflow velocity of 3 mm/s. Each line is a different time in increments of 100s.

airflow imposed at the boundary makes convective transport to dominate (s-shape curves). The oxygen profiles also show that the smoldering reaction is oxygen starved during the later stages of the ignition and during the whole propagation. The pressure profiles (Fig. 5.7c) show than the pressure gradient is nearly constant along the sample except for a bump at the smolder front. This drop is caused by the gases released from the reacting solid, which increase the gas velocity to roughly two times its valued at the boundary. The solid mass profiles (Fig. 5.7d) show that about 70% of the solid reacts at the smolder front and that during ignition the solid consumption by higher. For all cases

simulated, the maximum temperature difference between the solid and the gas was lower than 3 °C, which implies than both phase are in virtual thermal equilibrium.

Results of the spatial profiles for the reaction rates, temperature and oxygen concentration at the smoldering front are presented in Fig. 5.8 (left of opposed, right for forward). It is seen that the model predicts that both fronts consume all the incoming oxygen. Considerable differences can be observed in the smolder-front structure for the two propagation modes. In opposed smoldering combustion (left of Fig. 5.8), the oxidation and the pyrolysis reactions overlap to form one single front. This is consistent with experimental observations, where the propagation front appears as one single smolder-front (Bar-Ilan *et al.* 2004b, Torero *et al.* 1993). The pyrolysis front combines contributions from the endothermic degradation of the foam and the β-foam. The oxidation front also has contributions from both, but it is dominated by the exothermic degradation of the β-foam. The starvation of oxygen occurs before the char oxidation is complete and this results in little heat provided to the front by this reaction (also in agreement with experimental observations (Bar-Ilan *et al.* 2004b, Torero *et al.* 1993)). The model predicts that both the pyrolysis and the oxidation fronts propagate at the same velocity in opposed smoldering combustion of PU (as Fig. 5.6 (left) also indicates).

The structure in forward smoldering combustion (right of Fig. 5.8) is quite different. The oxidation and the pyrolysis reactions form two distinct propagating fronts: the pyrolysis front followed by the oxidation front. This result is also in agreement with experimental observations of forward propagation (Bar-Ilan *et al.*

2004a, Torero and Fernandez-Pello 1996). The pyrolysis front combines both the endothermic degradation of the foam and the b-foam, but the former dominates. Forward smoldering combustion results in virtually no oxidation of the virgin foam, as all of it is converted to β-foam via pyrolysis, but has strong β-foam oxidation. The hot char region receives the fresh supply of oxidizer so the char oxidation is vigorous, and all the char is converted to solid residue. The model predicts that the pyrolysis front propagates about 0.07 mm/s faster than the oxidation front (as Fig 5.6 (right) also indicates). This finding was reported by Torero and Fernandez-Pello (1996) as an observation in their experiments, and it is due to the thermal wave traveling at a faster velocity than the oxidation wave. The resulting structure of the propagating wave with this characteristic is called 'reaction trailing' (Schult *et al.* 1996).

The effect of the inlet airflow on the self-sustained propagation velocities is presented in Fig. 5.9. Forward smoldering propagation is about 30% faster than opposed for the same inlet air velocity. The model predicts a sudden extinction of opposed smoldering combustion due to over-blowing (Leach *et al.* 1998, Kelley and Schult 2006). The results shown in Fig. 5.9 only applied to the ignition protocol implemented: the same as in Bar-Ilan *et al.* (2004a) and (2004b) but with the inlet forced-flow to its nominal value u_0 since the beginning ($t = 0$). It is expected that the results will change if the ignition protocol changes, especially at low airflow velocities.

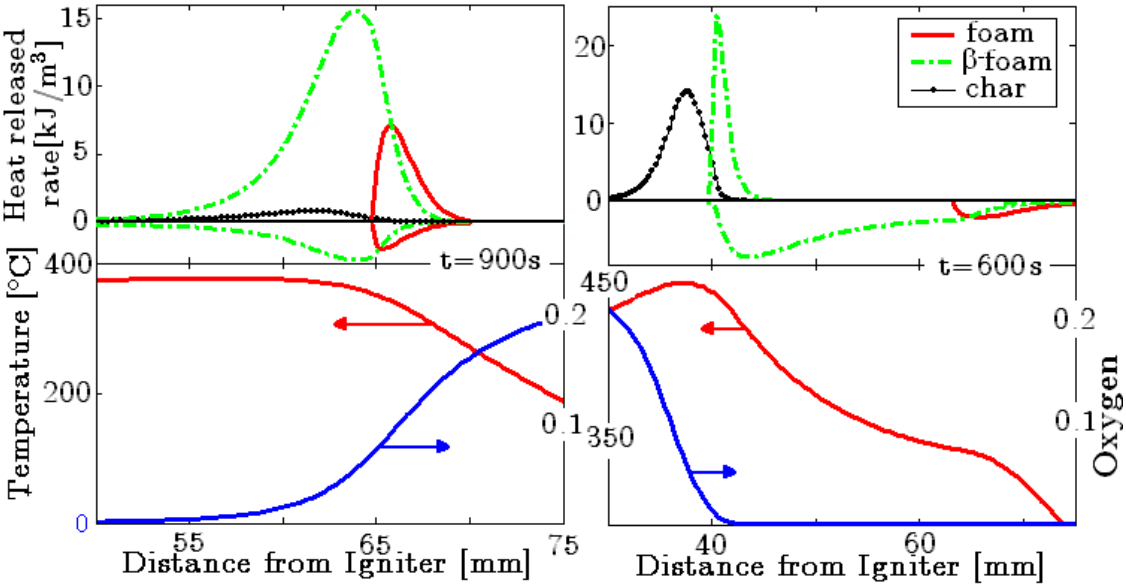

Figure 5.8. Numerical results for the front structure during self-propagation for; left) opposed smoldering with an inlet airflow of 3 mm/s; and right) forward smoldering with an inlet airflow of 5 mm/s. Top figures show the heat-released rate of each reaction (positive for oxidation, negative for pyrolysis). Bottom figures show the temperature and oxygen profiles.

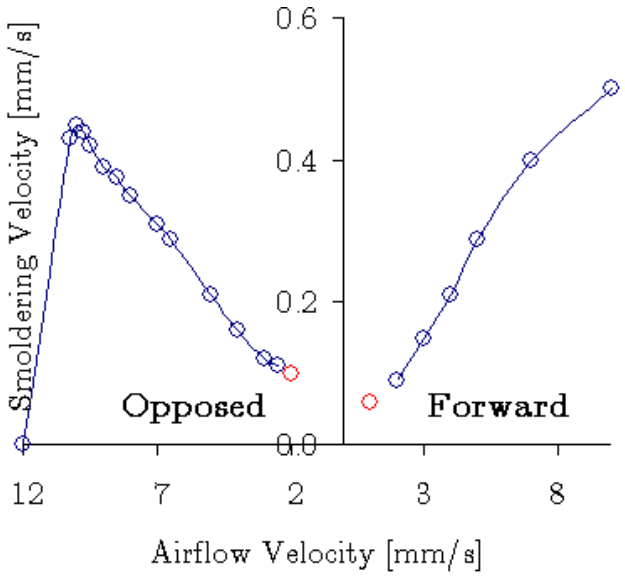

Figure 5.9: Self-sustained propagation velocity of the smoldering front in opposed and forward configurations. A red circle means halfway quenched.

5.8 Conclusions

The novel model presented here accounts for the most complete one-dimensional description of the chemical reactions and the transport mechanisms in smoldering combustion to date. Using a 5-step mechanism, the model of smoldering ignition and propagation in a porous media describes well both opposed and forward propagation. Specifically, the model predicts the reaction-front thermal and species structure, the onset of smoldering ignition, the propagation rate and the temperature profiles. The present model results, despite the inaccuracies, reproduce the most important features of the process and represent major a improvement in the modeling of smoldering combustion.

The fact that it is possible to predict the experimental observations in both opposed and forward propagation is a significant step forward in the development of numerical models of smoldering combustion. This is particularly relevant in multidimensional simulations where classification between forward and opposed propagation modes is no longer rigorous.

Chapter 6

Conclusions

"… he had never dined with a duchess, never received a prize, never been interviewed, never produced anything which the public could understand, nor experienced anything since his schoolboy amours which nice people could regard as romantic. He was, in fact, an authentic scientist"

Arrowsmith, Sinclair Lewis (1885-1951).

6.1 Conclusions

A computational study has been carried out to investigate smoldering ignition and propagation in polyurethane foam. The one-dimensional, transient, governing equations for smoldering combustion in a porous fuel have been solved accounting for improved solid-phase chemical kinetics.

The study of the thermal and oxidative degradation kinetics conducted in chapter 3 offers a methodology to apply solid-phase mechanisms to solid

materials from thermogravimetric experiments, and provides the kinetic parameters needed to compute the reaction rates in numerical models. Two different mechanisms were investigated and quantified using this methodology: a previously proposed 3-step (Ohlemiller 1985) and a new 5-step.

The 3-step mechanism has been applied here to model smoldering combustion of polyurethane foam for the first time (chapter 4). Previous attempts to model the process in polyurethane used the kinetics of cellulose or other solid materials (Ohlemiller 1979, Leach *et al.* 1997, Leach *et al.* 1998, Leach *et al.* 2000). The only two existing microgravity experiments in forward smoldering conducted previously have been used for comparison and calibration of the numerical results. The model predicts well the propagation characteristics and captures the extinction mechanism at low airflows, but the accuracy is low at low temperature.

The new 5-step mechanism is an extension upon the 3-step mechanism. It includes two additional reactions in order to capture the kinetic behavior observed in thermogravimetric experiments of polyurethane. This new mechanism offers an improved description of the thermal decomposition of polyurethane foam. A numerical model combining the transport mechanisms of mass and heat in porous media, together with the 5-step chemical mechanism, is developed here and represents a complete one-dimensional model of smoldering combustion. The microgravity experiments conducted previously in forward and opposed propagation have been used for comparison and calibration of the numerical results. The model reproduces the most important features of the process and compared well to the experiments. This work represents the first

successful attempt to model both forward and opposed smoldering combustion with the same kinetic mechanism and same kinetic parameters.

Realistic episodes of smoldering combustion involve most of the times multidimensional propagation (two or three spatial dimensions). In these situations, the smoldering front is not planar and does not propagate uniformly in space. Thus, the oxidizer gas would arrive to the reaction front from different directions, resulting in more possible propagation modes than just the forward and opposed. A numerical model with a comprehensive kinetic mechanism capable of modeling opposed and forward propagation, like the one presented here, is an essential step towards multidimensional simulations of the process.

6.2 Future Work

The topics that should be a natural extension of this work are the weak points of and the new frontiers opened by this thesis. These consist of:

- The thermochemistry of polyurethane remains poorly understood. This could be overcome conducting calorimetry experiments (*e.g.* DSC) in combination with thermogravimetric experiments. The use of the methodology presented in chapter 3 to extract the thermochemical parameters is recommended.
- Further thermogravimetric studies should be conducted with the same polyurethane foam used in the microgravity experiments of Bar-Ilan *et al.* (2004a and 2004b). These experiments should also address the effects in the

degradation kinetics of atmospheres with different oxygen concentrations. This will allow the determination of the oxygen coefficient in the Arrhenius expression used in chapter 3.

- The effect of the specific surface of the porous media on the reactivity of the solid could be addressed including a submodel that calculates the local conditions at the microstructure level.
- The 5-step mechanism does not include the secondary char oxidation (even though it is present in the thermogravimetric experiments). This reaction is known to take place in forward smoldering combustion when the reaction is strong (e.g. at 5 mm/s in Bar-Ilan *et al.* 2004a) and it is a pathway to the transition to flaming. In principle, the inclusion of this last kinetic reaction into the numerical model presented in chapter 5 should predict the transition to flaming as a thermal runaway.
- A multidimensional model is the most important future work that this thesis encourages. The description of the degradation kinetics has been advanced to the point that two- and even three-dimensional computational studies can be conducted. These computational models should be used first to predict the unburnt layer of foam nest to the samples walls seen in most smoldering combustion experiments.
- The inclusion of buoyancy-induced flows could be attained by adding the density-times-gravity term into Darcy's law equation (Eq. 5.17). Simulations with buoyancy make more sense in multidimensional domains, where recirculation flows could be established.

References

- I.Y. Akkutlu, Y.C. Yortsos, 2003, The dynamics of in-situ combustion fronts in porous media, *Combustion and Flame* 134, pp. 229-247.
- J.T. Alander, A. Autere, J. Mäntykoski, K.I. Keskinen, 1994. Distributed genetic algorithm for fitting of model parameters of chemical reaction kinetics, *Proceedings of the 2nd Finnish Workshop on Genetic Algorithms and their Applications*, Report 94-2, 16-18, pp. 115-126.
- S. Alexopoulos, D.D. Drysdale, 1988, The Transition from Smouldering to Flaming Combustion, *Fire and Materials* 13, pp. 37-44.
- J.D. Anderson, 1995, *Computational Fluid Dynamics: the Basics with Applications,* McGraw-Hill, New York, NY.
- M.K. Anderson, R.T. Sleight, J.L. Torero, 2000, Downward smolder of polyurethane foam: ignition signatures, *Fire Safety Journal* 35, pp. 131-147.

- R.A. Anthenien, S.D. Tse, A.C. Fernandez-Pello, 2005, On the trajectories of embers initially elevated or lofted by ground fire plumes in high winds, *Fire Safety Journal* (in press).
- Auerbach, 1989, Evaluation of kinetic-parameters appropriate for modeling urethane foam insulation performance, *Journal of Thermal Analysis* 35, pp. 1629-1641.
- V. Babrauskas, J.F. Krasny, 1985, Fire Behavior of Upholstered Furniture, *National Bureau of Standards* (NIST) Monograph 173.
- V. Babrauskas, J.F. Krasny, 1997, Upholstered Furniture Transition from Smoldering to Flaming, *Journal of Forensic Sciences* 42, pp. 1029-1031.
- Bar-Ilan, 2004, *The Effects of Buoyancy on Smoldering Combustion and its Transition to Flame*, PhD. Thesis, Department of Mechanical Engineering, University of California at Berkeley.
- Bar-Ilan, G. Rein, A.C. Fernandez-Pello, J.L. Torero, D.L. Urban, 2004a, Forced Forward Smoldering Experiments in Microgravity, *Experimental Thermal and Fluid Science* 28, pp. 743-751. http://repositories.cdlib.org/postprints/341
- Bar-Ilan, G. Rein, D.C. Walther, A.C. Fernandez-Pello, J.L. Torero, D.L. Urban, 2004b, The effect of buoyancy on opposed smoldering, *Combustion Science and Technology* 176, pp. 2027-2055. http://repositories.cdlib.org/postprints/350

- Bar-Ilan, O. Putzeys, G. Rein, A.C. Fernandez-Pello, D.L. Urban, 2005, Transition from Forward Smoldering to Flaming in Small Polyurethane Foam Samples, *Proceedings of the Combustion Institute* 30 (2) pp. 2295-2302.
- Bayliss ,B. Matkowsky, 1990, Two Routes to Chaos in Condensed Phase Combustion, *SIAM Journal Applied Mathematics* 50 (2), pp. 437-459.
- Bertschi, R.J. Yokelson, D.E. Ward, R.E. Babbitt, R.A. Susott, J.G. Goode, W.M. Hao. 2003, Trace gas and particle emissions from fires in large diameter and belowground biomass fuels, *Journal of Geophysical Research* 108 (D13), pp. 8.1-8.12.
- C.L. Beyler, Marcelo M. Hirschler, 2001, Thermal Decomposition of Polymers, *SFPE Handbook of Fire Protection Engineering* (3rd Ed), Section 1, Chapter 7, pp. 1-110.
- R. Bilbao, J.F. Mastral, J. Ceamanos ,M.E. Aldea, 1996, Kinetics of the thermal decomposition of polyurethane foams in nitrogen and air atmospheres, *Journal of Analytical and Applied Pyrolysis* 37, pp. 69-82.
- H.H. Biswell, 1989, *Prescribed Burning in California Wildlands Vegetation Management*, University of California Press, Berkeley, CA.
- Branca, C. Di Blasi, A. Casu, V. Morone, C. Costa, 2003, Reaction kinetics and morphological changes of a rigid polyurethane foam during combustion. *Thermochimica Acta* 399, pp. 127–137.
- S. Brereton, R.M. Laing, 1992, Analysis of injury and death from burning upholstered furniture, *New Zealand Medical Journal* 105, pp. 429-32.

- P.N. Brown, G.D. Byrne, A.C. Hindmarsh, 1989, VODE: A Variable-Coefficient ODE Solver, *SIAM Journal on Scientific Computing* 10 (5), pp. 1038-1051.
- J. Buckmaster, D. Lozinski, 1996, An elementary discussion of forward smoldering, *Combustion and Flame* 104 (3), pp. 300-310.
- E. Cantwell, A.C. Fernandez-Pello, Smoldering Combustion under Low Gravity, 1990, *AIAA 28th Aerospace Meeting*, Reno, NV. Paper AIAA-90-0648.
- C.Y.H. Chao, J.H. Wang, 2001a, Comparison of the Thermal Decomposition Behavior of a Non-Fire Retarded and a Fire Retarded Flexible Polyurethane Foam, *Journal of Fire Science* 19, pp. 137-155.
- C.Y.H. Chao, J.H. Wang, 2001b, Transition from smoldering to flaming combustion of horizontally oriented flexible polyurethane foam with natural convection, *Combustion and Flame* 127, pp. 2252-2264.
- Y. Chen, C.W. Kauffman, M. Sichel, J. Fangrat, and Y. Guo, 1990, The Transition from Smoldering to Glowing to Flaming Combustion, *Easter States Section Fall Meeting*, The Combustion Institute, paper #68. Florida.
- E. Chornet ,C. Roy, 1980, Compensation Effect in the Thermal Decomposition of Cellulosic Materials, *Thermochimica Acta* 35, pp. 389-393.
- J.A. Conesa, A. Marcilla, J.A. Caballero, R. Font, 2001, Comments on the validity and utility of the different methods for kinetic analysis of thermogravimetric data, *Journal of Analytical and Applied Pyrolysis* 58-59, pp. 617-633.

- F.S. Costa ,D.V. Sandberg, 2004, Mathematical model of a smoldering log, *Combustion and Flame* 139 (3), pp. 227-238.
- G. Debenest, V.V. Mourzenko, J.-F. Thovert, 2005a, Smouldering in fixed beds of oil shale grains. A three-dimensional microscale numerical model, *Combustion Theory and Modelling* 9 (1), pp. 113–135.
- G. Debenest, V.V. Mourzenko, J.-F. Thovert, 2005b, Smouldering in fixed beds of oil shale grains: governing parameters and global regimes, *Combustion Theory and Modelling* 9 (2), pp. 301–321.
- M.A. Decker, D.A. Schult, 2004, Dynamics of smoulder waves near extinction, *Combustion Theory and Modelling* 8 (3), pp. 491–512.
- Di Blasi, 1995, Mechanisms of two-dimensional smoldering propagation through packed fuel beds, *Combustion Science and Technology* 106, pp. 103-124.
- C.M. Dick, C. Denecker, J.J. Liggat, M.H. Mohammed, C.E. Snape, G. Seeley, C. Lindsay, B. Eling, P. Chaffanjon, 2000, Solid state 13C and in situ 1H NMR study on the effect of melamine on the thermal degradation of a flexible polyurethane foam, *Polymer International* 49 (10), pp. 1177-1182.
- S.S. Dosanjh, P.J. Pagni, A.C. Fernandez-Pello, 1987, Forced cocurrent smoldering combustion, *Combustion and Flame* 68 (2), pp. 131-142
- S.S. Dosanjh, J. Peterson, A.C. Fernandez-Pello, P.J. Pagni, 1986, Buoyancy Effects on Smoldering Combustion, *Acta Astronautica* 13, pp. 689-696.

- S.S. Dosanjh, P.J Pagni, 1987, Forced countercurrent smoldering combustion, *Proceedings of the 1987 ASME/JSME Thermal Engineering Joint Conference* (Ed. P.J. Marto, I. Tanasawa), pp. 165-173.

- Drysdale, 1999, *An Introduction to Fire Dynamic*, 2nd edition, John Wiley & Sons, West Sussex (UK).

- L. Elliott, D.B. Ingham, A.G. Kyne, N.S. Mera, M. Pourkashanian, C.W. Wilson, 2004, Genetic Algorithms for Optimisation of Chemical Kinetics Reaction Mechanisms, *Progress in Energy and Combustion Science* 30, pp. 297-328.

- G.M. Faeth, 1989, Closing Address, *Space Station Freedom Modular Combustion Facility Assessment Workshop*, NASA LeRC, Cleveland, OH, May 17.

- F. Fiorino, 2003, Lessons From Swissair Crash, *Aviation Week & Space Technology* 158 (15), p. 62.

- J. Florio, J.B. Henderson, F.L. Test, 1989, Experimental determination of volumetric heat transfer coefficients in decomposing polymer composites, *Porous Media, Mixtures and Multiphase Heat transfer* (ASME Winter Annual Meeting, San Francisco, CA), HTD-Vol. 117, pp. 51-60.

- R. Font, A. Fullana, J.A. Caballero, J. Candela, A. García, 2001, Pyrolysis study of polyurethane, *Journal of Analytical and Applied Pyrolysis* 58-59 (1), pp. 63-77.
- J.A. Foster, 2001, Evolutionary Computations, *Nature* 2001 Vol. 2, pp. 428-436.
- D.A. Frank-Kamenetskii, 1955, *Diffusion and Heat Exchange in Chemical Kinetics*, Princeton University Press, Princeton, NJ.
- W.H. Fransden, 1991, Burning rate of smoldering peat, *Northwest Science* 65, pp. 166-172.
- R. Friedman, 1993, Risk and Issues in Fire Safety on The Space Station, *NASA Technical memorandum* 106403.
- R. Friedman, 1998, Fire Safety in Extraterrestrial Environments, *NASA Technical Memorandum* 1998-207417, Lewis Research Center, Cleveland, OH, May 1998.
- A.K. Galwey, 2004, Is the science of thermal analysis kinetics based on solid foundations?: A literature appraisal, *Thermochimica Acta* 413 (1-2), pp. 139-183.
- S. Garcia, 1999, *Experimental Design Optimization and Thermophysical Parameter Estimation of Composite Materials Using Genetic Algorithms*, PhD Thesis, Virginia Polytechnic Institute (and Universite de Nantes).
- Goldberg, 1989, *Genetic Algorithms: In Search, Optimization and Machine Learning*, Addison-Wesley, Reading, MA.

- O. Grexa, M. Janssens, R. White, M. Dietenberger, 1996, Fundamental Thermophysical Properties of Materials Derived from the Cone Calorimeter Measurements, *Proceedings of Wood and Fire Safety 3rd International Scientific Conference*, Slovakia, p. 139-147.
- M. Grønli, M.J. Antal, G. Varhegyi, 1999, A round-robin study of cellulose pyrolysis kinetics by thermogravimetry, *Industrial and Engineering Chemistry Research* 38, pp. 2238-2244.
- J.R. Hall, 2004, The Smoking-Material Fire Problem, Fire Analysis and Research Division of *The National Fire Protection Association*, Quincy, MA (USA).
- C.C. Hardy, R.D. Ottmar, J.L. Peterson, J.C. Core, P. Seamon, (eds), 2002, *Smoke Management Guide for Prescribed and Wildland Fire*: 2001 Edition, PMS 420-2, 226 pp., Natural Wildfire Coordination Group, Natural Interagency Fire Center, Boise, Idaho.
- R.A Hartford, W.H. Frandsen, 1992, When it's hot, it's hot etc. or maybe it's not! (Surface flaming may not portend extensive soil heating), *International Journal of Wildland Fire* 2, pp. 139-44.
- C.J. Hilado, D.P. Brauer, E.M. Olcomendy, A. Furst, 1979, Toxicity of gases from Smoldering combustion, *Proceedings of the West Pharmaceutical Society* 22, pp.199-200.
- M.G. Hille, S.L. Stephens, 2005, Mixed conifer forest duff consumption during prescribed fires: tree crown impact, *Forest Science* 51 (5).

- H. Hotta, Y. Oka, O. Sugawa, 1987, Interaction between hot layer and updraft from a smoldering fire source - Part I An experimental approach, *Fire Science and Technology* 7 (2), pp. 17-25.
- Y. Hshieh, D. Hirsch, H. Beeson, 2003, Evaluation of Polyimide Foam as a Fire Barrier for Spacecraft Cushion Materials, *Journal of Fire Sciences* 21, pp. 485-501.
- C.R. Houck, J.A. Joines, M.G. Kay, 1995, GAOT: A Genetic Algorithm for Function Optimization: a Matlab Implementation, *North Carolina State University* Report NCSU-IE TR 95-09. http://www.ie.ncsu.edu.
- F.P. Incropera, D.P. DeWitt, 1996, *Fundamentals of Heat and Mass Transfer*, 4th ed., Wiley, New York, NY.
- R.D. Irons, T.W. Clarkson, J. Schulz, R. Eberhardt, B. Weiss, P. Todd, G.W. Morgenthaler, G. Oberdorster, M.J. Utell, 1994, Hazard identification and risk assessment in the extended spaceflight environment, *Acta Astronautica* 33, pp. 277-287.
- E.M. Kallman, 2005, *Numerical Modeling of Microgravity Smoldering Combustion in Polyurethane Foam*, PhD. Thesis, Department of Mechanical Engineering, University of California at Berkeley.
- W. Kaminsky, 1985, Thermal recycling of polymers, *Journal of Analytical and Applied Pyrolysis* 8, pp. 439-448.

- T. Kashiwagi, H. Nambu, 1992, Global kinetic constants for thermal oxidative degradation of a cellulosic paper, *Combustion and Flame* 88, pp. 345-368.
- J.B. Kauffman, D.L. Cummings, D.E. Ward, 1998, Fire in the Brazilian Amazon, 2, Biomass, nutrient pools and losses in cattle pastures, *Oecologia* 113, pp. 415-427.
- M.L. Kelley, D.A. Schult, 2006, Modeling extinction in forced opposed flow smolder, *Combustion Theory and Modelling* 10 (1), pp. 133-143.
- M.D. King, H.D. Ross, 1998, Overview of the NASA Microgravity Combustion Program, *AIAA Journal* 36 (8), pp. 1337-1345.
- H.E. Kissinger, 1957, Reaction kinetics in differential thermal analysis, *Analytical Chemistry* 29 (11), pp. 1702-1706.
- N. Koga, 1995, A review of the mutual dependence of Arrhenius parameters evaluated by the thermoanalytical study of solid-state reactions: The kinetic compensation effect, *Thermochimica Acta* 244, pp. 1-20.
- C.K. Law, G.M. Faeth, 1994, Opportunities and challenges of combustion in microgravity, *Progress in Energy and Combustion Science* 20 (1), pp. 65-113.
- S.V. Leach, J.L. Ellzey, O.A. Ezekoye, 1997, A numerical study of reverse smoldering, *Combustion Science and Technology* 130 (1-6), pp. 247-267.
- S.V. Leach, J.L. Ellzey, O.A. Ezekoye, 1998, Convection pyrolysis and Damkohler number effects on extinction of reverse smoldering combustion, *Proceedings of the Combustion Institute* 27 pp. 2873-2880.

- S.V. Leach, G. Rein, J.L. Ellzey, O.A. Ezekoye, J.L. Torero, 2000, Kinetic and fuel property effects on forward smoldering combustion, *Combustion and Flame* 120 (3), pp. 346-358.
- S.V. Levchik, E.D. Weil, 2004, Thermal decomposition, combustion and fire-retardancy of polyurethanes—a review of the recent literature, *Polymer International* 53, pp.1585-1610.
- Lozinski, J. Buckmaster, 1995, Quenching of reverse smolder, *Combustion and Flame* 102 (1-2), pp. 87-100.
- R.R. Mahajan, P.S. Makashir, E.M. Kurian, 2000, Thermal and Spectroscopic Studies on High Density Polyurethane Foam, *Journal of Polymer Materials* 17, pp.47-52.
- V. Mamleev, S. Bourbigot, M. Le Bras, S. Duquesne, J. Sestak, 2000, Modelling of nonisothermal kinetics in thermogravimetry, *Physical Chemistry Chemical Physics* 2, pp. 4796-4803.
- B.J. Meacham, V. Motevalli, 1992, Characterization of smoke from smoldering combustion for the evaluation of light scattering type smoke detector response, *Journal of Fire Protection Engineering* 4 (1), pp. 17-28.
- K. Miyanishi, E.A. Johnson, 2002, Process and patterns of duff consumption in the mixedwood boreal forest, *Canadian Journal of Forest Research* 32, pp. 1285-1295.
- Mulholland, T.J. Ohlemiller, 1982, Aerosol characterization of a smoldering source, *Aerosol Science and Technology* 1, pp. 59-71.

- NASA, 2003, Research Needs in Fire Safety for the Human Exploration and Utilization of Space, *Proceedings and Research Plan*, NASA CP-2003-212103 (Ed. G.A. Ruff).
- J.L. Newhall, A.C. Fernandez-Pello, P.J. Pagni, 1989, Experimental Observations of the Effect of Pressure and Buoyancy on Cellulose Co-current Smoldering, *Fire and Materials* 14, pp. 145-150.
- D.A. Nield, A. Bejan, 1992, *Convection in Porous Media*, Springer-Verlag, New York, NY.
- M.A. Nolter, D.H. Vice, 2004, Looking back at the Centralia coal fire: a synopsis of its present status, *International Journal of Coal Geology* 59 (1-2), pp. 99-106.
- J. Oberg, 2001, *Star-Crossed Orbits: Inside the U.S.-Russian Space Alliance*, McGraw-Hill, New York, NY (USA).
- R.A. Ogle, J.L. Shumacher, 1998, Fire Patterns on Upholstered Furniture: Smoldering vs. Flaming combustion, *Fire Technology* 34 (3) pp.247-265.
- T.J. Ohlemiller, J. Bellan, F. Rogers, 1979, A model of smoldering combustion applied to flexible polyurethane foams, *Combustion and Flame* 36, pp. 197-215.
- T.J. Ohlemiller, D.A. Lucca, 1983, An experimental comparison of forward and reverse smolder propagation in permeable fuel beds, *Combustion and Flame* 54 (1-3), pp. 131-147.

- T.J. Ohlemiller, 1985, Modeling of Smoldering Combustion Propagation, *Progress in Energy and Combustion Science* 11, pp. 277-310.
- T.J. Ohlemiller, 1990, Forward Smolder Propagation and the Transition to Flaming in Cellulosic Insulation, *Combustion and Flame* 81, pp. 341-353
- T.J. Ohlemiller, 2002, Smoldering Combustion, *SFPE Handbook of Fire Protection Engineering* (3rd Ed.), Chapter 2, pp. 200-210. http://fire.nist.gov/bfrlpubs/fire02/art074.html
- S.L. Olson, H.R. Baum, T. Kashiwagi, 1998, Finger-like smoldering over thin cellulosic sheets in microgravity, *Proceedings of the Combustion Institute* 27, pp. 2525-2533.
- M. Ortiz-Molina, T-Y. Toong, N. Moussa, G. Tesoro, 1979, Smoldering Combustion of Flexible Polyurethane Foams and its Transition to Flaming or Extinguishment, *Proceedings of the Combustion Institute* 17, pp. 1191-1200.
- S.E. Page, F. Siegert, J.O. Rieley, H.-D.V. Boehm, A. Jaya, S. Limin, 2002, The amount of carbon released from peat and forest fires in Indonesia during 1997, *Nature* 420, pp. 61-61.
- P.J. Pagni, 1993, Causes of the 20 October 1991 Oakland Hills Conflagration, *Fire Safety Journal* 21, pp. 331-339.
- K.N. Palmer, 1957, Smoldering Combustion in Dusts and Fibrous Materials, *Combustion and Flame* 1, pp. 129-154.
- H. Palmer, 1989, Closing Address, *International Microgravity Workshop*, NASA LeRC, Cleveland, OH, January 25.

- E. Pastor, L. Zarate, E. Planas, J. Arnaldos, 2003, Mathematical models and calculation systems for the study of wildland fire behaviour, *Progress in Energy and Combustion Science* 29 (2), pp. 139-153.
- T. Paulos, F. Issacci, I. Catton, G.E. Apostolakis, 1994, *Proceedings of 2nd Probabilistic Safety Assessment and Management Conference* (Ed. G.E Apostolakis), San Diego, CA, Vol. 3, pp. 099-15-099-20.
- L. Peng, C. Lu, J. Zhou, L. Zhang, F. You, 2005, Smoldering Combustion of Horizontally Oriented Polyurethane Foam with Controlled Air Supply, Proceedings of the 8th International Symposium on Fire Safety Science, Beijing, China. Paper BR2-4.
- W. Polifke, W. Geng, K. Döbbeling, 1998, Optimization of Rate Coefficients for Simplified Reaction Mechanisms with Genetic Algorithms, *Combustion and Flame* 113, pp. 119-134.
- Prakash, 2005, Coal fires - A natural or man made hazard?, University of Alaska Fairbanks. http://www.gi.alaska.edu/~prakash/coalfires
- O. Putzeys, A. Bar-Ilan, G. Rein, A.C. Fernandez-Pello, D.L. Urban, 2006, The role of the Secondary Char Oxidation in Smoldering and its Transition to Flaming by Ultrasound Probing, *31th International Symposium on Combustion*, Heidelberg, Germany (submitted).
- O. Putzeys, R. Titus, A. Bar-Ilan, D.L. Urban, A.C. Fernandez-Pello, 2005, Observations of Forward Smoldering and the Transition to Flaming in Small

Polyurethane Foam Samples with Ultrasound Probing, *43rd AIAA Aerospace Sciences Meeting* (2005). Paper 2005-0715.

- J.G. Quintiere, M. Birky, F. Macdonald,G. Smith, 1982, An analysis of smoldering fires in closed compartments and their hazard due to carbon monoxide, *Fire and Materials* 6 (3-4), pp. 99-110.
- E.R.C. Rabelo, C.A.G. Veras, J.A. Carvalho, E.C. Alvarado, D.V. Sandberg, J.C. Santos, 2004, Log smoldering after an amazonian deforestation fire, *Atmospheric Environment* 38 (2), pp. 203-211.
- M. Ravey, E.M. Pearce, 1997, Flexible polyurethane foam. I. Thermal decomposition of a polyether-based, water-blown commercial type of flexible polyurethane foam, *Journal of Applied Polymer Science* 63 (1), pp. 47-74.
- Rein, 1999, *A Numerical Simulation of Forward Smoldering*, B.S Thesis, ICAI College of Engineering, Universidad Pontificia de Comillas, Madrid (Spain).
- G. Rein, A. Bar-Ilan, A.C. Fernandez-Pello, J.L. Ellzey, J.L. Torero, D.L. Urban, 2005, Modeling of One-Dimensional Smoldering of Polyurethane in Microgravity Conditions, *Proceedings of the Combustion Institute* 30 (2), pp. 2327-2334. http://repositories.cdlib.org/postprints/342
- S. Renner, 2005, *Status of Fires at Abandoned Underground Coal Mines in Colorado*, Colorado Division of Minerals and Geology, State of Colorado, Denver, USA.

- F.E. Roger, T.J. Ohlemiller, A. Kurtz, M. Summerfield, 1978, Studies of the Smoldering Combustion of Flexible Polyurethane Cushioning Materials, *Journal of Fire and Flammability* 9, pp. 5-13.
- F.E. Rogers, T.J. Ohlemiller, 1980, Smolder Characteristics of Flexible Polyurethane Foams, *Journal of Fire and Flammability* 11 pp.32-44.
- F.E. Rogers, T.J. Ohlemiller, 1981, Pyrolysis kinetics of a polyurethane foam by thermogravimetry: a general kinetic model, *Journal of Macromolecular Science A* 15 (l), pp.169-185.
- M.S. Saidi, M.R. Hajaligol, F. Rasouli, 2004, Numerical simulation of a burning cigarette during puffing, *Journal of Analytical and Applied Pyrolysis* 72, pp. 141-152.
- H.A. Schneider, 1992, Thermogravimetric kinetics of polymer degradation: Science or Fiction?, *Polymer Engineering and Science* 32 (17), pp. 1309-1315.
- D.A. Schult, B.J. Matkowsky, V.A. Volpert, A.C. Fernandez-Pello, 1995, Propagation and extinction of forced opposed flow smolder waves, *Combustion and Flame* 101 (4), pp. 471-490.
- D.A. Schult, B.J. Matkowsky, V.A. Volpert, A.C. Fernandez-Pello, 1996, Forced forward smolder combustion, *Combustion and Flame* 104 (1-2), pp. 1-26.
- R. Siegel, J.R. Howell, 2001, *Thermal Radiation Heat Transfer*, 4th ed., Taylor and Francis, New York, NY.

- S.L. Stephens, M.A. Finney, 2002, Prescribed fire mortality of Sierra Nevada mixed conifer tree species: effects of crown damage and forest floor combustion, *Forest Ecology and Management* 161, pp. 261-271.
- D.P. Stocker, S.L. Olson, D.L. Urban, J.L. Torero, D.C. Walther, A.C. Fernandez- Pello, 1996, Small-Scale Smoldering Combustion Experiments in Microgravity, *Proceedings of the Combustion Institute* 26, pp. 1361 1368.
- G.B. Stracher, T.P. Taylor, 2004, Coal fires burning out of control around the world: thermodynamic recipe for environmental catastrophe, *International Journal of Coal Geology* 59, pp. 7-17.
- Y. Sui-Hang, 2005, City University of Hong-Kong. Personal communications about results to be submitted for publication.
- M. Summerfield, T.J. Ohlemiller, H.W. Sandusky, 1978, Thermophysical model of steady-draw smoking and Predictions of overall cigarette behavior, *Combustion and Flame* 33, pp. 263-279.
- J.S. T'ien, H. Shih, C. Jiang, H.D. Ross, F.J. Miller, A.C. Fernandez-Pello, J.L. Torero, D.C. Walther, 2001, Mechanisms of Flame Spread and Smolder Wave Propagation, *Microgravity Combustion: Fire in Free Fall,* H.D. Ross (Editor), Academic Press, pp. 299-417.
- P. Todd, M.V. Sklar, W.F. Ramirez, G.J. Smith, G.W. Morgenthaler, J.T. McKinnon, G. Oberdörster, J. Schulz, 1994, Inhalation risk in low-gravity spacecraft, *Acta Astronautica* 33, pp. 305-315.

- J.L. Torero, A.C. Fernandez-Pello, M. Kitano, 1993, Opposed forced flow smoldering of polyurethane foam, *Combustion Science and Technology* 91, pp. 95-117.
- J.L. Torero, A.C. Fernandez-Pello, 1996, Forward smolder of polyurethane foam in forced air flow, *Combustion and Flame* 106, pp. 89-109.
- J.L. Torero, A.C. Fernandez-Pello, D.L. Urban, 1994, Experimental Observations of the Effect of Gravity Changes on Smoldering Combustion, *AIAA Journal* 32, pp. 991-996.
- J.L. Torero, J.I. Gerhard, 2005, personal communications, The University of Edinburgh.
- J.L. Torero, A.C. Fernandez-Pello, 1996, Forward smolder of polyurethane foam in forced air flow, *Combustion and Flame* 106, pp. 89-109.
- J.L. Torero, A.C. Fernandez-Pello, 1995, Natural Convection Smolder of Polyurethane Foam, Upward Propagation, *Fire Safety Journal* 24, 35-52.
- S.D. Tse, A.C. Fernandez-Pello, K. Miyasaka, 1996, Controlling Mechanisms in the Transition from Smoldering to Flaming of Flexible Polyurethane foam, *Proceedings of the Combustion Institute* 26, pp. 1505-1513.
- S.D. Tse, R.A. Anthenien, A.C. Fernandez-Pello, K. Miyasaka, 1999, An Application of Ultrasonic Tomographic Imaging to Study Smoldering Combustion, *Combustion and Flame* 116 (1-2), pp. 120-135.

- J.P. Vantelon, B. Lodeho, S. Pignoux, J.L. Ellzey, J.L. Torero, 2005, Experimental observations on the thermal degradation of a porous bed of tires, *Proceeding of the Combustion Institute* 30 (2), pp. 2239-2246.
- P.J. Wakelyn, P.K. Adair, R.H. Barker, 2005, Do open flame ignition resistance treatments for cellulosic and cellulosic blend fabrics also reduce cigarette ignitions?, *Fire and Materials* 29, pp. 15–26.
- D.C. Walther, A.C. Fernandez-Pello, D.L. Urban, 1999, Space Shuttle Based Microgravity Smoldering Combustion Experiments, *Combustion and Flame* 116, pp. 398-414. http://repositories.cdlib.org/postprints/770
- D.C. Walther, 1998, *A Study of Opposed Flow Smoldering of Polyurethane Foam: Comparison Between Normal- and Microgravity*, PhD. Thesis, Department of Mechanical Engineering, University of California at Berkeley.
- D.C. Walther, R.A. Anthenien, C. Fernandez-Pello, 2000, Smolder ignition of polyurethane foam: effect of oxygen concentration, *Fire Safety Journal* 34 (4), pp. 343-359. http://repositories.cdlib.org/postprints/769
- Q. Wang, J. Li, J.E. Winandy, 2004, Chemical mechanism of fire retarding of boric acid on wood, *Wood Science Technololy* 38, pp. 375–389.
- J-I. Watanabe, T. Tanaka, 2004, Experimental Investigation into Penetration of a Weak Fire Plume into a Hot Upper Layer, *Journal of Fire Sciences* 22, pp. 404-420.

- F.J. Weinberg, F.B. Carleton, D. Dunn-Rankin, 2003, Development of electrically charged extinguishant dispersions for use in microgravity, *Combustion Science and Technology* 175, pp. 2161-2179.
- D. Wolf, R. Moros, 1997, Estimating rate constants of heterogeneous catalytic reactions without supposion of rate determining surface steps - an application of a genetic algorithm, *Chemical Engineering Science* 52, pp. 1189-1199.
- J-W. Wu, W.-F. Sung, H.-S. Chu, 1999, Thermal conductivity of polyurethane foams, *International Journal of Heat and Mass Transfer* 42, pp. 2211-2217.
- S.C. Yi, E.-S. Song, M.R. Hajaligol, 2001a, Mathematical Model of Smoldering Combustion in a Carbonaceous Porous Medium Part 1- Development of Pyrolysis and Combustion Models for a Cylindrical Geometry, *Journal of Fire Science* 19, pp. 429-447.
- S.C. Yi, E.-S. Song, W.-D. Joung, S.-G. Oh, S.K. Moon, M.R. Hajaligol, 2001b, Mathematical Model of Smoldering Combustion in a Carbonaceous Porous Medium Part 2- Sensitivity Analysis of Model Parameters., *Journal of Fire Science* 19, pp. 449-460.